JOURNAL OF RESEARCH of the National Bureau of Standards
Vol. 87, No. 5, September-October 1982

Contents

Library of Congress Catalog Card Number: 63-37059

For sale by the Superintendent of Documents, U.S. Government Printing Office
Washington, DC 20402
Single copy price $5.50 Domestic; $6.90 Foreign.
Subscription price: $18.00 a year; $22.50 foreign mailing.
UNITED STATES GOVERNMENT PRINTING OFFICE, WASHINGTON: 1982

JOURNAL OF RESEARCH of the National Bureau of Standards
Vol. 87, No. 5, September–October 1982

Consensus Values and Weighting Factors

Robert C. Paule* and John Mandel*

National Bureau of Standards, Washington, DC 20234

May 12, 1982

A method is presented for the statistical analysis of sets of data which are assembled from multiple experiments. The analysis recognizes the existence of both within group and between group variabilities, and calculates appropriate weighting factors based on the observed variability for each group. The weighting factors are used to calculate a "best" consensus value from the overall experiment. The technique for obtaining the consensus value is applicable to either the determination of the weighted average value, or to the parameters associated with a weighted least squares regression problem. The calculations are made by using an iterative technique with a truncated Taylor series expansion. The calculations are straightforward, and are easily programmed on a desktop computer.

An examination of the observed variabilities, both within groups and between groups, leads to considerable insight into the overall experiment and greatly aids in the design of future experiments.

Key words: ANOVA (within-between), components of variance, consensus values, design of experiments, pooling of variance, weighted average, weighted least squares regression.

1. Introduction

e purpose of this article is to discuss the problem of calculating "best" estimates from a series of experimental results. It will be convenient to refer to these estimates as consensus values. Since experimental data frequently come from many different sources, with each having its own characteristic variability, the statistician's problem centers on the appropriate weighting of the data to obtain the consensus value(s). In order to achieve this aim, the statistical analysis should recognize the existence of both within group and between group variability. Both types of variability are considered here to be random effects and are described by their associated components of variance: the within set component of variance for group i, $\sigma^2_{w_i}$, and the between set component of variance, σ^2_b.

Early attempts to solve the consensus value problem have not explicitly recognized the existence of the between set component of variance. Attempts, such as the Birge ratio method [1],[1] are adversely affected by this omission.

In this article we will deal with two types of problems. The first is essentially the calculation of a weighted average value and its statistical uncertainty. The second problem arises in the fitting of a straight line or curve to a set of data. The estimates both for the average and the parameters of the fitted curve can be thought of as consensus values, i.e., they should be the consensus of the observed data. Both problems can involve several sources of error. It will turn out that, because of the similarity of the weighting problems in both types of situations, a theoretical solution common to both problems can be derived. A solution for a more restricted form of the first problem has been previously reported [2,3]. The mathematical aspects of the general problem are outlined in the current paper.

An understanding of the nature of random error processes associated with measurement systems is required to develop appropriate weighting factors. The weighting factors that are derived are not arbitrary, but are controlled by the nature of the variability of the data.

2. Illustrative Examples

For purposes of exposition, artificial examples of data sets will be used as illustrative material. Later in this paper it will be shown that the procedures developed are useful for the analysis of actual laboratory data.

To develop some feeling for "what is appropriate weighting", let us examine two specific examples. For the first example, consider that three measurements are each made by method A and by method B, and that the method A results are more precise. Assume, both here and throughout this manuscript, that the relative accuracies of the methods are not known. Let the following be the measured values, and the corresponding coded

*National Measurement Laboratory

[1]Figures in brackets indicate literature references located at the end of this paper.

values which are obtained by subtracting 200 from the measured values.

Method	A			B		
Measured Values	201.1	201.9	201.5	216	225	203
Coded Values	1.1	1.9	1.5	16	25	3

For ease of presentation, our evaluations will be made using the coded values. Giving the same weight to all six coded values result in a straight average of 8.1. Note that the addition or loss of a single method B measurement would likely result in a relatively large change of this average. This is not desirable. Intuitively, we know that we should give greater weight to the more precise (and stable) method A results.

For the second example, consider that the measurements by method A and B are equally precise, but that many more measurements were made by method A than by method B.

Method	A						B	
Coded Values (Measured Values−200.)	2.0	1.0	1.5	1.8	1.2	1.7	16.3	16.8

In this example, the values by the two methods differ widely. Here again, we should not take a straight average ($\bar{Y} = 5.3$). To do so would strongly favor method A, and we have no basis for preferring this method. For these data, it is better to take separate averages for each method, and to then average the two averages ($\bar{Y} = 9.0$). Note that this is a form of weighting, and that it does not let the larger number of A measurements overpower the B measurements.

3. Basic Statistics of Weighted Averages

It is well known that the weighted average of n values of Y is calculated by the formula:

$$\tilde{Y} = \frac{\sum_{i=1}^{n} \omega_i Y_i}{\sum_{i=1}^{n} \omega_i} = a_1 Y_1 + a_2 Y_2 + \ldots$$

where ω_i is the weight associated with the value Y_i and the a's are the corresponding coefficients. Statistical theory shows that the variance of this weighted average is minimized when the individual weights are taken as the inverse of the variance of the individual Y_i, that is, $\omega_i = 1/\mathrm{Var}(Y_i)$. Low weights are given to values with high variance.

Next consider the weighted average of m average values, $\bar{Y}_i$:

$$\tilde{Y} = \frac{\sum_{i=1}^{m} \omega_i \bar{Y}_i}{\sum_{i=1}^{m} \omega_i} \tag{1}$$

where now $\omega_i = 1/\mathrm{Var}(\bar{Y}_i)$. If both the $\bar{Y}_i$ and the $\mathrm{Var}(\bar{Y}_i)$ are known, then the weighted average of (1) is easily calculated, and this is the consensus value. The estimation of the proper value for the variance of $\bar{Y}_i$, however, is not always a simple process. To better understand the problem let us return to the second example, given above. It is easy to obtain $\bar{Y}_A = 1.533$ and the variance estimate

$$s^2(\bar{Y}_A) = \frac{s^2(Y_A)}{n_A} = \frac{\sum_{i=1}^{6} (Y_i - \bar{Y}_A)^2}{(6-1)\cdot 6} = 0.0238 = (0.154)^2$$

and $\bar{Y}_B = 16.55$ and $s^2(\bar{Y}_B) = 0.0625 = (0.250)^2$, but one questions the reasonableness of the estimated variances. How can the variances be so small, and the two averages be so far apart? The answer is that the above variance calculations only describe the internal variability of the A or the B measurements, and do not recognize the variability between the sets of measurements. It is quite common, even among very good measurements, to find large differences between different sets of measurements [4]. To obtain a realistic estimate of Var $(\bar{Y}_i)$, or correspondingly of ω_i, one must evaluate a between set component of variance and include it in Var $(\bar{Y}_i)$.

The use of a between set component of variance, in effect, treats the collection of systematic errors from the various measurement sets as a source of random variability. The existence of systematic errors in a measurement process may require a word of explanation. The systematic errors that are being described are errors that remain after the extensive scientific development of a measurement process. All major sources of error should have been eliminated, and calibrations with multiple standards should have been made. What frequently happens in this process is that many within set errors are eliminated along with the larger between set errors, such that the sensitivity of the analytical method

increases to the point that a lower level of systematic error can now be detected. There are practical limitations to the pursuit of this process, and frequently one must live with a certain detectable level of between set systematic error. Effects such as interferences due to minor sample components will vary in different laboratory environments and these effects are extremely difficult to eliminate.

An essential point in our analysis is the assumption that no information on systematic errors is available that would allow us to place more confidence in any one set of measurements as compared to the others. Thus, in this analysis all sets have equal standing with regard to their possible systematic errors. Our technique can, however, be extended to cover situations involving different assumptions.

The calculation of the between set component of variance is readily accomplished by an iterative procedure, described in section 4. The sample estimate of $\mathrm{Var}(\bar{Y}_i)$ for method i, is obtained by combining the within set component of variance, $s^2_{w_i}$, and the between set component of variance, s^2_b. For the second example:

$$s^2(\bar{Y}_\mathrm{A}) = \frac{s^2_{w\mathrm{A}}}{6} + s^2_b$$

$$s^2(\bar{Y}_\mathrm{B}) = \frac{s^2_{w\mathrm{B}}}{2} + s^2_b$$

The within set component of variance for method A is:

$$s^2_{w\mathrm{A}} = \frac{\sum_{i=1}^{6} (Y_i - \bar{Y}_\mathrm{A})^2}{(6-1)} = 0.1427$$

Similarly,

$$s^2_{w\mathrm{B}} = 0.1250$$

and $s^2_{w\mathrm{A}}/6$ and $s^2_{w\mathrm{B}}/2$ are equal to 0.0238 and 0.0625, the quantities that we had previously (and incorrectly) called $s^2(\bar{Y}_\mathrm{A})$ and $s^2(\bar{Y}_\mathrm{B})$. For the proper $s^2(\bar{Y}_i)$ one needs to add in s^2_b. With an available s^2_b one calculates estimates for $s^2(\bar{Y}_A)$ and $s^2(\bar{Y}_B)$ and the corresponding weights, ω_A and ω_B, and then proceeds by eq (1) to obtain a valid estimate of the consensus value, $\tilde{Y}$.

If the $s^2_{w_i}$ are quite similar, as they are in the above example, one can make an improvement by using a more stable pooled s^2_w. There should, of course, be a reasonable scientific and statistical basis for pooling the within set variability. For the current example,

$$s^2_w = \frac{\sum_{i=1}^{6} (Y_{\mathrm{A}_i} - \bar{Y}_\mathrm{A})^2 + \sum_{i=1}^{2} (Y_{\mathrm{B}_i} - \bar{Y}_\mathrm{B})^2}{(6\text{-}1) + (2\text{-}1)} = 0.1398 \tag{2}$$

so that

$$s^2(\bar{Y}_\mathrm{A}) = \frac{0.1398}{6} + s^2_b$$

and

$$s^2(\bar{Y}_\mathrm{B}) = \frac{0.1398}{2} + s^2_b$$

To summarize: The weighting constants used to calculate the consensus value are obtained by taking the inverse of the variances of the various set $\bar{Y}_i$. The proper variances are a combination of the within and the between set components of variance. Under certain circumstances, a more stable pooled within set component of variance may be used.

4. Calculation of the Between Set Component of Variance

The proper weight for $\bar{Y}_i$ is $\omega_i = 1/\mathrm{Var}(\bar{Y}_i)$ and the estimate of this quantity is:

$$\omega_i = \left[\frac{s^2_{w_i}}{n_i} + s^2_b\right]^{-1} \tag{3}$$

Depending on the nature of the data, the within set variance may or may not be pooled. For either case, however, s^2_b must be evaluated. This is accomplished in the following way.

From the definition of ω_i we obtain the relation:

$$\omega_i \mathrm{Var}(\bar{Y}_i) = 1$$

or equivalently (4)

$$\mathrm{Var}(\sqrt{\omega_i}\bar{Y}_i) = 1$$

For any given set of ω_i, this variance can be estimated from the sample by the formula

$$s^2(\omega_i \bar{Y}_i) = \frac{\sum_{i=1}^{m} \omega_i (\bar{Y}_i - \tilde{Y})^2}{(m-1)}$$

Equating this estimate to its expected value (unity, see eq (4)), we obtain

$$\frac{\sum_{i=1}^{m} \omega_i(\overline{Y}_i - \widetilde{Y})^2}{(m-1)} = 1 \qquad (5)$$

where $\widetilde{Y}$ is the estimate of the consensus value as given by eq (1). The estimate of $\widetilde{Y}$ depends on knowing the ω_i. These can be calculated from eq (3), once s_b^2 is known. Thus, the only problem is to estimate s_b^2. Equation (5) provides the means for calculating s_b^2 through an iterative process.

Define the function:

$$F(s_b^2) = \sum_{i=1}^{m} \omega_i(\overline{Y}_i - \widetilde{Y})^2 - (m-1) \qquad (6)$$

In view of eq (5), s_b^2 must be such that $F(s_b^2) = 0$. For ease of notation let $s_b^2 = v$. Start with an arbitrarily selected initial value, v_o. It is desired to find an adjustment, dv, such that $F(v_o + dv) = 0$. Using a truncated Taylor series expansion, one obtains:

$$F(v_o + dv) \approx F_o + \left(\frac{\partial F}{\partial v}\right)_o dv = 0$$

and

$$dv = -\left(\frac{Fo}{\frac{\partial F}{\partial v}}\right)_o$$

Evaluating the partial derivative in this equation, one obtains:

$$dv = \frac{Fo}{\left[\sum_{i=1}^{m} \omega_i^2 (\overline{Y}_i - \widetilde{Y})^2\right]_o} \qquad (7)$$

The adjusted (new) value for v is:

$$\text{New } v_o = \text{Old } v_o + dv$$

This new value is now introduced in eq (1), (3), (6), and (7) and the procedure is iterated until dv is satisfactorily close to zero. If at any point in the iteration process a negative value is obtained for v, this value should be replaced by zero and the iteration continued. The last v is the s_b^2 we seek. The ω_i and Y are also obtained from this last iteration.

The small data set of our second example will now be used to illustrate the iterative procedure. Let the first estimate for s_b^2 be 100. In calculating the ω_i from eq (3), it is seen that the first term of the right-hand side is a fixed quantity and that the values for the A and B sets have been previously calculated to be .0238 and .0625, respectively. Thus, $\omega_A = 1/(.0238 + 100.) = .0099976$ and $\omega_B = .0099938$. The $\overline{Y}_A$ and $\overline{Y}_B$ are 1.533 and 16.550, respectively.

From eq (1), $\widetilde{Y} = 9.0400$
From eq (6), $F_o = .1270$
From eq (7), $dv = 11.28$

The next iteration would start with a value of 111.28 for s_b^2, and would repeat the above set of calculations with this new value. After two additional iterations, v is equal to 112.7120 and dv is less than .0001. The final $\widetilde{Y}$ is 9.0402. (The uncoded Y is, of course, 209.0402.)

In this illustration the initial v value was reasonably close to its final estimate. More discrepant initial values will require only a few additional iterations. It can be shown that the iteration process always converges.

The pooled estimate of the s_w^2 (= 0.1398) could have been used for the above iterative calculations. The final results would be very similar ($s_b^2 = 112.7085$ and $\widetilde{Y} = 9.0399$). For either case, the iterative calculations are easily programmed on a desktop computer.

5. Discussion

The above iterative calculations for the weights and the weighted average are recommended. The calculations are based on the recognition of both within and between group variability. The calculated consensus value is, in general, neither the grand average of all measurements, nor the average of measurement set averages. These overall averages merely describe two opposite weighting situations from our more general weighting eq (3). To illustrate this point consider the case where a pooled s_w^2 is used in eq (3). When the s_b^2 term of this equation is zero, the weights for the $\overline{Y}_i$ are all proportional to n_i. All individual *measurements* are therefore weighted equally. When, however, s_b^2 is relatively large, the s_w^2/n_i term of eq (3) is essentially without effect, and all the measurement set *averages* are weighted equally. Equation (3) also gives proper weighting for all intermediate cases. In addition, it describes the situation where the within set components of variance are different for different sets of measurements, and takes account of any differences in the number of replicates (n_i) in the various groups.

The ready availability of programmable desktop computers strongly encourages the use the iterative approach. Since one can easily do the calculations, there is little reason to not use proper weighting.

The examples to this point have been chosen to be easily worked by hand. They describe situations where the intuitive answers are obvious. The examples use of only two measurement sets, however, is not recommended in practice since there is a very limited sampling of measured differences between sets. Such a limited sampling results in a s_b^2 estimate that is quite uncertain. The use of many sets of measurements is recommended since this results in greater stability of the estimates.

6. Calculation of the Standard Error of the Weighted Average

All practical applications of the weighted average will require some estimate of its uncertainty. Accordingly, the standard error (standard deviation) of the weighted average should be calculated. The derivation of the standard error of $\tilde{Y}$ is straightforward if one considers the final ω_i estimates as constants.

$$\tilde{Y} = \frac{\sum_i \omega_i \bar{Y}_i}{\sum_i \omega_i}$$

and

$$\mathrm{Var}(\tilde{Y}) = \frac{\sum_i \omega_i^2 \mathrm{Var}(\bar{Y}_i)}{(\sum_i \omega_i)^2} = \frac{\sum_i \omega_i^2 (1/\omega_i)}{(\sum_i \omega_i)^2} = \frac{1}{\sum_i \omega_i}$$

The sample estimate of the standard error of $\tilde{Y}$ is easily obtained from the final iteration of $\tilde{Y}$. It is simply the inverse of the square root of the sum of the weights. Note that the latter quantity has already been calculated as the denominator of $\tilde{Y}$.

$$\text{Standard Error} = \frac{1}{\sqrt{\sum_i \omega_i}}$$

The standard error is reduced by the use of a larger number of sets of measurements, i.e., by more ω_i.

The standard error associated with the $\tilde{Y} = 209.04$ from our previously worked example is calculated as follows:

$$\text{Standard Error} = \frac{1}{\sqrt{(.0238+112.7120)^{-1}+(.0625+112.7120)^{-1}}} = 7.51$$

This value is seen to be quite reasonable when one remembers that the uncoded group averages for methods A and B were 201.53 and 216.55. Notice in this example that the between set component of variance is the predominant factor in the standard error.

7. Example of an Interlaboratory Experiment Using the Weighted Average

Five laboratories have made a number of determinations for the heat of vaporization of cadmium [5]. In this experiment, each laboratory had a noticeably different replication precision, and each performed a different number of determinations to obtain its average value. We now wish to determine the consensus value (weighted average) from this interlaboratory experiment. The information from the experiment is listed below, along with the s_b^2 calculated by the iterative procedure.

Lab i	Avg. Value	n_i	$s_{w_i}^2/n_i$	s_b^2
1	27,044	6	3	
2	26,022	4	76	
3	26,340	2	464 $\times 10^3$	105×10^3
4	26,787	2	3	
5	26,796	4	14	

In the process of examining the data, the following three averages were calculated.

Average of averages	26,598
Average of individual measurements	26,655
Iterative weighted average	26,713

One notes that the iterative weighted average does not fall between the other two averages. How can this happen? Basically, it is caused by the recognition of the individual within group variances in the weights for the iterative weighted average. To better understand the three averaging processes, let us order the laboratory heat values and include the three sets of "weights" that were used for the averages.

	Weights For Avg. of				
Ordered Avg. Values	Avg. of Averages	Measurements	Iterative Procedure	$s_{w_i}^2/n_i$	s_b^2
26,022	1	4	5.5	76	
26,340	1	2	1.8	464	
26,787	1	2	9.3 $\times 10^{-6}$	3 $\times 10^3$	105×10^3
26,796	1	4	8.5	14	
27,044	1	6	9.3	3	

Note that the second and third columns contain relative weights while the fourth column contains absolute weights. The relative weights cause no problem for the calculation of the weighted average since inspection of eq (1) shows that any constant multiplier for the relative weights will cancel out. An inspection of the three columns of weights, as well as the ordered laboratory heat values, shows that the weights for the iterative procedure most strongly favor the higher laboratory heat values. Column five of the table, in turn, shows why the iterative weights most strongly favor the higher laboratory heat values; the observed within group variability is smaller for the laboratories that have the higher heat values. This causes the $\mathrm{Var}(\overline{Y_i})$ for these laboratories to be relatively small and the weights to be relatively large.

This example with actual laboratory data shows that one cannot automatically assume that the average of averages and the average of measurements will bracket the consensus value (weighted average). The weighted average should be calculated. It is more sensitive to the overall experiment and it responds to both the within- and the between group variability.

It will next be shown that the iterative treatment of weighting factors can be easily extended to the problem of fitting lines by weighted least squares (regression).

8. Fitting Lines by Weighted Least Squares

According to statistical theory, the above defined estimate of the weighted average is the value that minimizes the sum of the weighted squared deviations of the observed data (from the weighted average value). It is a least squares estimate. A similar treatment is used in weighted linear regression. Here, a pair of parameters, namely the intercept and the slope of the line, are estimated, rather than a single average. The procedure, however, is again the minimization of the weighted sum of squares of deviations. Here, too, both within set and between set components of variance should be evaluated.

Consider the situation where a laboratory calibrates an instrument using a series of standards. The laboratory may not always make the same number of replicate measurements with the different standards. Thus there are different sets of replicate instrument measurements (Y) corresponding to a series of accurately determined standard values (X). An example of a linear calibration process is given in figure 1. Let us assume that the linearity of the calibration curve has previously been established. An examination of the figure shows that the variability in the Y direction among replicates obtained at the same X value is relatively small when compared with the scatter of the clusters of points about the straight line. Thus, two sources of variability are suggested by the data. The Y replication variability associated with a given X value is analogous to the previously described within set component of variance, $s^2_{w_i}$, and the variation shown by the scatter of the clusters of points about the fitted line is analogous to the between set components of variance, s^2_b.

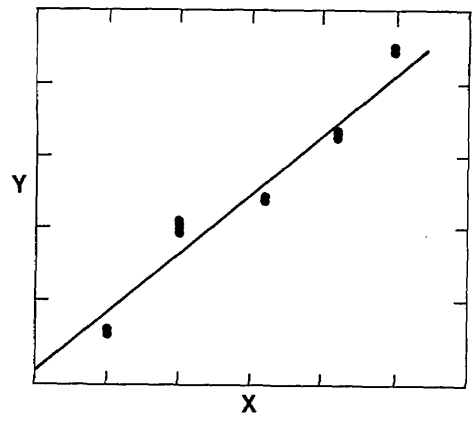

Figure 1

The observed variance for the j-th replicate Y_{ij} measurement made at a given X_i value will consist of the sum of the within- and the between set components of variance.

$$s^2(Y_{ij}) = s^2_{w_i} + s^2_b$$

For convenience of calculation, it is desirable to deal with the averages of the replicate measurements. The average of n_i replicate measurements is denoted as $\overline{Y_i}$. The observed variances for the averages are given by:

$$s^2(\overline{Y_i}) = \frac{s^2_{w_i}}{n_i} + s^2_b$$

The within set variances of the above equation can be evaluated for each distinct X_i value. It is possible, if there is a consistent measurement process over the full range of values, to obtain a pooled estimate of the within set component of variance. This pooled estimate is obtained in the same manner as described by eq (2), above. In the current application, the different X_i values correspond to the previously described different measurement sets and there are now as many summations in the numerator and denominator of eq (2) as there are distinct X_i values.

Let us now assume that an appropriate between set component of variance is available. The weights, $\omega_i =$

$1/\mathrm{Var}(\overline{Y}_i)$ can be evaluated, and a standard weighted linear regression of $\overline{Y}_i$ on X_i can be carried out (see either the Appendix, or Ref. [6]). Thus, the regression problem using weighted least squares centers on the determination of s_b^2.

The s_b^2 value, for the regression case with an intercept and slope, can be determined by the general iterative approach given above. Equation (3) now refers to the within- and between set random errors in the Y measurements. It is now used along with the following modified iteration equations:

$$F(s_b^2) = \sum_{i=1}^{m} \omega_i(\overline{Y}_i - \hat{Y}_i)^2 - (m-2) \tag{8}$$

$$ds_b^2 = \frac{\mathrm{Fo}}{\left[\sum_{i=1}^{m} \omega_i^2 (\overline{Y}_i - \hat{Y}_i)^2\right]_o} \tag{9}$$

where

$\hat{Y}_i$ = weighted least squares fitted value, i.e.,

$\hat{Y}_i = a + bX_i$

The major modification is that instead of using $\tilde{Y}$, we use a weighted least squares fitted value $\hat{Y}_i$. Equation (8) uses $(m\text{-}2)$ rather than $(m\text{-}1)$ degrees of freedom since we are now estimating two parameters, i.e., the intercept and the slope.

The procedure for iteration is little changed. An arbitrary initial estimate for s_b^2 is taken and used with (3) to obtain the weights. Next, a weighted linear regression is made of $\overline{Y}_i$ on X_i to obtain estimates a, b, and $\hat{Y}_i$. This is followed by the use of eq (8) and (9) to calculate a correction for s_b^2. The whole procedure is then repeated until the correction for s_b^2 is negligible. The final s_b^2, a, b, and $\hat{Y}_i$ are then saved for further interpretation and use.

The above procedure for performing a weighted linear least squares fit can be easily extended to a weighted quadratic, or higher order, regression of $\overline{Y}_i$ on X_i. For example, to fit the equation $Y_i = a + bX_i + cX_i^2$ change, in equation (8), the $(m\text{-}2)$ to $(m\text{-}3)$ to account for the addition of coefficient c, and use a quadratic fitted $\hat{Y}_i$ in eq (8) and (9).

9. An Example of a Weighted Least Squares Fit

Let us examine the effect of different weighting factors on the determination of the intercept and slope of a calibration line. A greatly simplified example is shown in figure 2. The true line has both unit intercept and slope. For this example, let us assume that "interferences" for the $X = 1$ and the $X = 5$ standard samples are such that the measured values will be about 0.2 units high. Similarly, the $X = 2$ and $X = 4$ standards yield results that are about 0.2 units low. Duplicate measurements are made, and for simplicity assume that these measurements have a fixed s_w^2 value of 0.0008 (as shown in fig. 2). With equal numbers of replicate measurements, both the unweighted and the iterative weighted regression calculations give the correct values for the intercept and the slope.

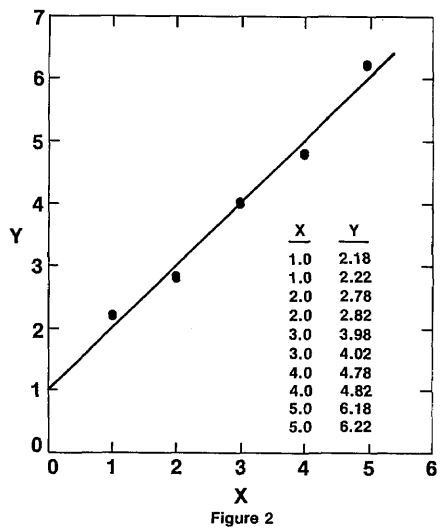

Figure 2

Let us now, however, say that the experimenter is particularly interested in determining the intercept and that he/she therefore makes six rather than two replicate measurements using the X = 1 standard. For the sake of simplicity, assume that the six Y measurements again center at 2.2 and that $s_w^2 = .0008$. Even though everything looks nominally the same, the unweighted regression calculation gives an intercept of 1.145 and a slope of 0.9636. Obviously, the six points at X = 1 have pulled the left side of the line upward. If we carried out the regression calculation using only the average Y value for each X value we would obtain the correct intercept and slope values. The average Y values are not affected by the number of measurements used in each average.

In this example, in which appreciably more measurements were made for one standard than for the others, and the replication error was relatively small, the

unweighted regression leads to erroneous results. A proper weighting procedure must prevent the measurements at one standard from unduly influencing the fit. Equation (3) of our iterative weighted regression calculations will properly control the weighting. In this example, the s_b^2 term in eq (3) dominates the weighting. Use of the iterative weighted linear regression gives $a = 1.0008$ and $b = 0.9998$. If the data from this example were real laboratory data, then our calculated a and b would be the appropriate sample estimates.

10. Design of Experiments

The interferences associated with the five standards of the above illustrative example have been ideally and artificially balanced. In real life situations the order in which the interferences will occur will tend to be more random. When the replication error is small, i.e., s_w^2 is small relative to s_b^2, the positions of the (X_i, Y_i) points will be mainly affected by these random sample interferences. In that case, the use of a larger number of standards over the range of measurement interest is recommended since this favors a more even distribution of these interferences, and a more accurate determination of the line. Furthermore when s_w^2 is small relative to s_b^2, the use of large numbers of *replicate* measurements is not recommended since these measurements are very inefficient in determining the position of the (X_i, Y_i) points.

Consider next the situation shown in figure 3, where s_w^2 is large relative to s_b^2. Here all of the average points (X_i, Y_i) are very uncertain. The interferences of each standard sample is now completely overshadowed by the variability in the replicate measurements. For this situation one should make many replicate measurements with all of the standard samples so as to minimize the replication uncertainty.

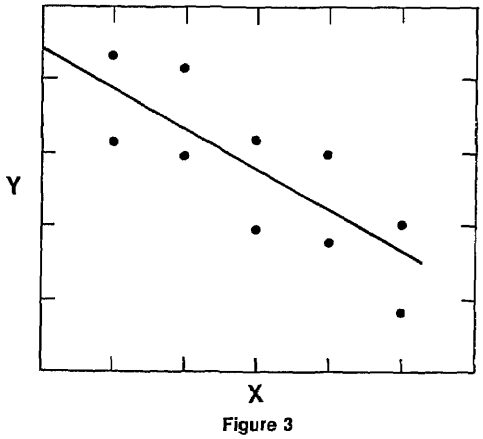

Figure 3

11. Summary and Conclusions

Calculation of consensus values, both in the form of the weighted average or the weighted least squares regression, requires a knowledge of the within- and the between set components of variance. The individual or the pooled within set components of variance can be directly calculated from the experimental data. The between set component of variance can conveniently be calculated from the experimental data using an iterative technique which is based on a truncated Taylor series expansion. Consensus value(s) are also obtained by this iterative technique.

A simple intuitive understanding of the within- and between set components of variance allows one to more efficiently design experiments for obtaining consensus values.

The logical arguments for use of the within- and between set components of variance can be extended to other areas of statistical analysis. Work is in progress for extending the current techniques to nested analyses of variance.

12. References

[1] Birge, R. T., The Calculation of Errors by the Method of Least Squares, Phys. Rev., **40**, 207–227 (1932).

[2] Mandel, J. and Paule, R. C., Interlaboratory Evaluation of a Material with Unequal Numbers of Replicates, Anal. Chem., **42**, 1194-7 (1970), and Correction, Anal. Chem., 43, 1287 (1971).

[3] Cochran, W. G., The Combination of Estimates from Different Experiments, Biometrics, 10, 101-29 (1954).

[4] Youden, W. J., Enduring Values, Technometrics, **14**, 1-11 (1972).

[5] Paule, R. C. and Mandel, J., Analysis of Interlaboratory Measurements on the Vapor Pressure of Cadmium and Silver, NBS Special Publication 260-21 (1971).

[6] Draper, N. R. and Smith, H., *Applied Regression Analysis*, 2nd ed., Section 2.11 (John Wiley and Sons, N.Y., 1981).

Appendix

The formulas for estimating the slope and intercept by weighted least squares are straightforward. The slope is calculated from the observed m sets of (X_i, Y_i) points.

$$b = \frac{\sum_{i=1}^{m} \omega_i (X_i - \tilde{X})(\bar{Y}_i - \tilde{Y})}{\sum_{i=1}^{m} \omega_i (X_i - \tilde{X})^2}$$

where

$$\tilde{X} = \frac{\sum_{i=1}^{m} \omega_i X_i}{\sum_{i=1}^{m} \omega_i}$$

and

$$\tilde{Y} = \frac{\sum_{i=1}^{m} \omega_i \bar{Y}_i}{\sum_{i=1}^{m} \omega_i}$$

The intercept is obtained by the following formula.

$$a = \tilde{Y} - b\tilde{X}$$

The interested reader may also wish to calculate the standard errors of the above estimates of the slope and the intercept, the formulas are:

$$s_b = \sqrt{\frac{1}{\sum_{i=1}^{m} \omega_i (X_i - \tilde{X})^2}}$$

$$s_a = \sqrt{\frac{\sum_{i=1}^{m} \omega_i X_i^2}{\left[\sum_{i=1}^{m} \omega_i\right]\left[\sum_{i=1}^{m} \omega_i (X_i - \tilde{X})^2\right]}}$$

A more detailed explanation of weighted least squares fitting processes is contained in Ref. [6].

JOURNAL OF RESEARCH of the National Bureau of Standards
Vol. 87, No. 5, September–October 1982

Report on the Sixth International Symposium on Temperature

B. W. Mangum* and G. T. Furukawa*

National Bureau of Standards, Washington, DC 20234

July 6, 1982

This is a report on the Sixth International Symposium of Temperature which was held in Washington, DC, USA, March 15–18, 1982. Included is a brief introduction discussing the timeliness of the symposium, its sponsors, and the publication of the proceedings. The remainder of the report is devoted to a summary of the Plenary and Technical sessions of the symposium.

Key words: fixed points, temperature scale; thermometers; thermometry; symposium.

I. Introduction

The Sixth International Symposium on Temperature was held in Washington, DC, March 15–18, 1982. The *five preceding symposia on Temperature* were in 1971, 1961, 1954, 1939, and 1919. The symposium in 1919 was held in Chicago and called the Symposium on Pyrometry. The symposia in 1939 and in 1954 were held in New York City and in Washington, DC, respectively; the fourth symposium was held in Columbus, Ohio in 1961; the fifth symposium was held in Washington, DC in 1971. Except for the Symposium on Pyrometry, the proceedings of these symposia have been published under the title *Temperature: Its Measurement and Control in Science and Industry*.

The sixth symposium was co-sponsored by the American Institute of Physics, the Instrument Society of America, and the National Bureau of Standards (NBS).

This symposium was held at a propitious time, coming just prior to the meeting of the Comité Consultatif de Thermométrie (CCT) on 30 March to 1 April 1982, during which that body deliberated on possible improvements in and extension of the International Practical Temperature Scale of 1968 (IPTS-68), deliberations which may lead to a new Scale in 1987. The symposium provided a forum for discussion of new developments in thermometry, as well as for reviews of the current situation. It brought to a focus the current research and results of many efforts in thermometry and revealed the areas where more work is needed, as well as areas which are now well in hand. Concomitantly, various problems with the IPTS-68 (non-agreement with thermodynamic temperatures, extension of the temperature range, adequacy of defining fixed points, standard interpolating instruments, etc.) were addressed which should assist the members of the CCT in devising a new and more comprehensive scale. Considering the enormous amount of work in thermometry, it is not surprising that there were some duplications at the symposium. Certain duplications are desirable, of course.

There were approximately 1200 registrants from 20 countries at the symposium and the exhibits, with about 480 symposium attendees. This was the first temperature symposium at which there were commercial exhibits of temperature equipment. Three hundred persons attended just to see the exhibits, approximately 90 in number.

The principal areas of thermometry covered at the symposium were: thermodynamic temperature measurements and temperature scales, temperature fixed points, spectroscopic (rotational, vibrational, NMR) and radiation thermometry, electronic thermometry, vapor pressure thermometry, resistance thermometry, thermocouple thermometry, medical thermometry, instrumentation, automation, and calibration.

II. The Proceedings

The papers presented at the symposium are scheduled for publication in September 1982 in *Temperature: Its Measurement and Control in Science and Industry* (American Institute of Physics, New York, 1982), Vol. 5. The editor of that publication is James F. Schooley of NBS, who was also the program chairman.

III. The Plenary and Technical Sessions

A. Plenary Session

At the Plenary session, the conference was opened by the conference's General Chairman, Lawrence G.

*Center for Absolute Physical Quantities, National Measurement Laboratory.

Rubin, of the National Magnet Laboratory, MIT, USA, who, in his brief introductory remarks, welcomed the attendees and wished them a fruitful meeting. He then introduced H. Preston-Thomas, of the National Research Council (NRC), Ottawa, Canada, who, in turn, introduced the keynote speaker, Ralph P. Hudson, of the International Bureau of Weights and Measures (BIPM), Sevres, France. Hudson's address was entitled, "Temperature Scales, the IPTS, and its Future Development."

In his remarks, Hudson gave a brief review of the basic concepts of internationally-agree-upon temperature scales, of events leading to the International Practical Temperature Scales (IPTS), and of the practical considerations which influence their construction and use. He mentioned some semi-official scales which are widely used in certain temperature ranges and discussed in detail the IPTS-68, the latest version of the IPTS, and its presently-perceived deficiencies. He indicated some of the ways in which the IPTS-68 could possibly be improved and extended in the near future, in the form of a new scale going to temperatures substantially lower than that of the IPTS-68. Some new primary thermometry data and instrumentation which will probably form the basis for constructing that revised scale were reviewed. The advantages and disadvantages of the prescribed standard instruments of the IPTS-68, including their temperature regions of use, were also discussed; some likely candidates for interpolation instruments for the revised scale and their possible ranges of utility were described in some detail. The desirability of removing the standard thermocouple from any future scale definition was documented. In his concluding remarks, the speaker briefly addressed the relationship between state-of-the-art metrology and the requirements of science and industry and some of the possible consequences of revising the scale.

Throughout his talk, Hudson pointed out some specific papers to be presented at the symposium which concerned thermodynamic temperature measurements and/or temperature scale work which he considered to be particularly timely and relevant to discussions of a new scale. The subject of the keynote address was itself very timely in that it put the various aspects of temperature scales in their proper perspective. This talk thus set the stage for the entire symposium.

B. Technical Sessions

Immediately following the keynote address, the technical sessions convened. There were 181 technical papers presented at the symposium, distributed among 33 technical sessions, three or four parallel sessions at a time. In addition, two afternoon sessions were devoted entirely to approximately 15 Manufacturer's Application Papers, and manufacturers' exhibits were open three afternoons for the benefit of the participants. In order to get comments from the symposium participants concerning temperature scales, the CCT held an open meeting on the last afternoon of the symposium.

A brief summary of the work reported at the technical sessions follows.

1. Fundamental Thermometry and Temperature Scales

Although direct and simple methods for accurate realization of thermodynamic temperatures remain about as elusive as ever, the review of the measurement of thermodynamic temperature by L.A. Guildner (NBS, USA) et el. showed that remarkable improvements in every technique have occurred in the eleven-year period since the fifth symposium. While gas thermometry retained superiority in accuracy except at the extremes of temperature, measurements by noise thermometry, acoustic thermometry, total- and spectral-radiation thermometry, and dielectric constant gas thermometry have reached a sufficiently high level of reliability to either stand by themselves or to improve our confidence in gas thermometer results.

H. Marshak (NBS, USA) presented details of work on thermodynamic thermometry using gamma-ray anisotropy. This method permits thermodynamic temperature measurement by the only technique currently feasible in the very lowest range, potentially from a few microkelvins to about 1 K, with an uncertainty of no more than a few percent. Marshak reported that results of noise-thermometer measurements agreed with his ^{60}Co gamma-ray anisotropy results to within 0.5% in the temperature range from 0.01 to 0.05 K.

The gas thermometry which sets the standard for thermodynamic temperatures from 2.6 to 27.1 K was performed at the National Physical Laboratory (NPL), UK, by K. H. Berry. He summarized that work and compared the resulting practical scale, NPL-75, with the IPTS-68, T_{58} (^4He vapor pressure scale), and T_{XISU} (the Iowa State Magnetic scale). Berry's work has been confirmed by other measurements, some of which were presented at the symposium.

D. Gugan, et al. (Bristol Univ., UK) discussed dielectric constant gas thermometry (DCGT) which, while nominally gas thermometry, depends on the change of the dielectric constant with gas density and, thus, is intensive in nature, in contrast to the extensive quality of regular gas thermometry. This method appears unusually attractive for its simplicity and high accuracy. With this very different approach, Gugan reported values

within 0.3 mK of Berry's results over the range from 4.2 to 27 K.

Gugan also discussed a re-analysis of his DCGT isotherm data and of Berry's constant volume gas thermometry (CVGT) isotherm results using a procedure known as surface-fitting. This is a procedure in which all the data from the isotherms are combined and then the isotherm temperatures and the functional forms of the virial coefficients are determined simultaneously from a single, weighted, least-squares fit. He substantiated the accuracy and smoothness of NPL-75 but the re-analysis suggests that the values assigned to Berry's isotherm temperatures need corrections of a few tenths of a millikelvin. The re-analysis also showed that DCGT is a good technique, that it is rather insensitive to details of analysis, and that its internal consistency is easy to examine. This fitting technique also showed the necessity of using the third virial coefficient for proper analysis of CVGT data.

Measurements by acoustic thermometry have been made at the NPL, UK, in the low-temperature range by A. R. Colclough. He summarized the theory and practice of acoustic thermometry, which as executed by him yielded results agreeing with Berry's values to within 1 mK over the range from 4.2 to 20.27 K. The one exception was a difference of 2.2 mK at 17 K.

The CVGT effort at the CSIRO National Measurement Laboratory (NML), Australia, was reported by W. R. G. Kemp et al., and that at the Kamerlingh Onnes Laboratory (KOL), the Netherlands, by P. P. M. Steur et al. Both of these groups of researchers used reference temperatures from NPL-75 and their results showed excellent consistency with the NPL results, from 13.8 to 27.1 K at the NML and from 4 to 27 K at the KOL.

Work is in progress to determine thermodynamic values by CVGT at higher temperatures. The KOL apparatus was designed for measurements up to 100 K, and initial values up to 40 K were reported at the symposium. A constant volume gas thermometer has been built also at the National Research Laboratory of Metrology (NRLM), Japan. Using this CVGT, H. Sakurai reported preliminary measurements of the temperature of the triple point of oxygen.

H. H. Plumb (NBS, USA) presented results of analyses of acoustical isotherms at temperatures from 9 to 34 K. He has obtained values for the ^{4}He second and third virial coefficients and they are $B=16.8925 - 383.095/T - 150.665/T^2$ (cm^3/mol) and $C=5788/T$ cm^6mol^{-2}, respectively. Plumb compared his measured isotherm slopes (i.e., the term linear in pressure) with those calculated from the second virial coefficients determined in other, non-acoustical experiments. He concluded that the close agreement of those slopes indicates the inadequacy of the generally-accepted Helmholtz-Kirchhoff correction, and that it is not applicable, in its predicted entirety, to the acoustical isotherm data that have been measured in the NBS acoustical thermometer.

A. R. Colclough described the refractive index thermometer that has been built and tested at the NPL, UK. He showed that the accuracy to be expected from this method should be comparable to that obtained from other methods.

M. R. Moldover (NBS, USA) et al. discussed the application of spherical resonators to the determination of the speed of sound of a gas such as argon at the zero pressure limit with estimated internal inconsistencies of $\pm 3 \times 10^{-6}$. He discussed the application of this technique for the determination of thermodynamic temperatures.

Preparations to extend the CVGT measurements at the NBS, USA, beyond the currently-reported range from 0 to 457 °C were described by L. A. Guildner et al. Current activities are focused on measuring temperature values between 500 and 800 °C, with an ultimate objective of measuring the thermodynamic temperature of the gold point.

R. A. Kamper (NBS Boulder, USA), in a paper entitled "Survey of Noise Thermometry" presented at the fifth temperature symposium in 1971 concluded, "Noise thermometry is and will remain a difficult and frustrating art." At that symposium there was only one other paper on noise thermometry, "Methods of Noise Thermometry above 400 °C," which was presented by A. Actis et al. (IMGC, Italy). At the sixth temperature symposium, ten papers on Johnson-noise thermometry were presented in two sessions by authors from six countries: Australia, Belgium, Italy, Japan, United States, and West Germany. Those papers covered the temperature range from 0.01 to beyond 1900 K. In a session on thermodynamic noise thermometry, R. J. Soulen et al. (NBS, USA) reported measurements of Johnson noise with Josephson junctions to determine temperatures in the range from 0.01 to 0.52 K with inaccuracies of ±0.5 to ±0.2%. G. Klempt (Univ. of Münster, FRG) measured liquid helium temperatures at 2.145 K with a total uncertainty of 0.3 mK. C. P. Pickup (CSIRO, Australia) measured a temperature of 135 °C with a standard deviation of 2.4 mK for a total integration time of 5.4×10^6 s and showed the IPTS-68 to be 12 mK too high. L. Crovini et al. (IMGC, Italy) measured temperatures in the range from 630 to 962 °C with a total uncertainty of 0.18 to 0.34 K with an integration time of up to 9600 s and showed differences from IPTS-68 of as much as 0.67 K at 850 °C.

Values of thermodynamic temperature at 327, 344, and 365 K were measured at the NPL, UK, by a total radiation thermometer. The results, reported by T. J.

Quinn et al., are in good agreement with the NBS gas thermometer measurements.

The accuracy of thermodynamic temperatures measured with spectral photoelectric pyrometers has improved rapidly and can be expected to be superior to the best gas thermometry at temperatures above the gold point. Results of new measurements at the CSIRO, Australia were reported by T. P. Jones et al. for the thermodynamic values of the freezing points of silver and copper, on the basis of the IPTS-68 value for the gold point. Similarly, M. Ohtsuka et al. reported results of measurements of the copper to silver interval by a monochromatic optical pyrometer at the NRC, Canada.

R. E. Bedford et al. (NRC, Canada) presented a paper on the measurement of the melting temperature of copper-71.9% silver eutectic, using a monochromatic optical pyrometer. The mean value for the melting temperature of the eutectic as determined from two eutectic ingots and from the freezing points of three silver ingots, was 1053.12 ± 0.10 K, relative to the silver point value of 1235.20 K.

P. B. Coates et al. (NPL, UK) reviewed the progress made at the NPL on the measurement of thermodynamic temperatures above the zinc point by photon-counting radiation pyrometry. The estimated total uncertainty of the method from the zinc point to the gold point was given as 50 mK. Measurements were recently obtained on Al, Ag, Cu, and Pd points. The preliminary value reported for the Pd point was 1555.3 ± 0.2 °C, based on the IPTS-68 value for the Au point. Preliminary results were given for the comparison of t_{68} and thermodynamic temperatures between 440 and 630 °C. Preliminary values for the Au and Ag points relative to the 630 °C reference temperature were also reported.

In view of the elaborate experimental techniques required to make accurate thermodynamic measurements, the need for a practical scale above 0.5 K, say, remains as great as ever. As mentioned earlier, a revision of the International Practical Scale is in the offing and, this being the case, the work at the KOL to improve the helium vapor pressure equations, reported by M. Durieux et al., is particularly timely. Also, the work at the CSIRO, reported by R. C. Kemp, refines the interpolating techniques first put forward by C. G. M. Kirby (NRC), and establishes a combination of choice of fixed points, form of equation and derivation of constants that reduces the non-uniqueness (variation of corresponding values given by different standard platinum resistance thermometers (SPRTs)) to a nearly uniform 0.2 mK over the range from 13.8 K to 273 K. These should be very helpful in the deliberations of the CCT.

About 30 papers dealt with the realization of fixed or reference points, distributed throughout the temperature range from the superconductive transition point of W at about 0.015 K to the melting point of Ta at 3258 K.

For several years, the Office of Standard Reference Materials of the NBS (USA) has issued two superconductive fixed point devices, SRM 767, containing Pb, In, Al, Zn, and Cd, and SRM 768, containing $AuIn_2$, $AuAl_2$, Ir, Be, and W. To date, about 100 SRM 767 and 50 SRM 768 devices have been issued. J. F. Schooley et al. (NBS, USA) reviewed the progress made with superconductive transition points and discussed the reproducibilities of prototypes of SRM 767 and SRM 768 devices that were issued. For 22 SRM 767 devices tested, Pb, In, Al, Zn, and Cd with transition temperatures (T_c) at about 7.20, 3.41, 1.18, 0.85, and 0.52 K, respectively, showed standard deviations of 0.2, 0.2, 0.4, 0.4, and 0.3 mK, respectively. For the five SRM 768 devices tested, with T_c of the specimens ranging between 0.015 and 0.2 K, the T_c among samples showed measurable differences which were attributed principally to ferromagnetic impurities. Consequently, each device was calibrated against the NBS-CTS-1 and given individual T_c values which were reproducible at the level of from 0.1 mK to 0.2 mK.

Temperature values of the superconductive transition points of Pb, In, Al, Zn, and Cd of SRM 767 have been assigned on the 1976 Provisional 0.5 K to 30 K Temperature Scale (EPT-76) and, hence, the device provides 5 of the 11 reference points of that scale. A. E. El-Samahy (KOL, the Netherlands) et al. discussed how the transitions compared in eight different devices, three each at KOL and NPL and two at NML. The results at the KOL and NPL were correlated through common temperature scales, the NPL-75 and the T_{X1}; the results at NML, obtained on the T_{XISU} Scale, made the comparison slightly less certain, however. The spreads in the transitions for the six devices at KOL and NPL were 1.1, 0.4, 0.6, 1.5, and 0.7 mK for Pb, In, Al, Zn, and Cd, respectively. If the two devices at the NML were included, the spreads increased to 1.7, 0.5, and 0.9 mK for Pb, In, and Al, respectively. Since single crystals of superconductive materials have been found to have sharper transitions than those of the polycrystalline materials, a suggestion was made to circulate an SRM 767 device with single crystals for comparison.

In 1978 the CCT initiated a program for international intercomparison of fixed points by means of sealed cells. F. Pavese (IMGC, Italy) summarized the results of the intercomparison of the triple points of Ar, 0_2, e-H_2,

CH_4, N_2, Ne, and e-D_2. Eleven laboratories were involved, with varying degrees of participation, and eight or nine different cell designs were compared. The number of cells of each gas that was tested varied. The results obtained with Ar were the best, with an rms difference of ±0.1 mK. Oxygen cells showed some systematic differences that require further analysis and measurements; the cells with best agreement are within ±0.2 mK. Methane measurements agreed to within ±0.3 mK; measurements repeated later, however, showed shifts larger than this value. Neon cells showed a small systematic difference that ranged from about ±0.2 to ±0.4 mK. The question was raised as to whether the difference could be attributed to variations in the isotopic composition of the samples. More measurements or further analyses are required on the e-H_2, e-D_2, and N_2 cells.

A number of reports concerned investigations of triple points of cryogenic substances (sealed in miniature pressure cells) using adiabatic cryostat techniques. Also, some triple-point measurements, obtained by using a condensation-type cryostat, were reported. Both techniques involve the measurements of equilibrium melting points at known increasing amounts of sample melted. The range of the melting points becomes narrower as the purity of the samples increases. The triple point may be taken as the average over a selected range of sample melted (F), as the extrapolated value at $F=1$, or as the extrapolated value at $1/F=0$. The latter value assumes that the system follows the ideal solution law, that the observations are at equilibrium, and that the impurities remain in the liquid or that the distribution coefficient of the impurities in the liquid and solid solutions can be obtained.

G. Bonnier et al. (INM, France) discussed the results of investigations of the thermal behavior of sealed cells of different shapes. A cell with compartments for five different gases, which has been used successfully in triple-point measurements, was described.

F. Pavese et al. (IMGC, Italy) reviewed the developments made at IMGC in 10 years of research on the triple points of sealed cells, having filled about 50 cells with a dozen different substances during that time. The cells that have been built were chiefly narrow cylinders which could be readily inserted into a top-loading, adiabatic cryostat. Gases that were investigated include Ar, 0_2, CH_4, Ne, C_2H_6, and others.

G. T. Furukawa (NBS, USA) discussed the results of a comparison of the triple points of six sealed cells of argon, of which three were NBS cells (each of a different design) and one each was from IMGC, NRC, and NRLM. Six SPRTs were used in the study. The results of these six cells agreed to within ±0.1 mK. The average triple-point value for the three NBS cells, obtained with five SPRTs, was reported to be 83.8003 K (S.D.= 0.017 mK) on the NBS-IPTS-68 or 83.7970 K on the NPL-IPTS-68. The results obtained with all six SPRTs showed that their calibrations were consistent to well within the reproducibility of the argon triple point.

W. R. G. Kemp (CSIRO, Australia) reported the triple-point temperature of e-D_2 to be 18.6909 K and that of n-D_2 to be 18.709 ± 0.001 K. These values were obtained from melting-point measurements using a condensation-type adiabatic cryostat. For the e-D_2 measurements, hydrous ferric oxide was placed in the sample vessel to aid conversion of the D_2; the melting range was 0.2 mK and the reproducibility was ±0.1 mK. Nominal purity of the sample was 99.5 percent. Further measurements obtained after purification of the sample gave results which were the same as the original results. For the n-D_2 measurements, the sample chamber contained no catalyst. The melting range in this case was not as small as that obtained with the e-D_2, possibly due to some conversion from the para to the ortho state. From another experiment using the same adiabatic cryostat and method, W. R. G. Kemp et al. (CSIRO, Australia) reported the triple-point temperature of Xe to be 161.388 ± 0.001 K. The relatively broader range of melting points found for Xe was attributed to its being a mixture of isotopes.

There were three papers on the triple point of water. G. T. Furukawa et al. (NBS, USA) reported standard deviations of 8 μK for measurements conducted over 4 or 5 days, testing before each measurement that the ice mantle was free to move on a slight tilting of the cell. (The well-known rotational impulse test may not assure the mantle to be free from slight sticking to the thermometer well.) High quality cells should be essentially free of air; a residual air pressure of 130 Pa causes about 0.01 mK lowering of the triple point. Of the 21 cells that were compared, 3 cells which increased the spread of the triple points from 0.05 to nearly 0.2 mK were considered substandard. J. Ancsin (NRC, Canada) presented results on the melting curves of water at the triple point and at one-atmosphere pressure of air, 0_2, He, Ar, CH_4, Kr, Xe, and CO_2 in sealed cells. A linear relation was obtained between the liquidus points of the ice and the solubility of the above substances. The results showed that a pressure of one atmosphere lowers the melting point by 7.3 mK. J. V. McAllan (CSIRO, Australia) reported that a pressure of one atmosphere of air lowers the melting point by 7.474 ±0.01 mK and that the difference between the air-saturated ice point and the triple point is 9.85 ± 0.1 mK.

Three papers concerned with the triple point of gallium were presented. B. W. Mangum (NBS, USA) discussed triple-point measurements of 10 Ga cells prepared using samples from three sources. Three of the cells were all plastic, while the other seven cells were stainless steel coated with Teflon wherever Ga was in contact. The triple points of the three all-plastic cells were found to be within a band of 0.04 mK; when the seven stainless steel cells were included, the band widened to 0.23 mK. The lower values obtained for the steel cells were attributed to contamination by the steel through pin holes in the Teflon. The average Ga triple-point temperature obtained with five SPRTs on the sample of highest purity in an all-plastic cell was given as 29.77398 ± 0.00014 °C.

M. V. Chattle (NPL, UK) et al. presented results of the comparison measurements obtained at three laboratories (NPL, INM, and IMGC) on the triple points and melting points of three Ga cells, one furnished by each of the laboratories. The Ga samples in the NPL and INM cells were 99.9999 percent pure, while the sample in the IMGC was 99.99999 percent pure. Two SPRTs were used at each of the laboratories, one SPRT calibrated at the NPL and the other locally calibrated. The overall average temperature of each cell, as determined by the three laboratories, agreed to within 0.19 mK. The IMGC cell, with the purer sample, tended to give higher values. The average triple-point temperature of the three cells was found to be 29.77373 °C; the freezing point was on the average 1.98 mK lower. lower.

B. N. Oleinik et al. (Mendeleyev Res. Inst. Metrol., USSR) submitted a paper on the realization of the melting point of approximately 99.997 percent pure gallium. The melting-point temperature obtained using three SPRTs, was 29.7704 ± 0.0004 °C (or 29.7724 °C for the triple point).

Several papers were presented on fixed points suitable for biomedical applications. J. D. Cox et al. (NPL, UK) described different techniques for realizing the triple points of water, phenoxybenzene, 1,3-dioxolan-2-one, and n-icosane in which they obtained standard deviations of the means of 0.2, 0.2, 0.5, and 0.5 mK, respectively. The "outer solid-sheath method" with sample solidified on the outer cell walls was preferred for realizing the triple point, instead of solidifying the sample around the thermometer well and then obtaining an "inner melt".

M. E. Glicksman (Rensselaer Polytechnic Institute, USA) et al. described a technique for zone-refining succinonitrile to a purity estimated to be at lease 99.9996 percent. The measurements of its triple-point temperature were shown to be reproducible to ±0.1 mK. The triple-point value reported was 58.0805 ± 0.004 °C.

J. M. Figueroa et al. (NBS, USA) presented a paper on measurements of the triple point of Rb. A calibrated bead-type thermistor was used for freezing and melting experiments of six cells containing nominally 99.9 percent pure Rb. The value 39.265 ± 0.014 °C was reported for the Rb triple point. Freezing points of any given cell were found to be reproducible to ± 0.003 °C.

S. Sawada (NRLM, Japan) reported results of measurements of the triple-point temperature of In sealed in glass. Three samples of In ranging in purity from 99.999 to 99.9999% were investigated. From the measurements with three SPRTs, the triple-point value of 156.6296 ± 0.0003 °C was obtained. In another paper, M. Hanafy (NIS, Egypt) et al. discussed melting-point measurements obtained with minature In cells containing about 70 g of In. The melting-point temperature obtained by using calibrated thermistors was reported to be 156.65 ± 0.02 °C.

There were two Cd point papers. G. T. Furukawa et al. (NBS, USA) reported results of freezing-point measurements of five Cd cells prepared from two sample sources. They reported the cells to agree to within ± 0.1 mK and they found the average freezing-point temperature, obtained with eight newly-calibrated SPRTs, to be 321.1082 °C (S.D.= 0.1 m°C). The relatively broad range (0.9 m°C) of the results was attributed to the possible presence of excess moisture in some of the mica-insulated SPRTs. The Cd point was stated to be useful in checking the calibration of SPRTs on the IPTS-68 to within ± 0.5 mK and for detecting SPRTs of poor insulation resistance. J. V. McAllan et al. (CSIRO, Australia) presented results of monitoring the IPTS-68 calibrations of 43 thermometers of eight different designs at the Cd point, obtaining a value of 321.10814 °C (S.D.= 0.71 mK) for the Cd freezing point. The authors found good-quality industrial platinum resistance thermometers (PRTs) with a temperature coefficient of resistance of 0.00385 $°C^{-1}$ to give temperature values at the Cd point to within ± 1 mK of that determined with the IPTS standards.

J. V. McAllan (CSIRO, Australia) investigated the melting and freezing behavior of copper-71.9% silver eutectic and of sodium chloride, using a PRT. The standard deviation of the mean melting point (779.898 °C) of the eutectic was 0.009 °C; that of the freezing point (802.31 °C) was 0.02 °C.

Zhu Ci-Zhun (NIM, PRC) discussed the use of sealed freezing-point cells at high temperatures, sealed in order to avoid chemical contamination. Graphite crucibles containing the samples were sealed in fused-silica cells with an appropriate amount of Ar gas to give a pressure of 1 atm at the freezing point. Results showed the reproducibility of the plateau temperatures for Sb and Cu to be within 5 and 10 mK to 20 mK, respectively.

For optical pyrometry, blackbody cavities operate reliably near the gold point; above about 1800 K, however, the operation of blackbodies becomes more difficult. A. Cezairliyan (NBS, USA) reviewed the use of the radiance temperature of metals at their melting points (1800 to 3300 K) as possible high temperature reference points. For the measured radiance temperatures of Fe, Pd, Ti, Zr, V, Nb, Mo, and Ta, which range from about 1670 to 2846 K, the average deviation ranged from 0.3 K for Zr to 1.2 K for V. The need for additional work on the wavelength dependence of the radiance temperature was indicated.

The wire-bridge method for calibration of a thermocouple at the melting point of a metal, in which a short section of the pure metal joins the two legs of the thermocouple, is susceptible to errors from contamination of the metal by the thermocouple wires and permits only one measurement per "temperature sweep". M. Tischler et al. (INTI, Argentina) described a miniature graphite capsule sample holder of about 6 mm diameter and 12 mm length constructed with two external holes for insertion of thermocouple wires, suitable for repeated freezing- or melting-point calibrations of thermocouples. The graphite served to make the electrical contact between the wires. The inaccuracy of calibration obtained when using In, Sn, Cd, Pb, Zn, Sb, Al, Ag, Au, and Cu was estimated to be 0.2 or 0.3 K.

D. Rappaport (Galai Laboratories, Ltd., Israel) discussed a novel method for realizing secondary temperature reference points. These reference points utilize the first-order phase transitions in ferroelectric or ferromagnetic solids which, as a result of the non-linear and abrupt changes in loss mechanisms, self-stabilize at the reference temperature under applied voltage or magnetic field. He has constructed reference points over the range from 300 to 500 K, using the semiconductor/insulator phase transition in Nd-doped $BaTiO_3$. The devices are stable to 0.01 to 0.5 K, depending upon construction details, and are useful for thermocouple and infrared pyrometer calibration.

F. Sakuma et al. (NRLM, Japan) described the design of a set of blackbody fixed points of Cu, Ag, Al, Sb, and Zn for calibration of narrow-band radiation thermometers using silicon-photodiode detectors. Metal samples of about 26 cm^3 were contained in graphite crucibles. The estimated emissivity of the blackbody source was given as 0.999 ± 0.0005. The inaccuracy of realization of the blackbody fixed points was estimated to be ± 0.3 K.

3. Precision Platinum Resistance Thermometry

Five papers were presented on the subject of precision platinum resistance thermometry, with three of them devoted to the design of high temperature thermometers and the behavior of those thermometers when heated for long periods of time at 1000 °C and above.

R. J. Berry (NRC, Canada) presented results of studies of a reversible oxidation effect in PRTs operating in the temperature range from 0 to 630 °C. This effect is due to the formation and dissociation of a platinum oxide film on the surface of the Pt sensing element, which, he found, can cause changes in resistance ratios equivalent to as much as 24 mK. He outlined procedures for reducing temperature errors due to this effect in existing thermometers. Berry also discussed studies of the oxidation, stability, and insulation characteristics of Rosemount SPRTs.

H. J. Jung et al. (PTB, Berlin, FRG) reported results of a study of the stability of commercially-available high-temperature PRTs having a resistance of 5 Ω at 0 °C. The authors found that during a 500-hour exposure of four thermometers to 1000 °C, two of the thermometers indicated temperature values at the silver point that stayed within a range of 30 mK.

J. P. Evans (NBS, USA) discussed results obtained with some high temperature PRTs employing resistors of various designs, including the single layer bifilar helix design. Each thermometer had a resistance of 2.5 Ω at 0 °C. The thermometers proved to be satisfactory in some respects but deficient in others when they were exposed to 1100 °C for long periods. He also described a guarded-lead design that reduced the effects of electrical leakage when the thermometers were used at high temperatures.

Long Guang (Beijing Glass Res. Inst., PRC) et al. described precision high-temperature PRTs developed in China. The thermometer coil comprised a bifilar helix of 0.4 mm diameter Pt wire supported on a notched strip of quartz. The resistance of the thermometer at 0 °C is 0.25 Ω. Four such thermometers exposed to 1070 °C exhibited drift rates in R(0) which ranged from the equivalent of 0.5 to -4.2 mK per 100 hours at 1070 °C. Values of W(100) ranged from 1.392536 to 1.392776. The thermometers were reported to be mechanically durable and the silica sheath to be resistant to devitrification.

4. Cryogenic Thermometry

Five papers which were concerned with resistance thermometry at cryogenic temperatures were presented. P. R. Swinehart (Lake Shore Cryotronics, Inc., USA) discussed the properties of planar Ge thermometers and reported major advances in controlling As diffusion into Ga-doped Ge substrates. These planar Ge thermometers have a higher resistance than those of the bulk devices for a given sensitivity, but they are usable over a much

greater temperature range. Also, electrical contacts are better on these planar thermometers than they are on the bulk devices. Both short-term and long-term stabilities were reported to be ±0.5 mK at 4.2 K. Since these thermometers contain a p-n junction diode, they may be used as diode thermometers in the range from 100 K to 300 K.

T. Shiratori (NRLM, Japan) et al. reported results of tests of some Pt-0.5 mol% Co resistance thermometers, which were constructed as small and robust devices for industrial use over the temperature range from ~4 to ~500 K. They had an inaccuracy, including sensor interchangability and without calibration, of ±0.5 K over the range given above when referenced to a common resistance-temperature relationship. For a three-point calibration (0 °C, 77.3 K and 4.2 K), individual thermometers were reported to have a 0.1 K inaccuracy above 16 K.

Two papers were concerned with carbon-glass thermometry. B. W. Ricketson (Cryogenic Calibrations, Ltd., UK) et al. presented results of cycling carbon-glass thermometers between room temperature and 77 K. Some thermometers were reported to be stable to ±5 mK at 77 K over 30 cycles. Accuracies of fitting calibration data were determined and reported for different fitting procedures. With a fourth- or fifth-order polynomial, rms deviations of 0.5 mK were obtained in the range of 1.5 to 16 K. A tenth-order polynomial fitted the data from 1.5 to 300 K to about ±5 mK in the range from 16 to 300 K and to about ±0.5 mK in the range from 1.5 to 16 K.

Yao Quanfa (Shanghai Institute of Process Automation Instrumentation, PRC) et al. described their construction of carbon-glass thermometers and reported results of reproducibility tests of some of them. They obtained reproducibilities ranging from ±0.3 to ±2.1 mK at 4.2 K, when the thermometers were thermally cycled between 4.2 and 90 K. The low values of magnetoresistance obtained were reported to be in agreement with results reported by other workers.

R. L. Rusby (NPL, UK) reviewed the performance of Rh-Fe thermometers over a period of several years and reported the abilities of different equations and fitting procedures of accurately representing the calibration date of the thermometers. He reported that over 8.5 years the largest apparent shift among the thermometers at 20 K was 0.35 mK. He presented results of fitting data from calibrations at 13 points (6 points between the lambda point and the normal boiling point of ^{4}He, the Pb point, and another 6 points between 13.8 and 20.3 K; or the latter 6 points being replaced by points at 13.8, 17.0, 20.3 K, plus another 3 points between 24.56 and 26 K) with a 7th-order power series for 25 thermometers, showing that the fits were within 1.2 mK of the calibration obtained over the entire range using many more points. Based on these results, he proposed that the Rh-Fe thermometer be considered for the next IPTS as the interpolating instrument to be used between the Pt thermometer range and the helium vapor pressure range.

In the general field of cryogenic thermometry, L. G. Rubin (MIT, USA) et al. presented a comprehensive review covering the period from 1969 through 1981. The review concentrated on work done in the temperature range from 1 to ~ 100 K. The areas covered by the review were temperature scales; fixed points and vapor pressure thermometry; gas thermometry; resistance and diode thermometry; thermoelectric, capacitance and noise thermometry; nuclear quadrupole resonance, quartz crystal frequency, ferrite permeability, magneto-resistance and superconducting thermometers; environmental effects; and instrumentation, methods and materials. The paper has a bibliography of 406 references.

E. R. Pfeiffer et al. (NBS, USA) reported results of a comparison of three realizations of the EPT-76, as derived from the NBS 2-20 K Scale, the NBS version of the IPTS-68 and the NPL version of the EPT-76 (transferred by means of calibrated Rh-Fe thermometers). The authors concluded that the EPT-76 is non-unique by about 1 mK at several points over its 0.5 K to 30 K range.

H. Armbruster et al. (Texas A&M Univ., USA) presented designs of and procedures for constructing and using a gold/superconductor (e.g., Nb) thermocouple to measure temperatures between 20 mK and 9 K. The authors found that the sensitivity of the thermocouple is much better than that of carbon resistance thermometers and that its resolution is about 2 μK at 20 mK.

5. Industrial Platinum Resistance Thermometers

One session of the symposium, consisting of six papers, was devoted to a discussion of results obtained from studies of industrial PRTs. Papers on this subject were long overdue since, although such thermometers are widely used, there is a paucity of published information about them. Work on the behavior of industrial PRTs which was reported included studies of their thermal hysteresis and stress effects as a function of their design, the reproducibilities of general and specially-designed thermometers, the calibration characteristics and the equations required to fit their resistance-temperature behavior, and their possible use in high temperature resistance thermometry.

J. Severson presented a paper for D. J. Curtis, de-

ceased, (Rosemount, Inc., USA) which described his investigation of thermal hysteresis of industrial PRTs due to thermal stresses introduced in different designs. Curtis found that the measured hysteresis, proportional to the temperature span, was consistent with a theory in which thermal stresses played the dominant role. Element designs which minimize hysteresis errors were developed and presented.

B. W. Mangum et al. (NBS, USA) reported the results of an investigation of the stability of 60 small industrial PRTs from 5 manufacturers upon thermal cycling from 0 to ~250 °C. Most of the thermometers underwent calibration drifts and showed effects due to the presence of moisture. Fifty percent of the thermometers had changes in R_0 greater than the equivalent of 0.015 °C and 25% had changes greater than the equivalent of 0.05 °C. Generally, no improvement was found in the stability of the resistance ratio, $R(t)/R_0$, over that of the resistance itself.

The paper by N. M. Bass (CSIRO, Australia) described techniques for assembling industrial PRTs which can operate in the temperature range from 0 to 500 °C with an uncertainty of ±0.02 °C, using both ceramic encapsulated Pt wire sensors and Pt film on ceramic substrate sensors which are commercially available. He gave a detailed prescription for the cleaning and assembly of such a thermometer. Two critical aspects of the construction are (1) the heating of the sensors and the assemblies in an open-ended fused-silica tube at 500 °C for 24 hours under a stream of dry 0_2 provided by the boil-off from a Dewar of liquid oxygen, and (2) a 0.5 mm diameter hole in the four-pin plastic socket inserted in the top of the fused-silica sheath, which allows air to be drawn into the thermometer on each cooling cycle so that all internal components remain oxidized.

J. J. Connolly (CSIRO, Australia) presented results on the stability, upon heating up to 250 °C for 24 to 100 hours, and on the resistance-temperature relation of 87 industrial PRTs (67 of which originated from a single manufacturer) obtained during routine calibrations in the range from 0 to 250 °C. Since the manufacturer of the 67 thermometers takes great care to dry components during assembly, his thermometers have had many hours at 500 °C prior to being received for calibration. For these short-term stability measurements, Connolly found that the industrial PRTs were sufficiently stable and predictable for measuring temperatures to an uncertainty of about ±10 mK up to at least 250 °C. This uncertainty refers to the equivalent temperature difference between the experimental value and the fitted value of the resistance ratio, using the IPTS-68 equations. A cubic term in the equations gives a better fit.

J. V. McAllan (CSIRO, Australia) discussed results of his investigation of 26 industrial ceramic-based PRTs, prepared from sensors from 6 manufacturers as described by N. M. Bass, except that McAllan heated all of his sensors for about 100 hours at 800 °C under a slow stream of dry oxygen. He found that such thermometers could have practical applications in routine laboratory measurements to inaccuracies of 0.1 K at temperatures up to 960 °C and that, with care, difference measurements could be made to 0.02 K at 960 °C. McAllan found that the departures at the Al point from the IPTS-68 equation, obtained by calibration at the triple point of water, 99 °C, and the Zn point, depended more on construction details than on wire purity. He believes that although the thermometer scale provided by such instruments may not agree with that of the purest Pt, the departures for many sensors will be less than 0.05 K at temperatures up to 660 °C and may not be much worse up to 960 °C. They might thus serve as an inexpensive and convenient way for transferring a temperature scale to another laboratory with an inaccuracy of less than ±0.05 K.

A. Actis et al. (IMGC, Italy) presented results of an investigation of 27 wire-wound industrial PRTs from 6 manufacturers. The thermometers were calibrated over the temperature range from −200 to 420 °C. The authors tried fitting several different interpolating equations to the data and found that alumina-insulated thermometers, constructed such as to have their coils partially free to expand and contract, required three calibration points, in addition to that at 0 °C, in order to reduce uncertainties to within ±0.01 °C over the range from 0 to 420 °C. For the range from −100 to 200 °C, the range in which the biggest demand for precision temperature measurements is concentrated, they found that a quadratic equation with a deviation function could provide temperatures with uncertainties within ±0.015 °C, if suitable correction terms were applied below 0 °C.

6. Automatic and Precision Resistance Thermometry

A session on automatic and precision resistance thermometry contained papers by a number of individuals (and companies) who have long been active in the resistance thermometry field, and have recently developed new, high-precision bridges based on microprocessor technology. These new bridges are similar in that they may be easily interfaced with desk calculators and mini-computers, but are most remarkable not for their similarities but rather for their radically different modes of operation.

C. G. M. Kirby (NRC, Canada) described an automatic resistance thermometer bridge that closely resembles a manual instrument described by the same

author at the fifth temperature symposium in 1971. His circuit uses several high-input-impedance operational amplifiers provided with isolated power supplies, in conjunction with a precision inductive divider. The bridge operates with a 30 Hz sine-wave excitation, and although it is presently configured to make use of a commerical desk-top calculator for all bridge functions, an earlier model was developed that used a dedicated microprocessor chip. The author claimed that the direct use of a desk-top calculator provides significant advantages in cost and flexibility.

R. D. Cutkosky (NBS, USA) described two automatic resistance thermometer bridges for new and special applications. These are additions to a family of bridges of which the first member was described in the 1980 Conference on Precision Electromagnetic Measurements. The instruments, which use 15 or 30 Hz square-waves and a special five-stage transformer, rely upon a dedicated microprocessor and an intricate timing algorithm to achieve a high degree of freedom from electrical interference. The instruments are claimed to be accurate to one part in 10^7 of reading, with a least count of 1 $\mu\Omega$.

P. C. F. Wolfendale et al. (Automatic Systems Laboratories, Ltd., UK) described a new line of high-precision resistance bridges for resistance thermometry. These bridges make use of three-stage transformers in which the excitation current is provided by feedback amplifiers, causing their input impedances to be so high that they can be connected directly across the resistances under test. This scheme has been used by others in 400 Hz bridges, but these authors have chosen to operate at 3/2 times the line frequency to reduce frequency-dependent errors and for interference rejection. In practice, this means either a 75 or 90 Hz operation. The stabilization of a feedback amplifier under these conditions is not a simple matter. The authors appear to have devoted a great deal of effort to this problem, and have developed a circuit that could be useful for a number of other applications.

N. L. Brown et al. (Neil Brown Instrument Systems, Inc., USA) described a new automatic resistance thermometer bridge. This instrument appears to be very flexible with many self-checking features. As with the other instruments described above, it makes extensive use of transformers and feedback amplifiers. A number of original circuits are contained in this instrument, including a binary inductive divider with low-impedance solid-state switching. The instrument is capable of very high precision, and is designed to operate at 384 Hz, which is remote from most power line harmonics, and is, in addition, a good choice for circuits which combine transformers and feedback amplifiers.

7. Time Response

Time response is an important parameter of thermometry where accurate measurements of rapidly varying temperatures are required. In a session on the time response of thermometers, T. M. Dauphinee (NRC, Canada) reviewed temperature measurements that are obtained simultaneously with salinity (conductivity) and pressure measurements in ocean environments. The measurements require short response times with only a few mK error in order to obtain an accurate profile of the ocean. Cable considerations require the use of a single wire for both power and signal, with cable armor and/or sea return. The design of thermometers of Pt and Cu wires with 8 to 250 ms response times was described. For faster response (a few ms), the application of thermistors and multi-junction thermocouples was discussed. For improving the accuracy of measurements, techniques were given for measuring the resistance differences between the thermometer and the reference resistor. Electronic circuitry for measurements using ac excitation was also described.

T. W. Kerlin (Univ. of Tenn., USA) et al. described two methods for evaluating the time response of installed thermometers. In the first method, from measurements of the thermometer response at two or more fluid flow conditions, the intrinsic response that is independent of the fluid condition as well as the surface response that depends on the fluid conditions are determined. The response of the thermometer in other fluids is then estimated from heat transfer correlations for the fluids. In the second method, the time response is estimated by measuring the transient response of the installed thermometer as the excitation current is applied or removed. This response is analyzed to predict the response of the thermometer to a change in fluid temperature.

P. J. Giarratano et al. (NBS, Boulder, USA) discussed the design and performance of a thin Pt film as both heater and thermometer for transient heat transfer measurements. Procedures for vapor-depositing Pt films on both surfaces of a quartz disk of 0.15875 cm thickness were given. Two calibrations of the Pt films in the range from 76 to 293 K showed about ±1.0 percent change for one film and ±0.5 percent change for the other film. The response time at 77 K was shown to be about 0.1 ms. The measured thermal conductivity of the quartz substrate was shown to be in satisfactory agreement with published values.

R. M. Carroll et al. (ONRL, USA) described the construction of Type K, MgO-insulated, sheathed thermocouples and their response times under various conditions. The response time of an insulated-junction, Type 304 stainless steel-sheathed thermocouple of 1.6 mm

diameter was reduced 50 percent when the tip diameter was reduced 8 percent by swaging. When the thermocouple wires were "side-welded" to the stainless-steel sheath, the response time was reduced by about 90%. When a thermowell is used, the response time is governed principally by the well. To reduce the response time, the use of a good thermal conductor is recommended for filling the space between the well and the thermocouple.

D. Linenberger et al. (NBS, Boulder, USA) presented results of investigations of the response-time at 4, 76, and 295 K of thermometers which included Ge resistance thermometers, carbon resistors, diodes, and a silicon-on-sapphire resistance device. The technique involved measurement of the thermal response of a thermometer to changes in self heating when a step change was made in the excitation current. At 4 K, time constants of less than 1 μs seem to be possible. Measurements were made in both gas and liquid phases of He at 4 K and of N_2 at 76 K. The time constants were found to be nearly the same for the two phases of He, to be larger for gaseous N_2 than for liquid N_2, and to be larger at 76 K than at 4 K (e.g., the increases in N_2 gas compared to those in He gas were 100 to 180 times for carbon resistors, about 1.5 times for carbon-fiber resistors, about 100 times for Ge resistors, about 140,000 times for silicon-on-sapphire resistors, and 30 to 14,000 times for diodes).

8. Electronic, Nuclear and Ultrasonic Thermometry

Developments of various types of temperature-related properties for thermometry, employing specialized circuitry and electronics, were discussed in the session on electronic thermometry. K. P. Shambrook (Doric Scientific, USA) reviewed the application to temperature measurements of thermocouples, metal resistance thermometers, thermistors, and diodes. The discussion included problems of connecting the sensors to readout instruments, signal conditioning, common-mode and normal-mode noise, noise rejection, multiplexing, cabling, and thermocouple reference junction compensation. For the instruments, methods of linearization of the signal were described. Advantages of analog and digital readout were compared.

A. Ohte et al. (Yokogawa Electric Works, Ltd., Japan) described the features and the performance of a fully-automatic, precision nuclear quadrupole resonance (NQR) thermometer which is based upon the temperature dependence of the NQR absorption frequency of ^{35}Cl nuclei in $KClO_3$. The thermometer was calibrated over the temperature range from 90 to 398 K on the IPTS-68 at the NBS and the NQR frequency obtained as a function of temperature was accurately fitted by a 10th-degree polynomial. Since the ^{35}Cl (in $KClO_3$) NQR frequency-temperature relation is an inherent property of $KClO_3$, the thermometer serves as an excellent transfer standard and never needs recalibration. Also, other samples of pure $KClO_3$ have the same NQR frequency-temperature relationship and can be used without calibration. The authors found that the overall thermometer uncertainty, including that from probe interchangeability, reproducibility of absorption frequency, and frequency-temperature conversion using a polynomial approximation, was ±1 mK over the range from 90 to 398 K.

A. Ohte et al. (Yokogawa Electric Works, Ltd., Japan) described the development and performance of precision silicon-transistor thermometers. These are mass-producible electronic thermometers using inexpensive transistors as the temperature sensors. These thermometers are based on the propery of transistors that their base-emitter voltage decreases with increasing temperature. The authors reported reproducibilities of ±0.02 °C during a 1037-day test in which the sensors were cycled between room temperature and 125 °C. With the use of a novel linearizing circuit, different sensors required only a one-point temperature calibration to give linearities within ±0.1 °C over the temperature range from −50 to 125 °C. By using a more accurate linearizer and a three-point temperature calibration, the linearity can be improved to ±0.01 °C. There are some special high-temperature transistors which are suitable for use over the range of −75 to 200 °C. A variety of sensors, differently packaged, were assembled and assessed. With the advantages of small size, high accuracy and low cost, it is expected that these thermometers will find wide application in medical electronics, chemical and biological laboratories, agriculture, meteorology, and oceanography.

H. A. Tasman et al. (Commission of the European Communities, Joint Research Center, Karlsruhe Establishment, FRG) reviewed the developments and operating experiences of ultrasonic thin-wire thermometry for nuclear applications. The predominant method is that of using the pulse echo. The authors found that thoriated tungsten sensors were stable for short periods of time at temperatures above 2600 °C, e.g., they observed no change in calibration during a ½-hour test at 2860 °C. An error of less than 30 °C was obtained when fuel-rod centerline temperatures at 2400 to 2450 °C were monitored for 378 hours, and also when a clean environment at 2000 °C without fuel was monitored for 2000 hours. Although the thin-wire ultrasonic thermometer remains a complicated tool with occasional unsatisfactory reliability, it can provide

temperature profile data from environments where all other methods fail. The main difficulties are caused by interactions between the sensor and its protecting sheath.

L. C. Lynnworth (Panametrics, USA) reviewed thermometry using pulsed interrogation of multi-zone waveguides. He reported that, although some advances have been made in the theory and interpretation of test data, the greatest progress has been made in the application of this technique. The most important applications are in the temperature range from 2000 to 3000 °C.

M. G. Rao (Univ. of Southampton, UK) presented a brief review of the use of semiconductor junctions as cryogenic temperature sensors. Silicon, germanium and gallium-arsenide junctions were discussed. He indicated areas in which silicon-diode thermometers are being widely used.

9. Noise Thermometry in Industrial Environments

The subject of Johnson-noise thermometry in industrial environments was summarized by T. V. Blalock (Univ. of Tenn., USA) et al. The authors reported that most workers in noise thermometry employ a modification or extension of the noise-voltage-ratio method of Garrison and Lawson, while a few use noise power obtained from measurements of noise voltage and noise current, to determine Johnson-noise temperatures. They reviewed the theoretical foundation for Johnson-noise thermometry, gave a survey of several basic methods of noise thermometry which use conventional electronic signal processors, presented some applications of noise thermometry to temperature-scale metrology (e.g., at IMGC and CSIRO), and discussed some applications in process temperature instrumentation. They concluded that the progress in noise thermometry in the past 10 years was due to rapid improvements in signal-processor components and to the increased availability and power of digital computation.

H. Brixy (KFA-Jülich, FRG) et al. have applied Johnson-noise thermometry, using noise-voltage ratios and correlation methods, to nuclear reactors and industrial processes as high as 1150 °C. The authors claimed high reliability and accuracy even after long periods of operation in such environments.

M. C. Decréton (CEN/SCK Nuclear Research Center, Belgium) has employed a modified Johnson-noise-power method for measurement of temperatures up to 1500 °C, with a 0.3% agreement with thermocouple temperature indications, in tests conducted in temperature-regulated ovens. Niobium-shielded, alumina-insulated Pt and Re probes were used in those tests. A 10-second integration time per measurement was used.

T. R. Billeter (EG&G Idaho, Inc., USA) et al. presented results of a comparison involving high-temperature measurements obtained by using Johnson-noise thermometry and thermocouple thermometry. The temperature sensor consisted of W-Re thermocouple elements terminated in a Re coil, the latter serving as the noise-thermometer sensor. Comparisons made at temperatures up to 1500 °C generally showed agreement to within 4% of the readings. Nonthermal noise was a severe problem at temperatures above 1500 °C.

M. Imamura et al. (Yokogawa Electric Works, Ltd., Japan) reported on the development of an automatic commercial prototype Johnson-noise thermometer with an inaccuracy of ±0.3% from 77 to 1235 K.

T. V. Blalock (Univ. of Tenn., USA) et al. discussed the results of a Johnson-noise-power thermometer which was developed and applied to measurement of temperatures from 400 to 1770 K in nuclear reactors and to in-situ calibration of PRTs in nuclear power plants. For measurements of temperature and resistance in the temperature range from 273 to 1000 K, the uncertainties were within ±0.5% of the readings (99% confidence) for sensing resistors of 50 to 300 Ω, using cables as long as 18 m.

The major accomplishments of the above authors are the analysis and implementation of Johnson-noise thermometry systems over a wide temperature range, the virtual elimination of effects of spurious non-thermal-noise errors, and the application of Johnson-noise thermometry to temperature-scale metrology and to industrial conditions beyond the reach of conventional thermometers. The major problems discussed were the need to enlarge bandwidths and extend integration times to reduce uncertainties to the level (1 part in 10^6) achieved by other precision thermometers, problems with long cables, and effects of dielectrics in Johnson-noise thermometer sensors at high temperatures.

10. Thermocouples

Three sessions of the symposium were devoted entirely to the properties, performance, and applications of thermocouples. An enormous amount of work has been conducted in this area of thermometry.

Eight papers were presented that dealt with various aspects of the use and evaluation of nicrosil/nisil thermocouples. G. W. Burns (NBS, USA) reviewed experimental work on nicrosil/nisil thermocouples conducted since 1971, and discussed the present status of the use, availability, and standardization of the thermocouple in the United States. He concluded that

nicrosil/nisil can be a valuable addition to the family of letter-designated thermocouples.

N. A. Burley (MRL, Australian Department of Defence) et al. reported results of a joint investigation by MRL and NBS on the thermoelectric stability and the oxidation-resistance of nicrosil and nisil on the addition of Mg beyond their nominal composition. The oxidation-resistance and the thermoelectric stability of nisil were found to be enhanced as a direct function of initial Mg concentration in the range investigated, which was from 0.08 to 0.21 wt. %. There was also evidence of enhanced oxidation-resistance achieved by adding Mg to nicrosil, but no enhancement of thermoelectric stability was observed. Also, N. A. Burley et al. (MRL) presented a critical quantitative comparison of the properties and thermoelectric stability of the nicrosil/nisil thermocouple with those of letter-designated base-metal thermocouples.

T. P. Wang et al. (AMAX Specialty Metals Corp., USA) discussed thermoelectric stability data obtained for Type K and nicrosil/nisil thermocouples used in production furnaces operating in air and in reducing atmospheres at temperatures ranging from 500 to 1180 °C. It was found that, in general, the emf stability of nicrosil/nisil thermocouples was at least two to three times better than that of Type K thermocouples.

R. L. Anderson et al. (ORNL, USA) presented a paper on the thermoelectric stability of metal-sheathed thermocouples of various diameters (0.5 to 3 mm). Nickel-based thermocouples (Type K and nicrosil/nisil) with various combinations of sheath materials, such as Type 304 stainless steel and Inconel-600, were tested to determined the rate and extent of decalibration due to heating for various periods of time (for as long as about 1200 hours) at temperatures ranging from 600 to 1200 °C. Similar tests were also run at temperatures as high as 1350 °C with small diameter (0.5 mm), compacted-MgO-insulated, Type S and Type B thermocouples that had various sheath materials, including stainless steel, Inconel, and various Pt-Rh alloys. The results showed that the sheathed thermocouple is a complex system at elevated temperatures and that the thermoelements tend to become contaminated by the diffusion of materials from the sheaths through the insulation. It was found that the decalibration of nickel-based thermocouples was more severe in stainless-steel sheaths than in Inconel sheaths. Also, it was found that the small-diameter Type S thermocouples sheathed in either Pt-10% Rh or Pt-20% Rh tubing exhibit stability and reproducibility comparable to larger-diameter, bare-wire Type S thermocouples at temperatures up to at least 1200 °C.

E. H. McLaren et al. (NRC, Canada) presented results of extensive studies carried out on various noble- and base-metal thermocouples and on their individual thermoelements at temperatures in the 0 to 1100 °C range. Type S, Type K, and nicrosil/nisil thermocouples, as well as various Pt-Rh alloys, were included in the studies. The thermocouples and thermoelements were tested in metal-freezing-point cells in different temperature gradients, after they had been subjected to various thermal and mechanical treatments. Inhomogeneous oxidation was found to have a significant effect in the long-term degradation during service of both noble- and base-metal thermocouple alloys. The noble-metal thermocouples were reported to be much more homogeneous than the base-metal thermocouples.

A. Thurlbeck (UK Atomic Energy Authority) discussed the design and development of Type K thermocouples for measurements of coolant and fuel temperatures up to 850 °C in a gas-cooled nuclear reactor, and of W-Re thermocouples for measurements of fuel temperature up to 1500 °C. He presented results showing the reliability of those thermocouples during their 5 years of operation. He also described the use of some metal-sheathed nicrosil/nisil thermocouples for measuring the temperature of fuel-rod cladding during a brief in-pile experiment.

C. A. Mossman et al. (ORNL, USA) presented some methods of testing for thermocouple inhomogeneities and described the use of an inhomogeneity test system as a diagnostic tool to evaluate temperature measurement errors due to inhomogeneities.

In addition to these presentations on thermocouple thermometry, several authors discussed thermocouple performance and properties. R. L. Anderson et al. (ONRL, USA) presented results of thermal-cycling tests with metal-sheathed, compacted-MgO-insulated, Type K thermocouples of small diameter (0.5 mm). Experiments were conducted to determine the relative effect of differential thermal expansion, wire size, grain size, and manufacturing technology on the performance and reliability of thermocouples sheathed in stainless steel and in Inconel. They found that repeated heating and cooling of the sheathed thermocouples between 350 and 805 °C led to failure in the thermcouple wires by fracturing of the wire along grain boundaries embrittled by the formation of metal oxides. They also found that with smaller initial grain size in the thermoelement wire, the operating life was increased.

R. P. Reed (Sandia National Laboratories, USA) discussed diagnostics for validation of thermocouple data in applications in which thermocouples are used in hostile environments. The diagnostics include measurements of loop resistance, noise voltage, and circuit isolation and they reveal the occurrence, location, and nature of thermocouple failure. Reed also presented

a functional model of thermoelectric thermometry which can be used to reveal problems in complex circuits and allows a direct evaluation of errors.

D. D. Pollock (SUNY, Buffalo, USA) proposed a simplified spin-cluster mechanism to explain the thermoelectric properties of Ni and some of its alloys near their Curie temperatures. This mechanism is based primarily upon the temperature dependence of the electrons involved in the clusters.

J. Ohno et al. (Nippon Steel Corporation, Japan) described a differential thermometer developed for measurement of high-temperature combustion gases at temperatures of about 2000 °C. The temperatures of the gases are calculated by fitting the response curve of the thermocouple to temperatures up to about 1200 °C. Inaccuracies of about 1% were claimed.

Y. Kawate et al. (Kobe Steel, Ltd., Japan) described a technique for measuring the thickness of a blast furnace lining, and thus its erosion. The technique involved the use of a multiple thermocouple sensor, with several Type K thermocouples in the sheath and insulated from each other. This permitted the simultaneous measurement of temperature variations at a number of positions across the lining. By analyzing the signals obtained, an inaccuracy of less than 5% was obtained in the estimates of the lining thickness.

There were several presentations giving results of studies of thermocouples designed for use in nuclear reactors. S. C. Wilkins (EG&G, USA) discussed the development of small-diameter (0.3 to 0.7 mm) metal-sheathed thermocouples (both W-Re and Type K) for accurate and reliable measurement of the surface temperature of nuclear-fuel-rod cladding. He discussed fabrication and attachment techniques for such measurements and gave details of material compatibility.

C. P. Cannon (HEDL, USA) presented a paper on the fabrication and evaluation of metal-sheathed W-Re alloy thermocouples designed for measuring nuclear-reactor fuel-centerline temperatures as high as 2200 °C. W-5% Re/W-26% Re thermocouples, insulated with $Hf0_2$ tubing and sealed hermetically within a 1.6 mm diameter Re sheath, were found to undergo changes in emf output of less than 2% during out-of-pile tests run for 1000 hours at 2200 °C.

P. Siltanen (Imatran Voima Oy, Finland) et al. described their experiences with metal-sheathed Type K thermocouples used for measuring inlet and outlet reactor-core cooling-water temperature in a pressurized water reactor. The thermoelectric properties of inlet, but not outlet, thermocouples were found to be influenced by radiation, in proportion to the reactor power level. This was assumed to be the result of neutron reactions in the thermocouple wires.

R. W. McCulloch et al. (ORNL, USA) discussed results of an investigation in which they thermally cycled thermocouples. The authors gave criteria for the improvement in the lifetimes of 0.5 mm diameter metal-sheathed Type K thermocouples, used in nuclear-fuel-rod simulators to measure high temperatures (1200 °C) and to follow severe thermal transients (up to 50 °C/s). They found that improvements could be achieved in the reliability of such thermocouples by using better annealing schedules and better drawing techniques during the fabrication of the devices.

11. Thermistors

One session of the symposium, comprising five papers, was devoted entirely to thermistors. In that session, J. M. Zurbuchen et al. (Yellow Springs Instrument Co., Inc., USA) discussed the aging phenomena inherent in the multi-grain, multi-phase $NiMn_2O_4$ systems used in thermistors. Based on their observations, the authors concluded that aging, manifested as thermometric drift, is due to changes in the crystal structure of the material and to non-equilibrium degree of inversion.

T. H. LaMers et al. (Yellow Springs Instrument Co., Inc., USA) presented a paper on enhanced stability achieved for a recently-developed glass-coated, interchangeable disk thermistor. Results obtained during 2500 hours of aging at temperatures ranging from −80 to 250 °C indicate that the stability of these units is significantly better than that of uncoated interchangeable disks and is comparable to that of glass-coated bead thermistors.

M. Sapoff et al. (Thermometrics, Inc., USA) presented the results of an investigation to evaluate the exactness of fit of third-degree polynomials to the resistance-temperature relationship of thermistors. Seventeen different thermistor materials were evaluated over the temperature range of −80 to 260 °C. Analysis of the data indicated that the expression

$$\ln R_T = Ao + A_1/T + A_2/T^2 + A_3/T^3$$

was valid, to within measurement uncertainties, for temperature spans of 100 °C between −80 and 30 °C, spans of 150 °C between −60 and 260 °C, and spans of 200 °C between 0 and 260 °C.

R. L. Berger et al. (NIH, USA) described the design and construction of thermistors with response times of 5 ms. The authors also described a fast, low-noise, ac bridge with digital temperature output. They presented a computer technique for analyzing the thermal response of the thermistor and reaction vessel, yielding values

which compared favorably with their experimental results.

R. E. Wendt (Zurheide-Herrman, Inc., USA) presented a technique for tailoring the characteristics of perovskite-type oxide thermistors. By combining powders which exhibit different switching temperatures and controlling their relative distribution, he demonstrated that it is possible to obtain a log-linear characteristic over a relatively wide temperature range. Data were presented for a system comprising equal weights of six powders having rated switching temperatures evenly spaced from 15 to 115 °C.

12. Plasma Thermometry

In a session on plasma thermometry, the emphasis was on measurements of the very high temperatures of magnetically-confined fusion-type plasmas. P. C. Efthimion et al. (Princeton Univ., USA) and F. J. Stauffer (Univ. of Md., USA) discussed the measurements of "temperatures" in the range from a few hundred to a few kilo-electron volts (10^6 to $5x10^8$ K) in tokamaks, using electron-cyclotron resonance and emission-spectral-line Doppler-broadening techniques. These two new techniques were compared with other more established methods, such as Thomson laser scattering, and were found to agree quite well. Each of the two newly-developed methods offers unique features, such as time-resolved measurements over the entire length of the pulsed plasma discharge for the electron-cyclotron technique, and measurement of ion, rather than electron, temperatures for the Doppler-broadening technique.

D. H. Nettleton (NPL, UK) discussed the use of a wall-stabilized arc plasma as a radiometric standard. Using spectroscopic methods, the temperatures were measured to an uncertainty of less than 1% at approximately 14,000 K, thus allowing the emission from this plasma to be used as a radiometric standard.

13. Fast Radiation Thermometry

This was the first time in the history of the Temperature Symposia that an entire session was devoted to "fast radiation thermometry", "fast" meaning millisecond or shorter time-resolution. This indicates a definite increase in interest in rapid temperature-measurement techniques in the high-temperature region, both in connection with thermophysical-properties measurements and in specific high-temperature applications, such as gas turbines, high-temperature gases, and gas and dust explosions.

An accurate two-color microsecond-resolution pyrometer was described by G.M. Foley et al. (NBS, USA). This pyrometer was constructed in connection with a capacitor-discharge system for the measurement of thermophysical properties of substances at high temperatures. The pyrometer is capable of temperature measurements at 1.5 μs intervals in the range from 2000 to 6000 K, with a signal resolution of about 0.1%.

Development of a submicrosecond-resolution multi-wavelength pyrometer at the European Institute for Transuranium Elements was described by J. -F. Babelot (EITE, FRG) et al. This pyrometer also was built in connection with thermophysical-properties measurements at high temperatures utilizing a laser pulse technique. The time-resolution of the pyrometer was reported to be 10 ns and the spatial resolution was stated to be about 100 μm.

A summary of research occurring over the last 10 years at the Instituto di Metrologia "G. Colonnetti" was presented by F. Righini et al. (IMGC, Italy). The main emphasis was on millisecond-resolution pyrometry, which was developed in connection with thermophysical-properties measurements. The successful use of silicon photodetectors was discussed, and characteristics and performances of the fast pyrometers were presented.

In relation to applications to temperature measurements of gas and dust explosions, K. L. Cashdollar et al. (Bureau of Mines, USA) described the use of a rapid-scan spectrometer which has a wavelength range of 1.7 to 4.8 μm and a maximum rate of 800 scans/s. Also in this connection, multi-wavelength infrared pyrometers having about 20 μs response times were described.

Application of radiation thermometry to the development and control of gas turbine engines was described by T. G. R. Beynon (Land Pyrometers, Ltd., UK). The radiation thermometers that were used could operate in ambient temperatures from −60 to 550 °C under 30 atm pressure and continuous vibration. Their response times were a few microseconds.

The development of a packaged, automated instrument for temperature measurements in high-temperature gases based on the emission-absorption technique was described by S. A. Self et al. (Stanford Univ., USA). It employs optical fibers to transmit radiation from a standard lamp to the gas, and from the gas to a detector. The time-response of the instrument is 1 ms, and the instrument is intended for temperature measurements in the range from 2000 to 3000 K.

14. Optical Pyrometry

J. L. Gardner et al. (CSIRO, Australia) described the design and construction of a broadband, ratio optical pyrometer using silicon photodiode detectors. Design

considerations included the use of two closely spaced wavelengths at short wavelengths in order to minimize effects of variations in the emissivity with wavelength. Measurements with blackbody sources in the range from 600 to 900 °C in the region of 0.85 μm showed deviations from thermocouple readings of about 3 °C. The results were less satisfactory when the oxidation state of the surface was changing.

Jiang Schichang et al. (Shanghai Inst. of Process Automation Instrumentation, PRC) discussed the investigation of the calibration characteristics of the components of optical pyrometer systems. The relation between the mean effective wavelength and other properties of the detector and filter was investigated. The procedure for calibration of silicon photodiodes in the range from 700 to 1200 °C was described.

F. Sakuma et al. (NRLM, Japan) described a 900 nm narrow-band optical pyrometer system, with a silicon-photodiode detector, for establishing a temperature scale by calibration at blackbody fixed points in the range from 420 to 2000 °C. A quadratic relation that was fitted to the calibration data of the pyrometer system at the Al, Ag, and Cu points yields a temperature scale estimated to be accurate to ±0.5 °C.

B. Woerner (Inst. for Nuclear Energy, Stuggart University, FRG) presented a paper on the application of a special vacuum-photocell detector and electronic instrumentation to a standard optical pyrometer to obtain high linearity between measured radiance and output signal. Comparison measurements with standard optical-pyrometer techniques showed the photocell pyrometer to agree to within 0.1 K with tungsten strip lamps at temperatures up to 2500 K and to within 0.1 K with blackbody sources at temperatures up to 1700 K.

15. Applied Radiation Thermometry

One session was devoted entirely to applied radiation thermometry in the steel industry. The papers presented there described state-of-the-art techniques being introduced for temperature measurement and control of various processes in steel mills.

K. Tamura et al. (Kawasaki Steel Corporation, Japan) discussed the improved calibration procedures for radiation pyrometers used in their facilities. The uncertainty in the calibration was estimated to be less than ±2 °C.

J. E. Roney (Jones & Laughlin Steel Corporation, USA) discussed a technique used to compensate for the error caused by high levels of background radiation from flames, heating tubes, and hot walls of a processing furnace. He described three different configurations, each tailored to solve a specific measurement problem. In each configuration, two similar pyrometers are used. The first pyrometer is aimed directly at the surface of the steel of unknown temperature. Depending on the configuration, the second pyrometer is aimed at a target of known emissivity and/or temperature which has been placed within the furnace. From the difference between the two signals, the temperature of the hot steel surface can be determined. A measurement equation for the "dual pyrometer" method and some sample calculations which showed the effects of various sources of error were presented.

T. Iuchi et al. (Nippon Steel Corp., Japan) presented two methods for the simultaneous measurement of the temperature and the emittance of steel in processing furnaces. The technique is particularly useful in processes where both temperature and emittance of the source may change continuously during the measurement. Examples discussed included measurement and control of the temperature of a continuous annealing furnace for steel sheet and of a coating process for steel sheet.

Y. Tamura et al. (Sumitomo Metal Industries, Ltd., Japan) discussed two developments in the measurement of the temperature of steel in a reheating furnace. The first development involved the use of a water-cooled sight tube fabricated from castable ceramic. The second development was a heat-resistant data logger which tolerated exposure to 1200 °C for up to 4 hours. The logger could read thermocouple voltages at pre-selected time intervals and the readings were stored in a memory module within the logger. In an example of its application, thermocouples were fixed at various locations on a steel slab. The logger was placed on the slab and the assembly passed through a furnace. The time-temperature data subsequently retrieved from the logger were found to be very useful in analyzing the control and performance of the reheating furnace.

T. Yamada et al. (Nippon Kokan, Ltd., Japan) described a microcomputer-based camera employing a self-scanning silicon-photodiode linear array to measure and record temperature distributions on hot rolled products. Typical temperature distributions at various locations along the process line for rolled sheet and for H-shaped steel were presented.

J. Ohno (Nippon Steel Corp., Japan) discussed a new method for the determination of the temperature distribution within the field of view of a radiometer. This is based on the measurement of multi-spectral radiance. A typical application might be the determination of the temperature of a metal joint during a welding process.

16. Emissivities and Blackbody Furnaces

In a session on emissivities and blackbody furnaces, A. Ono (NRLM, Japan) presented results of a Monte

Carlo calculation of the apparent emissivities of cylindrical cavities with conical bottoms for which it was assumed that the cylindrical surfaces were diffuse and the conical surfaces were partially specular. He showed that apex angles of the cone near 60°, 90°, and 180° should be avoided because successive specular reflections on the cone can considerably reduce the apparent emissivity. He showed the advantage of choosing 120° as the apex angle in that a mirror-like conical bottom of that angle guides incident radiation onto the darkest part of the cavity by specular reflection. Thus, a higher degree of specularity gives a higher apparent emissivity. Consequently, by making a conical surface more specular, a perfect blackbody can be approached even if the conical surface is not black.

A. Ono (NRLM, Japan) et al. also presented results of their evaluation of the apparent emissivities of lateral holes formed on a Ta tube, determined both experimentally, by the integral blackbody method, and theoretically, by a Monte Carlo analysis. The apparent emissivities were determined experimentally by extrapolating the radiances of different-sized lateral holes to a view factor of zero, the condition at which the hole would be a perfect blackbody. The calculated apparent emissivities agreed with the experimental observations to within their uncertainties. The effects on the cavity quality of temperature distribution along the tube were also investigated.

S. Hattori et al. (NRLM, Japan) reviewed a new concept of an effective temperature to express the radiant characteristics of non-isothermal blackbody cavities. The effective (spectral) emissivity has been frequently used in the past as a quantity to express radiant characteristics of isothermal and non-isothermal cavities but this quantity explicitly depends on the wavelength of the radiation and on the temperature through the Planck relation for blackbody spectral radiance. Therefore, effective emissivities must be calculated for every wavelength and temperature associated with the radiation thermometers to be calibrated. The effective temperature of the cavity, however, depends neither on the wavelength of the radiation nor on the temperature of the cavity to a first-order approximation of temperature differences within a cavity. It depends only on the temperature distribution. The effective temperature can be regarded as the true temperature of the cavity. Beyond the first-order approximation, the author developed an empirical equation, taking into account the strong non-linear behavior of blackbody spectral radiance, which provides approximate effective temperatures accurate to better than 5% when the temperature distributions along the cylindrical axes are depressed by up to 10% at the apertures.

Zhu Yingsong (Shanghai Institute of Process Automation Instrumentation, PRC) et al. described the design, construction, and operation of two cylindro-conical heat-pipe blackbodies operating in a horizontal position over the temperature ranges from −50 to 50 °C and from 40 to 150 °C, respectively. The cavities are 6.0 cm in diameter and 30.0 cm long and are open to the atmosphere. One of the heat-pipe blackbodies is an ammonia/stainless-steel heat pipe which operates between −50 and 50 °C; the other is a water/copper heat pipe which operates in the range from 40 to 150 °C. Using the water/copper heat pipe, the authors obtained a temperature uniformity of ±0.03 °C over a 20.0 cm length from the cone apex in the temperature region from 110 to 150 °C. In the region of 40 to 110 °C, they obtained a uniformity of ±0.06 °C. For the ammonia/stainless-steel heat pipe, they obtained uniformities of ±0.01 °C in the region of -20 to 50 °C and ±0.02 °C in the range from -20 to -40 °C. They reported calculations that showed that the total effective emissivities of the conical part and of about four-tenths of the cylindrical part adjacent to the cone were greater than 0.999.

17. Spectroscopic Thermometry

Optical diagnostic techniques in which molecular vibrational and rotational populations are measured to determine temperature were discussed in two sessions entitled "Temperature Measurements in Hot Gaseous Media." Molecular-energy-level populations (mainly vibrational and rotational levels) are determined in "real time" (down to 10 ns) with fine spatial resolution (as small as 1 mm^3) by these non-contact methods.

Optical absorption and Raman spectroscopy, especially the non-linear optical technique of coherent anti-Stokes Raman spectroscopy (CARS) are now finding very practical application. For example, J. P. Taran et al. (Office National d'Etudes et de Recherches Aérospatiales, France), G. L. Switzer et al. (System Research Laboratories, Inc., USA), J. W. Fleming et al. (NRL, USA), J. F. Verdieck et al. (United Technologies Research Center, USA), L. A. Rahn et al. (Sandia National Laboratories, USA), and D. Klick et al. (Ford Motor Co., USA) discussed CARS thermometry in six presentations, giving results of investigations involving such practical applications as the study of well-stirred chemical reactors, hydrogen plasmas, laboratory "model" flames, jet engines, and internal-combustion engines. The study of internal-combustion engines received a good deal of attention, with presentations on this subject by L. A. Rahn and by D. Klick. The ability of the optical techniques to yield spatial and temporal temperature distributions is of great importance in such

work. M. C. Drake et al. (General Electric, USA) and P. P. Yaney et al. (Univ. of Dayton, USA) presented papers in which they described the application of conventional Raman spectroscopy to temperature measurement, with an emphasis on the study of turbulent combustion and mixing.

R. W. McCullough (Aeronautical Research Associates of Princeton, Inc., USA) et al. discussed the use of OH^- absorption for "real time" (to 10 kHz) temperature (spatially-averaged) measurements in a hypersonic propulsion test facility. H. G. Semerjian (NBS, USA) et al. presented a paper on the novel technique of optical tomography and its use in determining in "real-time", full spatial maps of inhomogeneous temperature fields.

The importance for accurate thermometry of a complete characterization of the fundamental molecular parameters which determine an observed optical spectrum was emphasized in two papers—one by C. C. Wang (Ford Motor Co., USA), dealing with OH^- absorption, and the other by M. C. Drake, dealing with linear (and to some extent non-linear) Raman spectroscopy. An accurate knowledge of molecular properties is required in order to achieve overall accuracies more closely commensurate with the reported precisions. In many cases, the systematic errors in these techniques lead to uncertainties which are 5 to 10 times larger than the random error. At the present time and under the best of conditions, measurement imprecision of the order of ±10 K can be achieved for temperatures averaged over 1 s to 10 s, in the 1000 to 3000 K region. Single-shot temperature measurements (10 ns to 10 ms) generally have relative imprecisions of 4 to 8% in this temperature range.

As another application of optical methods to thermometry, L. J. Bowie (Evanston Hospital, USA) described some spectroscopic techniques for measuring the temperature of liquids in cuvettes of analytical instruments, with particular application to clinical-laboratory instruments. The principle involved is the coupling of some temperature-dependent physical or chemical property of a fluid (e.g., viscosity or pH) to a spectral change which is sensitive to that same property. These techniques can be easily used to determine thermal equilibration times in absorption- or luminescence-dependent photometric devices. The use of suitably-calibrated materials permits the measurement of temperatures in cuvettes, which are otherwise generally inaccessible, with uncertainties of 0.1 °C or better. Through the use of this technique, Bowie and his colleagues have shown some commonly-used clinical-laboratory analyzers to have serious defects in temperature control and in the accuracy of the claimed temperature of reactions.

18. Biological and Human Comfort Thermometry

In a session on Biological and Human-Comfort Thermometry, J. Edrich (Univ. of Colorado, USA) et al. reviewed principles and techniques of microwave-thermography imaging of subcutaneous temperature distributions at 1 cm and 3 cm wavelengths. So far, this method uses comparison techniques in the detection of tumors, e.g., in the detection of breast cancer. This technique is currently being used in clinical tests as a diagnostic tool for the detection of cancer.

E. Mayer (Fraunhofer-Institut für Bauphysik, FRG) described the instruments and the methods used in studies of human thermal environments and of human comfort. The instruments used were a resultant-surface-temperature meter, a scanning radiometer, an air-temperature meter, a relative-humidity meter and an air-flow probe. Measurements obtained with these instruments permitted the calculation of an equivalent ideal temperature, a directional radiated heat loss, a directional skin temperature and directional heat flows.

An interesting paper, although somewhat removed from the theme of this symposium, was given by T. H. Benzinger (NBS, USA) who discussed a theory of the thermodynamics of living matter which permits the thermodynamic treatment and understanding of the multiple functions of living matter, the genetically-coded macromolecules of proteins, polynucleotides and membranes, their weak interactions and reversible conformational changes at moderate temperatures. The Gibbs-Helmholtz equation is inadequate in this regard in that it is incomplete. The complete equation for chemical equilibrium was given as

$$-RT \ln K(T) = \Delta H_0^0 - \left[T \int_0^T \frac{\Delta Cp^0(T') \cdot dT'}{T'} - \int_0^T \Delta Cp^0(T') \cdot dT'\right].$$

Through the use of this equation, Benzinger showed, as examples, that one can explain the experimental results on the unfolding of a protein and the unwinding of a polynucleotide double helix, results that cannot be explained through the use of the Gibbs-Helmholtz equation.

19. Fluidic, Self-Diffusion and Eddy-Current Thermometry

Several papers were presented on the application of the properties of gases for thermometry. R. M. Phillippi (HDL, USA) et al. described the application of capillary-flow properties of gases to thermometry. The change in gas pressure with change in capillary flow caused by temperature change was amplified using fluidic pressure

amplifiers to a level where commercial pressure transducers could be activated. The upper temperature limit is governed by the melting point of the refractory material used for the capillary. Tests with various capillary materials and gases up to 2500 °C gave an estimated inaccuracy of about one percent.

The self-diffusion coefficient of a gas is related to the 3/2 power of the absolute temperature. M. Lamvik (ITV, Norway) described the application of self diffusion to thermometry. An equation was derived for the case of diffusion of helium in hot nitrogen gas for the temperature range from 1000 K to 5000 K.

K. Sano et al. (Nippon Kokan, Ltd., Japan) discussed results of an investigation which used induced eddy currents for temperature measurement of steel plates. The primary coil was operated at 25 kHz and the eddy-current field was detected by two secondary coils. Test measurements between room temperature and 70 °C with the steel plate in a water bath showed good linearity (about ±1 or ±2 °C) between the eddy-current output and the temperature. Steel samples of different permeability show different eddy-current outputs.

20. Automation

The automation of precision measurements has resulted in new techniques for measurements as well as new measurement instruments and systems. Automation of precision measurements requires considerable care beyond the simple recording of data, and consideration must be given not only to the performance of the automated instrumentation, but also to the design of the measurement method and to the structuring of the computer software. The following papers described some of the techniques, instrumentation and control circuitry that have been employed to successfully obtain precision measurements.

M. H. Cooper et al. (ORNL, USA) discussed the redundancy and self-checking techniques that they have developed to insure that measurements are equal in reliability and accuracy to those obtained with manually-operated laboratory potentiometers. Cognizance of the manner in which digital instruments operate is required so that the computer software programs can be structured to include self-checking techniques for the quantities that are measured, and the use of external standards for checking the accuracy of the automated instruments must be built into the measurement process. The measurement of additional physical parameters of sensors is often easily accomplished with automation, and the authors demonstrated the usefulness of measuring thermocouple-loop resistance in order to gain further insight into thermocouple performance.

C. G. M. Kirby (NRC, Canada) described the conversion of a calibration facility, formerly operated manually, to a system under computer control. Instrumentation requirements for automation, the construction of inexpensive digitally-controlled current sources for thermometers and digitally-controlled power supplies for stirred liquid baths, and controls for tube furnaces were described. Measurements are made by minimizing the rate of change of temperature rather than attempting to control to an exact temperature, and thermometer self-heating effects are determined for each thermometer under test.

C. T. Van Degrift et al. (NBS, USA) discussed the software and hardware architecture and performance of an automatic control and calibration system for low-temperature measurements. Provisions are made for the scheduling of complex combinations of measurement and control tasks in a versatile manner by the easy establishment of task sequences with definable macro commands, so that many different experiments in different laboratories can be quickly structured. The authors have applied their techniques to Ge, Rh-Fe, and Pt thermometry, and to tunnel-diode oscillators to sense temperature, pressure, dielectric constant and magnetic susceptibility.

21. Temperature Control and Calibration

In the area of temperature control, T. M. Kegel et al. (Univ. of New Hampshire, USA) discussed work on fluidic preamplifiers and fluidic power amplifiers to control the temperature of a combustion chamber, employing a feedback linearizing scheme for the power amplifier. Thus, all components in the furnace control are pneumatic.

Zhang Jipei et al. (Shanghai Institute of Process Automation Instrumentation, PRC) described a furnace for the comparison-calibration of PRTs of various types at temperatures up to 700 °C with uncertainties of 2 to 5 mK. The furnace is interesting in that one of the heaters is wound directly on the Cu temperature-equalizing block in which the thermometers are inserted, and the thermometer for temperature control is a Pt wire wound close to the heater on the surface of this block.

C. A. Busse et al. (Commission of the European Communities, Joint Research Centre, Italy) discussed the use of inert-gas-controlled heat pipes to obtain stable isothermal heat zones in furnaces over the range from 20 to 1100 °C. Details of heat pipe construction, gas pressure control, working fluids, and furnace design were presented.

Wang Zhensen (Shanghai Institute of Process Automation Instrumentation, PRC) described a very interesting compound thermometer, consisting of a Pt wire

in series with a Rh-Fe alloy wire, which enables them to obtain a sensitive and fairly linear response over the entire range from 4.2 to 300 K. Using this, the temperature controller requires no other sensor for control. Details were provided for construction of the controller, which contains a simple ac sensing bridge utilizing an inductive-divider set-point.

H. El-Shammaa et al. (National Institute of Standards, Egypt) reported that they now have facilities for calibration of SPRTs in the temperature range above 0 °C. They are able to realize precisely the triple point of water and the freezing points of Sn and Zn.

V. A. Chistyakov (Mendeleyev Res. Inst. of Metrology, USSR) et al. submitted a paper on the theoretical analysis of radiometer calibrations using blackbody sources. Procedural and instrumental errors were discussed.

IV. Conclusions

In our attempt to summarize the Sixth International Symposium on Temperature, there were some papers of the symposium which were not covered, but it has been our aim to give the general flavor and content of the symposium and not to give a comprehensive or detailed review. This summary is no substitute for having attended the symposium or for obtaining the proceedings of the symposium when they are published.

There have been many significant accomplishments in thermometry during the 11 years since the fifth symposium on temperature and a revolution has occurred in electronic instrumentation. Significant advances in thermometry have been made throughout the entire temperature range. During the next decade, we undoubtedly will not only make many more significant advances in thermometry but a new IPTS is expected to be developed. The new Scale will probably be promulgated in 1987 or thereabouts. Reactions to and realizations of that Scale will likely dominate several sessions of the Seventh Temperature Symposium.

We gratefully acknowledge discussions with and the assistance given by many colleagues in our writing this summary. In particular, we want to thank G. W. Burns, A. Cezairliyan, R. D. Cutkosky, J. P. Evans, L. A. Guildner, W. S. Hurst, M. L. Reilly, J. R. Roberts, G. J. Rosasco, M. Sapoff, and R. L. Shepard.

JOURNAL OF RESEARCH of the National Bureau of Standards
Vol. 87, No. 5, September-October 1982

Nondestructive Evaluation Methods for Quality Acceptance of Installed Building Materials

James R. Clifton* and Nicholas J. Carino*

National Bureau of Standards, Washington, DC 20234

July 29, 1982

A review of methods developed for the nondestructive evaluation (NDE) of building materials is presented. The generic features of NDE methods are discussed. This is followed by descriptions of specific methods. The principles underlying the operation of the methods are described, along with their typical applications, advantages, and limitations. A table is included summarizing the characteristics of various NDE methods.

Key words: building materials; concrete; evaluation; inspection; inplace testing; nondestructive testing; quality assurance.

INTRODUCTION

A nondestructive evaluation (NDE) method refers to a procedure for obtaining information about the properties of an object without altering that object, and contrasts with traditional destructive tests which permanently damage test objects. Another significant characteristic of many NDE methods is that they are capable of performing measurements not only on laboratory specimens but also on objects "in-situ." It is the latter attribute which makes NDE methods extremely valuable in the area of building technology. With today's emphasis on rehabilitation and renovation, as opposed to new construction, there is a need for methods to evaluate the condition of existing structures. Such an assessment is required in order to develop the best renovation scheme. In addition, NDE methods are valuable tools for periodic inspections of structural components to determine the degree of deterioration, if any, which may occur during service conditions. Finally, these methods may be used for quality assurance purposes to determine whether or not an item has been fabricated as intended. The purpose of this article is to review the NDE methods which have been developed for the examination of materials and structural components.

NDE methods typically measure the properties that are desired in an indirect manner, that is, they measure a characteristic which is somehow related to the property in question. Thus, the accuracy of property measurements based on NDE methods will depend on several factors. First, it will depend on the relationship between the desired property and the quantity actually measured by the NDE method. If the relationship is strong, then the property can be estimated quite accurately by means of the indirect measurement. Second, the accuracy will depend on how insensitive the indirect measurement is to factors which do not affect the property in question. For example, if an NDE method is used to estimate the strength of a material and if the NDE measurement is strongly influenced by the moisture content while strength is not, then the strength estimate will be imprecise unless corrections are made for the actual moisture content. Finally, the accuracy will depend on the precision of the NDE measurement. Thus, prior to employing an NDE method, the user must be fully aware of the principles and limitations inherent to the method. Otherwise, incorrect interpretations will result.

The material property of most interest in engineering applications is strength. NDE methods may be used to determine the strength of materials as well as to determine whether or not flaws are present in the material which have an adverse effect on its strength. Some of the indirect measurements used to estimate the desired properties include the velocity of ultrasonic waves through the material, the disturbances of magnetic fields by discontinuities in the material and the absorption of electro-magnetic radiation, such as x-rays. Because of great differences between the properties of metallic and non-metallic building materials, many of the NDE methods are not applicable to both classes of materials.

Steel, concrete and wood are the main structural materials, but the technology of nondestructive evaluation is not equally developed for all three types of materials. The most technically advanced methods are for steel inspection, which is in part due to the com-

*Center for Building Technology, National Measurement Laboratory.

paratively homogenous nature of steel compared to the other materials. Concrete is unique among construction materials in that it is manufactured on-site (or at a nearby concrete plant) using locally available materials. Thus, there is no such thing as a "grade" concrete which has well-defined physical and chemical properties analogous to a "grade" of steel. In addition, concrete is a macroscopically heterogenous material composed of cement, water, sand and rocks. For these reasons, NDE methods have been developed for specific application to concrete, and as will be explained some are not completely "nondestructive." The technology of NDE inspection is least developed for wood.

A key element of many NDE methods is the calibration standard or calibration curve which is necessary to translate the indirect measurement to an estimate of the desired property. The development of the calibration procedure is just as important as the development of the hardware for performing the indirect measurement, and this must be kept in mind when choosing among alternative methods for estimating a desired property. The "cost" of NDE inspection involves not only the cost of the apparatus but also the cost of the calibration. For example, many of the methods used for concrete inspection employ relatively inexpensive test apparatus, but their implementation requires laboratory testing to develop the applicable calibration curve. The need for calibration will be mentioned as each method is discussed.

Having presented this brief introduction to some of the generic characteristics of NDE methods, we will next discuss the principles, applications, advantages and disadvantages of methods which are felt to be applicable for the inspection of building materials and structural components. The methods are presented in alphabetical order beginning with acoustic methods and ending with visual inspection. A special section details a proposed procedure which combines two of the other methods for the purpose of improving the accuracy of strength prediction of concrete. Following this section, the utility of the various NDE methods is discussed in the Summary. Also, displayed in table form for the reader's convenience, is information on commonly used NDE methods, which should prove useful in selecting an NDE method for a specific application.

DESCRIPTION OF NDE METHODS

1. Acoustic Emission Method

In this method, stress waves originating from within the test material or object are detected using surface transducers. [1].[1] The acoustic waves are due to the sudden release of stored strain energy when either preexisting or newly created flaws propogate under the action of an applied stress field. The types of flaw propagation that can be detected include dislocation movement in metals and crack growth in metals or brittle solids such as concrete. Thus, acoustic emission is able to determine the onset of mechanical failure, i.e., yielding or fracture. The test object needs to be stressed so that creation, movement, or propogation of flaws will occur. Static flaws are not detected by acoustic emission.

1.1. Description of Method

Acoustic emission testing is a passive technique and only an acoustic wave detection instrument is required. The acoustic waves, which may have a frequency range from audible to ultrasonic, are detected by piezoelectric transducers attached to the surface of the test object. Flaw growth usually can be detected by a transducer located on the test object some distance from the flaw region (provided that the wave amplitude is sufficient to be detected). The transducers generally detect waves in the frequency range of 50 kHz to 10 MHz [1]. Detected signals are amplified and the amount of amplification depends on the source of the acoustic emission; signals from dislocation movement require greater amplification than signals from microcrack propagation. After amplification, the acoustic emission activity is processed and displayed. The most useful data are the rate of acoustic emission events and the cumulative number of events plotted as a function of time, applied load or number of load cycles.

1.2. Applications

The method has been used to monitor the in-service behavior of pressure vessels (including nuclear reactors), to detect the onset of rapid crack propagation under fatigue loading or due to stress corrosion, and to monitor the response of systems to proof-load tests. Because acoustic emissions give forewarning of ultimate failure, the technique can be used to indicate when loads should be reduced to prevent total failure. By using multiple pickup of acoustic signals with transducers at different locations and by electronic data processing, it is possible to pinpoint regions of high acoustic emission activity and thereby locate the area of law development or propagation.

1.3. Advantages and Limitations

The most significant advantage of the acoustic emission method is that it gives the response of the total struc-

[1]Figures in brackets indicate literature references at the end of this paper.

ture (or system) to applied loads. By observing the acoustic emission activity as loads are applied it is possible to monitor the rate of internal material deterioration taking place (yielding or fracture) as a function of load. It is generally possible to determine the stage of incipient failure as this is usually accompanied by a rise in the acoustic emission rate and rapid increase in the cumulative number of emissions.

A major difficulty in interpreting acoustic emission results is the separation of signals due to the loading system or microscopic slippage at joints in the test object from the signals due to flaw propagation in the material. Users of the technique must be aware of all the possible extraneous acoustic signals that may be detected by the transducers, and must take precautions not to confuse them with signals due to flaw growth. Some background noise may be eliminated by using low frequency filters, but usually it is necessary to properly plan an acoustic emission inspection to eliminate unwanted noises. Equipment costs vary from moderate ($10,000) to very expensive depending on whether a single- or multiple-pickup system is required for the particular application.

2. Acoustic Impact Method

2.1. Description of Method

Acoustic impact is the oldest and simplest form of acoustic inspection. In this method, audible stress waves are set up in a test object by mechanical impact and the frequency and damping characteristics of the vibrations can be used to infer the integrity of the test object [2]. In its most unsophisticated form, the test object is struck with a hammer and the operator listens to the "ringing" (which is due to resonant vibration of the object). In a more sophisticated form, a transducer is attached to the test object, and an amplifier and display unit are used to produce a visual display of the frequency and damping characteristics of the "ringing". By comparing the output with a standard of acceptable quality, a decision is made regarding the integrity of the object.

2.2. Applications

This method can be used to detect hollow zones and delaminations in concrete and masonry structures or it may be used to detect the location of studs behind wallboard. It also has been used to detect deliminations in laminar and composite materials and rot in wood. By measuring the transmission time in wood, it's modulus of elasticity can be determined.

2.3. Advantages and Limitations

The equipment required to carry out the test is relatively inexpensive and the test can be performed easily. However, because the "ringing" can be affected by the mass and geometry of the test object, an experienced operator may be needed to correctly interpret the results.

3. Cast-In-Place Pullout

The pullout test measures the force required to pull out a steel insert, having an enlarged end, which has been cast in concrete (fig. 1). The concrete is subject to a complex state of stresses by the pullout force, and a cone of concrete is removed at failure. The pullout forces are usually related to the compressive strength of the concrete, with the ratio of pullout strength (force divided by surface area of the conic frustum) to compressive strength being in the range of 0.1 to 0.3. Correlation graphs are used to relate pullout force to compressive strength. There are several commmercially available test apparatus for measuring the pullout resistance of concrete with prices varying from $1000 to $6000.

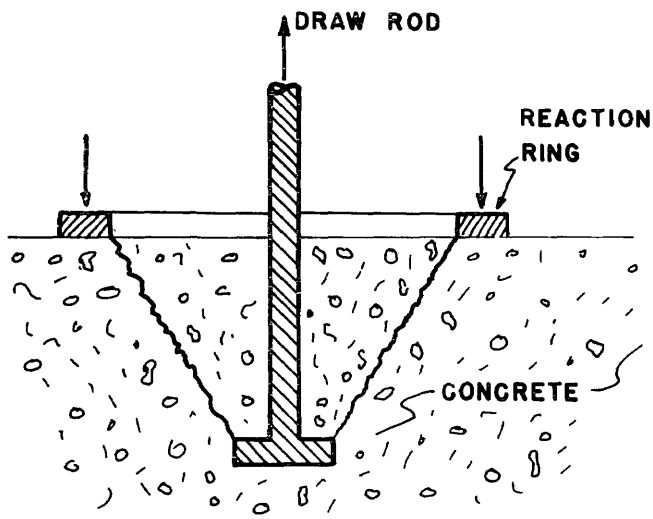

FIGURE 1. Schematic of cast-in-place pullout device.

3.1. Description of Method

The American Society for Testing and Materials (ASTM) has recently issued a test method, C900 [3] which describes the pullout assembly and gives allowable dimensions. The pullout insert is cast-in-place during placing of fresh concrete, and it is either pulled completely out of the concrete, or pulled until maximum load is reached, with a manually operated hollow tension ram exerting pressure through the steel reaction ring. Components of one possible test apparatus for pulling

out the insert are shown in figure 2.[2] Testing and calculation procedures are also given in ASTM C900. Techniques have been developed so that the inserts can be embedded deep in concrete, thereby permitting testing of the interior concrete.

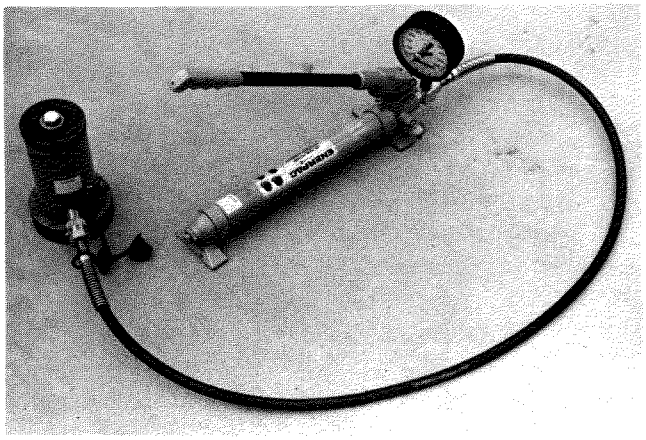

FIGURE 2. Components of one type of apparatus for performing pullout test.

Because the pullout insert is usually cast-in-place during placing of the fresh concrete, these tests must be planned in advance. Alternatively, hardened concrete can be drilled to receive the pullout insert. This necessitates drilling through the bottom or backside of a concrete slab for example, to the proper depth and width to permit the insertion of the enlarged head. A smaller hole, sufficient to permit insertion of the steel shaft, is drilled through the remaining portion of the concrete slab, the insert is placed through the bottom or backside, and the test is performed. This alternate method is currently being developed and is not covered by ASTM C900.

3.2. Reliability of Method

Malhotra [4] and Richards [5] have shown the pullout method is a reliable method for estimating the compressive strength of concrete. Malhotra found that the coefficients of variation for pullout test results were in the same range as those obtained from testing standard cylinders in compression. Correlation coefficients of 0.97 to 0.99 have been obtained for normal weight concrete from curve fitting of pullout and compression test results.

[2] In this paper several commercially available devices used for NDE tests of building materials are identified and discussed. Such identification does not imply recommendation or endorsement by the National Bureau of Standards.

3.3. Advantages and Limitations

The pullout technique is the only nondestructive test method which directly measures a strength property of concrete in place. The measured strength is thought to be a combination of tensile and shear strengths.

The major disadvantage of the pullout test is that a cone of concrete is sometimes pulled out necessitating minor repairs. However, if the pullout force is quickly released when failure is just initiated, the concrete cone will not be torn loose, and no repairs will be required. Another disadvantage is the need to plan where inserts are to be located and to make provisions for their placement prior to placing concrete. The feasibility of drilling holes into hardened concrete and inserting pullout devices is being explored [6]. This would eliminate the need to install the inserts prior to placing concrete.

4. Electrical Potential Measurements

Information on the corrosion state of metals can be obtained from measuring the electrical potential of the metal using a standard reference electrode and a voltmeter. As the electrical potential of a metal becomes more negative, the probability that corrosion has taken place increases.

4.1. Measurements on Steel in Concrete

The electrical potential method is commonly used to assess the corrosion condition of steel reinforcement in concrete. The electrical potentials of steel reinforcement are measured by making an electrical connection from a voltmeter to the reinforcement and a second electrical connection from the voltmeter to a reference cell in physical contact with the surface of the concrete (fig. 3). Dry concrete must be moistened before making electrical measurements. A saturated copper-copper sulfate electrode is usually used as the reference cell. The electrical potential of the reinforcement located below the reference cell is measured.

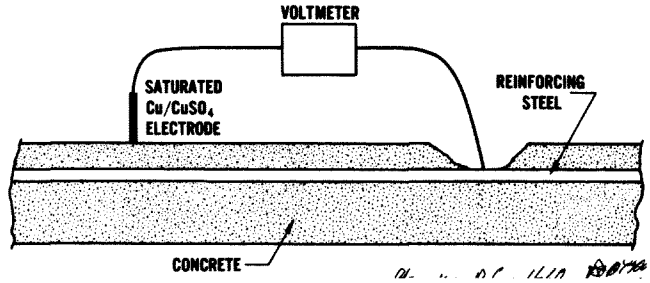

FIGURE 3. Measurement of electrical potential of steel reinforcing bars in concrete.

If the electrical potential of the steel reinforcement is more negative than -0.35 V versus the copper sulfate electrode, active corrosion is probably taking place. Values in the range of -0.30 to -0.35 V suggest that corrosive conditions are developing at the concrete-steel interface, while values less negative than -0.30 V indicate that the steel is probably passive, i.e., not corroding [7].

An electrical potential diagram of a concrete slab can be constructed in which areas of similar potentials are outlined. This can be used to identify those areas where reinforcement may be corroding.

4.2. Advantages and Limitations of Method

The equipment is inexpensive and only a moderate amount of user expertise is needed to make the measurements. Measurements of the electrical potential of steel reinforcement provide information concerning the probability for the occurrence of corrosion. However, information on either the rate or the extent of corrosion is not obtained. In addition, a direct electrical connection must be made to the reinforcing steel. If the steel is not exposed, then some concrete covering must be removed.

5. Electro-Magnetic Methods

The presence of flaws or changes in composition of metals will affect their electrical and magnetic properties. Therefore, it is possible to detect anomalies in metals by measuring changes in the electrical and magnetic characteristics of metals. NDE methods that function on the above basis include eddy current, magneto-inductive, and magnetic particle testing.

5.1. Eddy Current Inspection

Eddy current inspection is a versatile NDE method based upon the principles of electromagnetic induction and is only applicable to inspection of metals [1].

5.1.1. Description of Method

A coil carrying an alternating electric current will produce an alternating magnetic field opposing the flow of current into the coil (figure 4). When the coil is brought near a conductive material, this alternating magnetic field induces a closed-loop current flow in the material known as eddy current. The eddy currents will also be alternating, and, therefore, a secondary magnetic field is produced by them which opposes the magnetic field of the coil. Thus, when the energized coil is brought near a metal surface there will be a change in the current flow

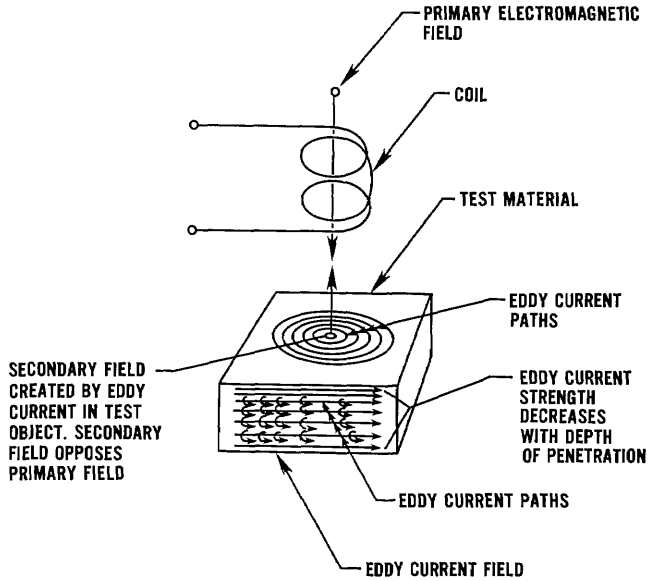

FIGURE 4. Establishment of eddy currents in a metallic building material [9].

in the coil. Measuring the changes in the current flow (or the coil impedence) is the basis of eddy current inspection.

The magnitude of the change in the coil current will depend on the intensity of the eddy currents induced in the metal. Factors which influence the intensity of eddy current flow include the following [8]:

1) the frequency and magnitude of the coil current,
2) the electrical conductivity of the metal,
3) the magnetic permeability of the metal,
4) the size and shape of the test object,
5) the proximity of the coil to the test object, and
6) the presence of discontinuities or inhomogeneities in the metal.

The electrical and magnetic properties of the metal are controlled by alloy composition, microstructure and residual stresses [1].

5.1.2. Eddy Current Inspection System

An eddy current device consists of the following components: inspection coil, an oscillator to provide coil excitation, a detector to monitor changes in coil impedance, and an output device to display the test results. Various kinds of coil geometries are available depending on the specific application. An important principle when inspecting for discontinuities is that the maximum signal is obtained when the eddy current flow is transverse to flaw. Thus, the user needs to understand the relationship

between coil configuration, eddy current flow and type of flaw to be detected.

The frequency of the excitation current affects the depth of the eddy currents and the sensitivity of flaw detection. Increasing the coil frequency will reduce penetration but increase sensitivity. Thus high coil frequencies should be used in attempting to detect small near-surface flaws. If it is desired to detect sub-surface flaws, a lower frequency should be used but the minimum detectable flaw size increases. Thus, there is a trade-off of penetrating ability versus sensitivity which is common to other inspection methods. The range of frequencies is from 200 Hz to 6 MHz [1], with the lower frequencies used primarily for inspecting ferromagnetic metals.

The detector circuit can also take on many forms depending on the application of the instrument. In any case, the changes in coil impedance that occur during inspection are small and bridge circuitry, similar to that used to monitor electrical resistance strain gages, is used to detect these changes. In making a measurement, the impedance bridge is first balanced by using an internal adjustment or placing the coil on a reference object of acceptable quality; then the coil is placed on the test object, and any difference between test object and reference object will result in an imbalance of the bridge which is indicated on the output device. The output device can be of many forms, such as audible alarms, meters, X-Y plotters, strip-chart recorders, magnetic tape, storage oscilloscopes, or a computer.

5.1.3. Instrument Calibration

Because there are many factors that may affect the coil impedance when a test is performed, the object used to calibrate the instrument must be carefully chosen. For example, to detect cracks, the reference object must have the same electrical and magnetic properties as the test object; otherwise differences in alloy composition could be interpreted as a crack. Therefore, a user must be knowledgeable in the operation of an eddy current device in order to properly calibrate it and to interpret test results.

5.1.4. Applications

Eddy current inspection has many uses including the detection of flaws such as cracks, porosity, or inclusions in metals; detection of changes in alloy composition or microstructure; and the measurement of the thickness of nonconductive coatings on a metal.

5.1.5. Advantages and Limitations

There are several important limitations to eddy current inspection. A major limitation is the depth at which discontinuities can be detected. The density of eddy currents rapidly decreases with increased distances below the surface of a metal. The depth of penetration is controlled by the resistivity and permeability of the metal and the coil frequency.

The strength of the signal due to a particular defect will depend on the proximity of the coil to the surface of the test object. As this distance, called "lift-off," increases the signal strength diminishes. The lift-off effect is so strong that it may mask signal changes due to defects. Care must be taken, therefore, to ensure uniform contact between coil and test object. This requirement may make it difficult to test objects with rough or irregular surface. The lift-off effect may be used, however, in measuring the thickness of nonconductive coatings on a conductive metals or non-magnetic metal coatings on magnetic metals. Proper calibration samples are required to use an eddy current instrument as a thickness gage.

5.2. Magneto-Inductive Methods

This technique is only applicable to ferromagnetic metals and is primarily used to distinguish between steel of different alloy composition and different heat treatments. The principle involved is electromagnetic induction and the equipment circuitry resembles a simple transformer in which the test object acts as the "core" [1]. There is a primary coil connected to a power supply delivering a low frequency (10 to 50 Hz) altering current, and a secondary coil feeding into an amplifier circuit. In the absence of a test object, the primary coil induces a small voltage in the secondary coil, but when a ferromagnetic object is introduced a much higher secondary voltage is induced. The magnitude of the induced voltage in the secondary coil is a function of the magnitization characteristics of the object, and changes in these characteristics are used to distinguish between samples of different properties. As in the case of eddy current inspection, this method can be used for quantitative measurement only after proper calibration is performed.

5.3. Cover Meters

Cover meters are portable, battery-operated magnetic devices that are primarily used to estimate the depth and location of reinforcing steel (bars and tendons) embedded in concrete. In addition, some information can be obtained regarding the dimensions of the reinforcement [4].

5.3.1. Principle and Applications

Cover meters are magnetic devices that are based on the magneto-inductive principle. A typical meter is shown in figure 5. A magnetic field is induced between the two faces of the probe, which houses a magnetic core, by an alternating current passing through a coil. If the magnetic field passes through concrete containing reinforcement, the induced secondary current is controlled by the reinforcement. The magnitude of this change in inductance is measured by a meter. For a given probe, the magnitude of the induced current is largely controlled by the distance between the steel reinforcement and the probe.

The induced current decreases as the distance from probe to the reinforcement increases because the magnetic flux intensity of a magnetic material decreases with the square of the distance. In addition, the magnetic permeability of the concrete, even though it is low, will have some affect on the reading. Therefore, the calibrated scales on the meters of commercial equipment are nonlinear. Also, a meter must be readjusted if a different probe is attached.

The probe is highly directional; i.e., a sharp maximum in induced current is observed when the long axis of the probe and reinforcement are aligned and when the probe is directly above the reinforcement.

The commercial cover meter shown in figure 5 can detect reinforcement with a concrete cover as thick as 8 inches (200 mm). Through the use of spacers of known thickness, the size of reinforcing between 0.38 to 2 in. (6 to 51 mm) can be estimated.

Another possible application of the cover meter is to estimate the thickness of slabs which are accessible from both sides. If a steel plate is aligned on one side with the probe on the other side, the measured induced current will give an indication of the thickness of the slab. For this application, a series of calibration tests must be first performed.

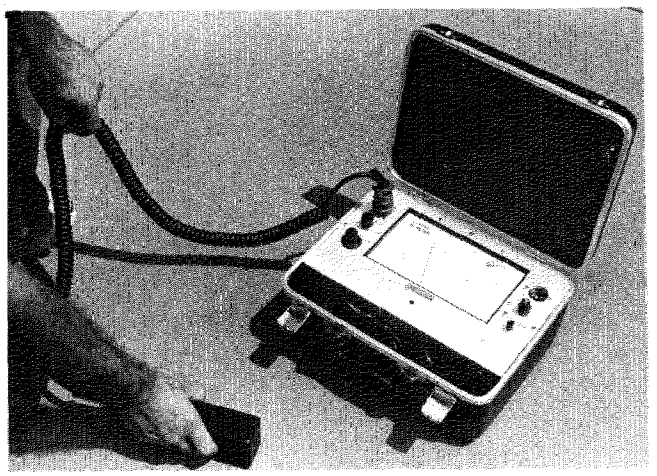

FIGURE 5. Cover meter used to detect steel reinforcement.

5.3.2. Advantages and Limitations

Cover meters are portable, inexpensive, instruments that can be easily used. They are most useful when reinforced concrete has only one layer of widely separated reinforcing bars. In highly reinforced concrete, the presence of secondary reinforcement makes the determination of the depth of concrete cover difficult. Furthermore, reinforcing bars running parallel to those being measured influence the induced current if the distance between bars is less than two or three times the cover distance [4].

5.4. Magnetic Particle Inspection

5.4.1. Principle of Method

This inspection method relies on the ability of cracks to alter the magnetic field within a metal so that fine magnetic powder will be attracted to the crack zone and cracks thereby identified [1, 10, 11]. To further understand the principle, consider a bar magnet in which the magnetic field passes through the magnet from south to north poles. If ferromagnetic particles are sprinkled over the middle surface of a crack free magnet, there will be no attraction because the magnetic field lies wholly within the magnet. Now consider the case in which the magnet is cracked; the two sides of the crack will act as north or south poles, and the magnetic field bridges the gap. However, some of the magnetic field will leak out of the magnet into the surrounding air space, and ferromagnetic powder will be attracted by the leakage field. Therefore, the attraction of the powder gives an indication of the presence of the crack. A subsurface crack would also produce a leakage field, but the response would be weaker than for a surface crack of the same size.

5.4.2. Application of Method

In using the magnetic particle method, it is necessary to magnetize the object being inspected, to apply ferromagnetic particles, and then to inspect for indications of cracks. There are two general types of magnetic fields that may be induced in the test object, circular and longitudinal fields. A circular field will be produced by passing an electric current through the test object, in which case the magnetic field would be concentric with the direction of current flow. A longitudinal field will be created by placing the part inside a coil carrying electric

current, in which case the magnetic field will be parallel to the longitudinal axis of the coil. The direction of the magnetic field relative to the test object controls which cracks will be detected. Strong leakage fields are produced by cracks which intersect the magnetic lines of force at an angle, and no leakage fields are produced by cracks parallel to the magnetic lines of force. Therefore, complete inspection of a part should involve rotation of the test object with respect to the magnetic field to make sure that all existing cracks intersect the magnetic field lines.

In field inspections, it usually is not practical to pass a current through the entire part or surround the part with a coil. Portable units are available that permit inspection of small portions of the test object at one time. For example, prods can be used to introduce a flow of current between two contact points on the object. In this case a circular magnetic field is induced. A yoke, i.e., a U-shaped electromagnet in which the poles are brought into contact with the test object, can also be used. With a yoke, a longitudinal magnetic field is set up in the object and the lines of force run from one pole to the other pole of the electromagnet. With either portable method, only a small portion of a large test object can be inspected at one time; 12 in (300 mm) is about the practical limit [1] for spacing between prod contacts.

The choice of current type used to magnetize the test object is important. If it is desired to detect subsurface cracks, direct current must be used because alternating current will only produce a surface magnetic field. The direct current may be from a constant or pulsating source, though the pulsating type is preferred because it imparts greater mobility to the ferromagnetic powder. The current supply is low voltage and very high amperage for user safety but still permits strong magnetization of the test object. Inspection is usually carried out with the current on but if the metal has high retentivity (permanent magnetism), the current may be turned off before applying the powder.

The powder used to indicate the leakage fields may be dry or suspended in a liquid. Dry powders are preferred for the best sensitivity to subsurface cracks and should be used with direct current while the wet powders are superior for detecting very fine surface cracks. To enhance visibility, various colors are available so that high contrast with the background can be achieved. In addition, fluorescent particles are available for increased visibility.

5.4.3. Advantages and Limitations

The magnetic particle inspection method has several advantages over other crack detection systems [1]. The equipment is portable, inexpensive, and simple to operate; positive crack indications are produced directly on the part and no electronic equipment is needed; and any shape part that is accessible can be inspected. However, there are some limitations that must be understood by the user. The method will only work with ferromagnetic metals. For complete inspection, each area needs to be inspected more than once using different magentic field directions and very large currents are needed to inspect large areas. Experience and skill is needed to properly interpret the particle indications and to recognize patterns which do not indicate cracks. Demagnetization may be required after inspecting steels with high magnetic retentivity. The maximum depth of flaw detection is about one-half inch (13 mm), and the minimum detectable flaw size increases as its depth increases.

6. Leak Testing Method

6.1. Principle of Method

Leak testing refers to the detection of holes in pipes and tanks which permit the escape of liquids or gases [9]. There are many different methods of leak testing but they can be generally classified into two categories. In the first category, the leaking system is monitored under normal operating conditions. This includes the use of pressure meters, the applications of a soap solution, or the use of audio or amplified listening devices. In the second category, a particular substance is added into the system flow to provide special indications of leakage. This includes such additives as colored dyes, Freon 12, helium gas, radioactive tracers, and odorous indicators.

6.2. Applications

Many leak detection methods are suitable for field application. Liquid storage vessels and above ground piping can usually be checked visually for leakage under normal operating conditions with no special equipment. Gas-carrying systems can usually best be checked in the field with a soap solution or, when Freon gas is added to the system, with a propane torch. These systems have no special power requirements and none of the equipment weighs more than 5 lbs (2 kg).

6.3. Advantages and Limitations

Leak detection methods can locate flaws too small to be found by any other NDE method. Gas leaks with rates as small as 10^{-12} cc/s can be detected with the use of radioactive tracers and radiation monitoring devices,

while a soapy water solution can locate leaks with rates as low as 10^{-3} cc/s [9].

Flaws can be detected only if they penetrate through a structure that can be held at pressure conditions differing from the surrounding atmosphere.

7. Microwaves

Microwaves are a form of electromagnetic radiation which has frequencies between 300 MHz and 300 GHz corresponding to wavelengths of one meter to one millimeter. Microwaves are generated in special vacuum tubes called klystrons and transported in a circuit by waveguides. Diodes are commonly used to detect microwaves.

7.1. Applications

Microwaves are reflected when they intercept a boundary between regions of different dielectric properties. They thus may be used for the detection of interfaces and voids. This technique can be used to detect delaminations and the presence of different materials in highway pavements [12-14]. The use of microwaves to estimate the moisture contents of roofing materials [15] and concrete [4] also has been explored. Similar to capacitance instruments (section 9) the effect of water on the dielectric properties of materials is determined. Boot and Watson [16] reported that the microwave technique only estimated the moisture content of concrete to within 12 to 30 percent of its mean value. Its low accuracy was largely attributed to the heterogeneity of concrete, and the internal scattering and diffraction it caused.

7.2. Limitations

The feasibility of using microwaves for inspecting installed construction materials has not been demonstrated. Further development work is required if the microwave method is to become a reliable field NDE method.

8. Moisture Detection Methods

Many of the problems encountered in a building are attributed to the presence of moisture. Visual inspection can reveal surface moisture, but even if a surface is dry, subsurface moisture can be present. Therefore, NDE methods are often used when making moisture inspections. Four NDE methods are commercially employed in moisture inspections: electrical resistance measurements; capacitance instruments; nuclear meters; and infrared thermography [15, 17, 18].

8.1. Electrical Resistance Probe

8.1.1. Principle and Applications

The resistance probe method involves the measurement of the electrical resistance of a material, which decreases as the moisture content increases. Most instruments consist of two closely spaced probes and a meter-battery assembly which are enclosed in one housing or in two attached assemblies. A commercial instrument is shown in figure 6. The probes are usually insulated except at the tips so that the region being measured lies between the tips of the probes. The probe can penetrate soft materials, such as roofing membranes, so that moisture located at various distances below the surface can be detected. Operation of a resistance probe is very simple. A voltage is impressed between the probes and the resistance is measured.

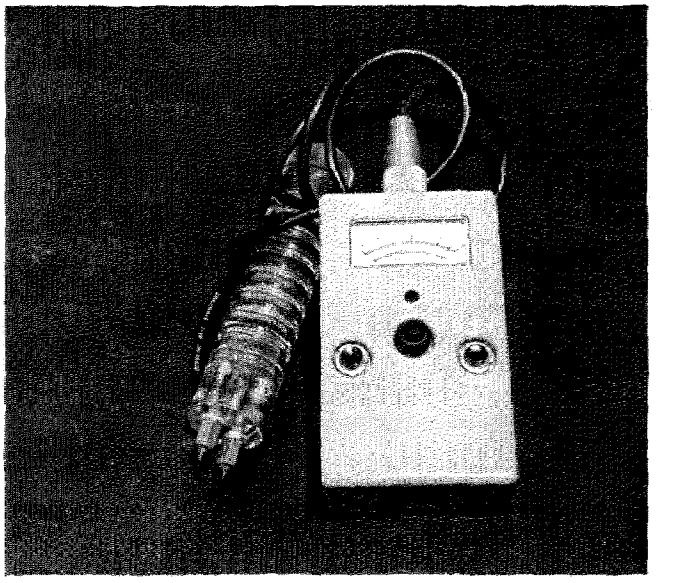

FIGURE 6. Electrical resistance instrument for detecting moisture.

Probe instruments have been used for moisture detection in plaster, brick, concrete and roofing materials. Similar procedures have been used for determining the electrical resistance of soils. In this application a 4-probe system is used.

8.1.2. Calibration

The electrical resistance probe instruments and other moisture measuring instruments are usually calibrated by obtaining relationships between their response and the moisture content of materials similar to those being inspected. The moisture contents of the specimens are gravimetrically determined, i.e., specimens are weighed

before and after oven drying with the differences in weight giving their moisture contents.

8.1.3. Advantages and Limitations

Electrical resistance probe instruments do not give a precise determination of moisture contents. The simple inexpensive instruments, while giving only a qualitative indication of wetness, are useful in identifying wet areas and for determining moisture migration patterns. More sophisticated instruments appear to be capable of giving semi-quantitative information if they are properly calibrated.

8.2. Capacitance Instruments

8.2.1. Principle and Applications

Capacitance instruments used to detect moisture are based on the principle that moisture can affect the dielectric properties of a material [17]. The dielectric constant, K, of a material is a relative measure of the ability of a material to store electrical energy and is given by:

$$K = C/Co \qquad (2)$$

where C is the capacitance of a material and C_o is the capacitance of vacuum.

The dielectric constants for many dry building materials are usually low, e.g., for dry roofing materials K ranges from 1 to 5, while water has a K of approximately 80 [17]. The value of K for a moist material will increase linearly as the volume fraction of water increases. Capacitance radio frequency instruments have been used to measure the moisture contents of paper products, wallboard, and roofing materials. Commercial capacitance instruments have various electrode configurations. The electrodes are attached to a constant frequency alternating current source and they establish an electrical field in the material being tested. Current flow or power loss is then measured which is indicative of moisture content. Most instruments operate in the radio frequency region of 1 to 30 MHz.

8.2.2. Advantages and Limitations

Capacitance instruments are portable and measurements can be taken rapidly. A recent investigation by Knab et al. [18] suggests that capacitance instruments may not give reliable quantitative measurements of the moisture contents of roofing systems. Further work appears required to establish the reliability of using this method for moisture measurements of building materials.

8.3. Nuclear Meters

8.3.1. Principle of Method

Fast neutrons, emitted during the decay of radioactive isotopes, are used in making moisture content measurements [16, 17]. Fast neutrons from the isotope source enter the material and are both scattered and slowed down by collision with the nuclei of the atoms composing the material (fig. 7). Nuclei of all materials slow down the neutrons by momentum exchange, but the reduction is greatest for collisions with hydrogen nuclei which have about the same mass as the neutrons. Some

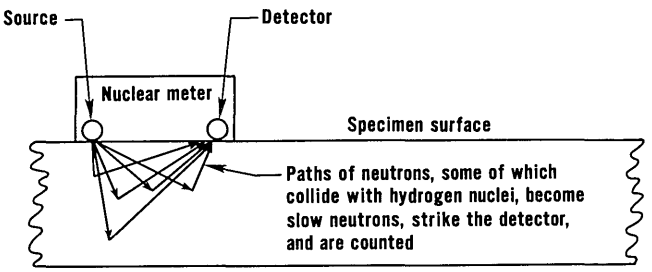

FIGURE 7. Process by which a nuclear meter detects moisture.

of the slow or thermal neutrons, are scattered in such a way that they reach the slow neutron detector in the instrument and are counted for a specified period of time. The thermal neutrons reaching the detector are much more likely to have collided with hydrogen nuclei than other atomic nuclei because the scattering cross-section of hydrogen is greater than that for other atoms. Thus, the method is capable of detecting moisture content. The detector largely measures the backscattering of slow neutrons which have collided with hydrogen nuclei in the surface region of the materials. For example, the depth of measurement is limited to between 2 to 8 in (51 to 203 mm) in soils.

8.3.2. Commercial Meters and Applications

Nuclear meters (fig. 8) are used to measure both moisture content and density of soils, portland-cement concrete, asphaltic concrete, and roofing materials [4, 15]. These meters consist of a shielded radioactive isotope source, a detector or counting device, and readout equipment. In commercial meters, the isotopes used are radium 226-beryllium, and americium 241-beryllium. Both americium and radium are alpha particle emitters and these particles interact with the nuclei of beryllium resulting in the emittance of fast neutrons.

In addition to neutron sources, most commercial nuclear moisture meters also have gamma ray sources.

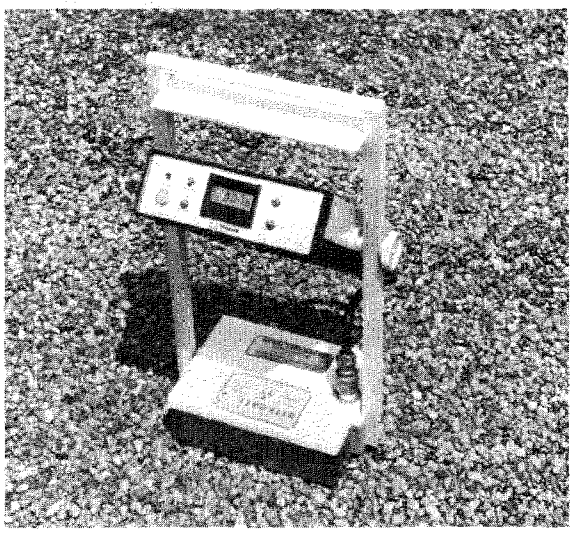

FIGURE 8. Nuclear meter used to measure moisture contents of materials.

The gamma rays are used to determine the density of materials. See section 13 for explanation of the principle.

8.3.3. Advantages and Limitations

Nuclear meters are portable and moisture measurements can rapidly be made on materials. However, the hydrogen atoms of building materials in addition to those of water will contribute to the number of detected thermal neutrons. For example, asphalt in a roofing membrane may contribute to a reading because it contains bonded hydrogen atoms. For hydrogen-containing materials, calibration of the meter is required using samples identical to those expected during field inspection. Also, a license must be obtained from the Nuclear Regulatory Commission for domestic use of the radioactive isotopes in the neutron source of the neutron moisture meters.

8.4. Infrared Thermography

In addition to detecting heat loss, infrared thermography can be used to detect moisture in building materials if heat is flowing through them. The presence of moisture will effect the heat transfer properties of materials which permits the identification of wet areas by thermography. The principle involved in making thermography scans is discussed in section 16. This method is being used in making aerial scans of roofs, whereby large roof areas and many buildings can be scanned in a relatively short time [15]. Hand held infrared cameras also are being used to measure heat losses and to detect moisture in roofing systems [19]. See section 16 for additional applications of this method.

In using the thermography method to detect moisture in roof systems, it is necessary to assume that temperature gradients are caused by moisture and are not associated with differences in roofing composition or thickness. Because construction and thickness variations can be present, results from thermographic inspections should be interpreted carefully.

9. Paint Inspection Gage (Tooke Gage)

9.1. Principle and Applications

The paint inspection gage is used to measure dry paint film thickness by the microscopic observation of a small V-groove cut into the paint film. In addition, the number of paint layers and their individual thickness can be determined. The thickness of dry coating applied to any type of surface (e.g., wood, metal, glass, or plastic) can be measured. A commercially available paint inspection gage, the Tooke Gage, is shown on figure 9. This gage is portable having overall dimensions of 4.5 x 3.5 x 1 in (114 x 89 x 25 mm) and weighing 26 oz. (.74 kg). Three cutting tips are furnished permitting the measurement of film thickness up to 50 mils (1.3 mm).

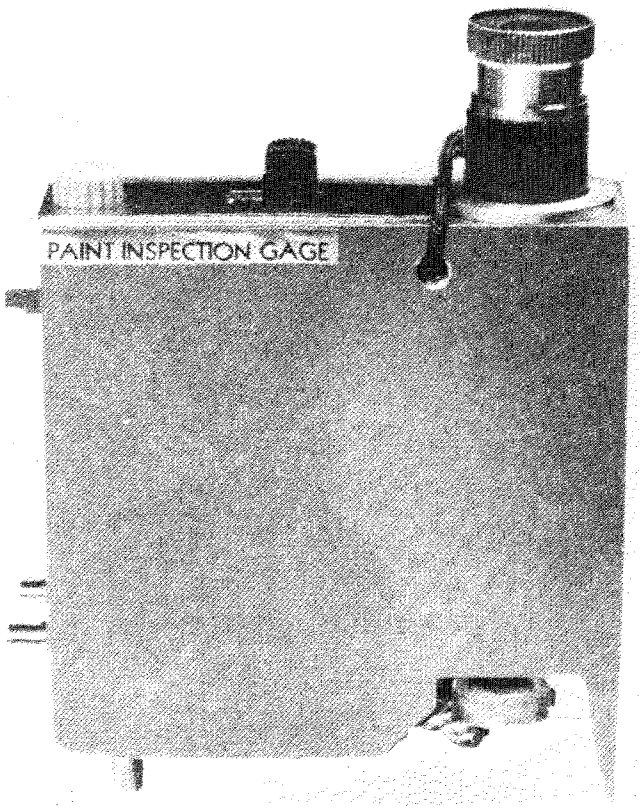

FIGURE 9. Tooke gage for measuring the thicknesses and/or number of paint layers.

9.2. Limitations

A disadvantage of this method is that a cut is made in the paint film which may need to be repaired, depending on the substrate and the severity of the environment.

10. Pin Hole Detector

10.1. Principle and Applications

A pin hole, or holiday detector, is used to determine the existence and location of pin holes (holidays) in nonconductive coatings applied to metals. Most commercial instruments consists of a probe or electrode which makes contact with the coating through a moist sponge and an earth lead such as an alligator clip (fig. 10) which is attached to an area of bare metal. When the moist sponge passes over a pin hole, an electrical circuit is completed which activates an audible alarm. Most detectors use a dc power source in the range of 9 to 67.5 V.

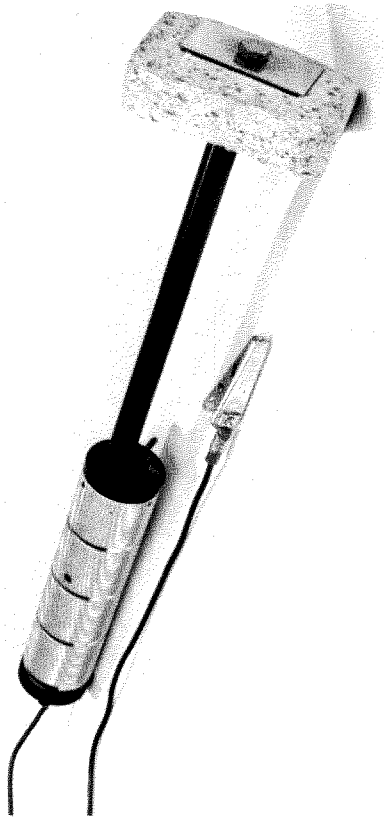

FIGURE 10. Device to inspect nonconductive coatings on metals for pin holes.

10.2. Advantages and Limitations

A large area can be rapidly surveyed for pin holes with this type of detector. Several problems can be encountered however, using this type of detector. If the metallic test object is completely coated so that a bare area does not exist, a portion of the coating must be removed so that the earth lead can make contact with the metal. Pin holes can be induced in weakened areas of a coating if high voltage (approximately 10 KV) detection is used. The results are quantitative, since no information on the size of a pin hole is obtained.

11. Proof Load Testing

11.1. Principle of Method

Proof load testing is based on the concept that a structural component or structure capable of surviving the stresses of a severe loading should be serviceable under normal operating conditions [9]. Proof loading requires the ability to overload a structure in a load pattern similar to operating conditions (e.g., high pressure in a pipeline).

11.2. Applications

Proof load testing can be used in conjunction with leak testing (section 6) in pressure vessels and pipeline inspection leak detection sensitivity levels. This method is usually used as a last resort to determine the adequacy of a structural system.

11.3. Advantages and Limitations

An entire structure can be tested in its "as-built" condition. However, the test may either cause the premature failure or the destruction of a structure. Proof load testing requires extensive planning and preparation, and is usually expensive.

12. Probe Penetration Method

12.1. Principle of Method

The probe penetration method is based on measuring the non-penetrating length steel probe which partly penetrates concrete when driven by a powder charge. This method is useful for assessing the quality and uniformity of concrete in situ, and for delineating areas of poor quality or deteriorated concrete in structures.

Probe penetration results have also been used to estimate the compressive strength of concrete by using correlation graphs. The graphs are constructed by plotting the exposed lengths of probes versus experimentally measured compressive strengths. This can be done by performing penetration tests on a concrete slab and taking core samples for compressive testing.

12.2. Probe Equipment and Use

The Windsor Probe is the most commonly selected, and possibly the only commercially available apparatus in the U.S. for measuring the penetration resistance of concrete. It consists of a special driving gun (fig. 11) into which a high-strength steel probe is inserted. This probe is driven into the concrete by firing a charge (a 32 caliber blank with a precise quantity of powder). A series of three measurements is made in each area using the spacer plate shown in figure 12. The length of a probe extending from the surface of concrete can be measured using a simple device as shown in figure 13.

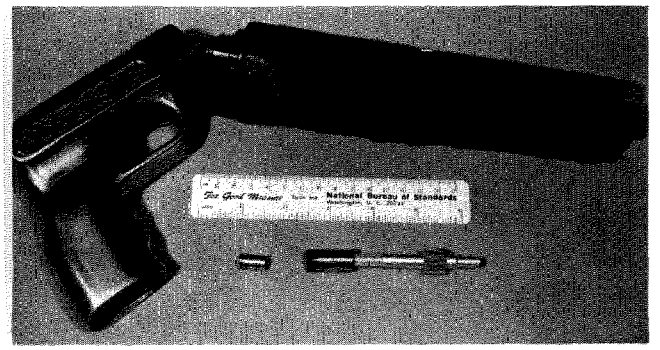

FIGURE 11. Windsor probe apparatus showing the gun, probe and blank cartridge.

FIGURE 12. Windsor probe in use.

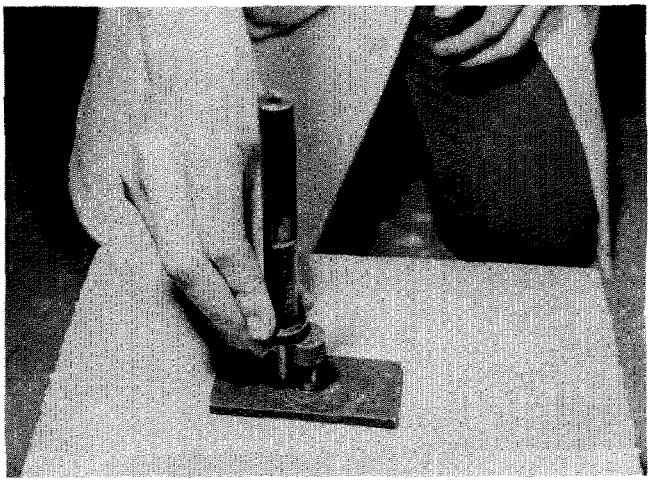

FIGURE 13. Device for measuring length of probe extending from surface of concrete.

Operating procedures for the Windsor Probe are given by the manufacturer. In addition, testing procedures are given in ASTM Standard C803 [20]. The probe can be easily operated by concrete inspectors, and is readily portable.

The manufacturer supplies a set of five calibration curves, each curve corresponding to a specific Moh's hardness for the coarse aggregate used in the concrete, by which probe measurements can be converted to compressive strength values. However, Arni [21] observed that use of the manufacturer's calibration curve often results in grossly incorrect estimates of the compressive strength of concretes. Therefore, it is recommended that the Windsor Probe should be calibrated by the individual user, and should be recalibrated whenever the type of aggregate or the concrete propagation is changed.

12.3. Applications

The Windsor Probe can be used for assessing the quality and uniformity of concrete because physical differences in concrete will affect its resistance to penetration. A probe will penetrate deeper as the density, subsurface hardness, and strength of the concrete decreases. Areas of poor concrete can be delineated by making a series of penetration tests at regularly spaced locations.

The Windsor Probe has been used to estimate the compressive strength of concrete. However, the relationship between the depth of penetration of the probe and the compressive strength can only be obtained empirically because penetration of the probe depends on a complex mixture of tensile, shear, and compressive forces [21]. The estimation of compressive strengths with the Windsor Probe, therefore, must be made using a correlation diagram with appropriate confidence limits.

The probe technique appears to be gaining acceptance as a practical NDE method for estimating the compressive strengths of concrete. Improved correlations between probe results and in-place strength can be obtained by keeping the curing conditions of the test specimens close to those expected for the in-place concrete and by making sure that the test concrete is representative of the in-place concrete. If the Windsor Probe is calibrated using concrete specimens taken from an early construction stage, the calibration chart could be used to estimate the strength of concrete placed during later stages (assuming that the concrete design is the same).

12.4. Advantages and Limitations

The Windsor Probe equipment is simple, durable, requires little maintenance, and can be used by inspectors in the field with little training. Care must be exercised, however, because a projectile is fired and safety glasses should be worn. The gun can only be fired when it is pushed against a special spacer plate.

The Windsor Probe primarily measures surface and subsurface hardness and does not yield precise measurements of the in situ strength of concrete. However, useful estimates of the compressive strength of concrete may be obtained if the probe is properly calibrated. The probe test is very useful in assessing the general quality and relative strength of concrete in different parts of a structure.

The Windsor Probe test does damage the concrete, leaving a hole of about 0.32 in (8 mm) in diameter for the depth of the probe and, also, may cause minor cracking and some surface spalling, necessitating minor repairs.

13. Radiography

Radiography enables the inspection of the internal structure of a test object through the use of penetrating radiation, which may be electromagnetic (X-ray, gamma rays, etc.) or particulate (neutrons) [1, 22, 23]. The object is exposed to a radiation beam and the intensity of the radiation passing through the object is reduced according to variations in thickness, density and absorption characteristics of the object. The quantity of radiation passing through the object is measured and used to deduce the internal structure of the test object. The types of radiation that have been most widely used are X-rays and gamma rays, with gamma rays being most commonly used during field inspections.

13.1. X-rays

X-rays are produced by bombarding a target material with fast moving, high energy electrons. The high energy electrons collide with electrons in the target, which are promoted to higher energy levels. X-rays are emitted as electrons fill the vacancies left by the promoted electrons. The generation of X-rays takes place in an evacuated chamber (X-ray tube) in which high energy electrons are generated by applying a very high voltage between an incandescent filament (the electron source) and the target material. By varying the voltage, X-rays with different penetrating abilities can be generated. For example, 200 kV (kilovolt) X-rays are capable of penetrating about 1 in (25 mm) of steel, while 400 kV X-rays can penetrate up to 2 in (51 mm) of steel [1], which is about the maximum attainable with portable equipment. In general, the penetrating ability of X-rays of a given energy level decreases as the density of the object increases. Portable gamma radiography units are available with greater penetrating capabilities than portable X-ray units. Therefore, gamma radiography is more commonly used for field inspections.

13.2. Gamma Rays

Gamma rays are physically indistinguishable from X-rays, the primary difference is the source. Gamma rays are the results of radioactive decay of unstable isotopes, and as a result there are some basic differences between gamma ray and X-ray radiography. Because gamma rays are due to nuclear disintegrations, a gamma ray source will lose its intensity with time and longer exposure times may be required for adequate inspection. In addition, each source produces rays of fixed penetrating ability. Isotopes of thulium, iridium, cesium, radium and colbalt have been used for radiography. Thulium has a penetrating ability of 1/2 in (13 mm) of steel, while cobalt produces gamma rays capable of penetrating up to 9 in (230 mm) of steel. The gamma sources usually used for inspecting concrete are given in table 1.

Note that the relative penetration abilities of the gamma rays are controlled by their energies.

13.3. Principle and Applications

Gamma or X-ray radiation is attenuated (reduced) when passing through materials. The extent of attenuation is dependent on the density and thickness of material, and on the energy of the rays. In radiography, differences in radiation attenuation produced by variations in the density and thickness of a material are

TABLE 1. *GAMMA RAY SOURCES [22]*

Radioactive Source	Gamma Energy (MeV)	Half-life ($t_{1/2}$)	Optimum Working Thickness of Concrete (mm)	Dose Rate[a]
Iridium 192	0.296 and 0.613	70 days	30-200	0.55
Cesium 137	0.66	33 years	100-300	0.39
Colbalt 60	1.17 and 1.33	5.3 years	150-450	1.35

[a]Roentgens per hour per curie at 1 m. One curie is equal to 3.7×10^{10} disintegrations per second.

recorded on photographic film. For example, when reinforced concrete is radiographically inspected, steel reinforcement attenuates the radiation more than concrete and appears as a lighter area in the film. Voids and cracks in the concrete will appear as darker areas on the film due to less attenuation of the incident radiation.

In practice, penetrating rays generated by a suitable source are allowed to pass through materials, with emerging radiation being recorded on X-ray film held in a light-tight cassette. Some of the applications of gamma radiography are inspection of concrete to locate reinforcing bars, and to determine if excess porosity or voids are present [24]; inspecting welds for cracks, voids, and slag inclusion; and inspecting masonry walls for the presence of reinforcement or grout.

13.4. Advantages and Limitations

Radiography provides a method for readily characterizing the internal features of an in-place material or building component. This method is applicable to a variety of materials. Portable gamma radiography units can have greater penetrating abilities than portable X-ray units.

The most important drawback of radiography is the health hazard associated with the penetrating radiation. A radiographic inspection program should be planned and executed by individuals who have been trained and are qualified to perform this type of inspection. All personnel involved in radiographic inspection must carry devices that monitor the radiation dosage to which they have been exposed and must be protected so that the dosage rate does not surpass Federal limits. Gamma ray sources are inherently hazardous because they emit rays continuously and high energy sources have extremely high penetrating ability. As a result, gamma ray sources require large amounts of shielding material which limits the portability of gamma radiography equipment. The use of gamma ray producing isotopes is closely controlled by the Nuclear Regulatory Commission, and a license is required to use them.

14. Seismic Testing

14.1. Principle of Method

Seismic testing is the evaluation of material integrity by analysis of shock wave transmission rates and effects [9]. An array of sensing devices around an explosive charge of known energy (the most common shock load input system) is used to record shock wave transmission rates. These shock wave transmission rates can be related to material densities. Vibrational patterns induced from shock loading can be used to determine resonant frequencies in structures.

14.2. Applications

Seismic testing can measure soil densities and locate density variation boundaries (figure 14). Soil density

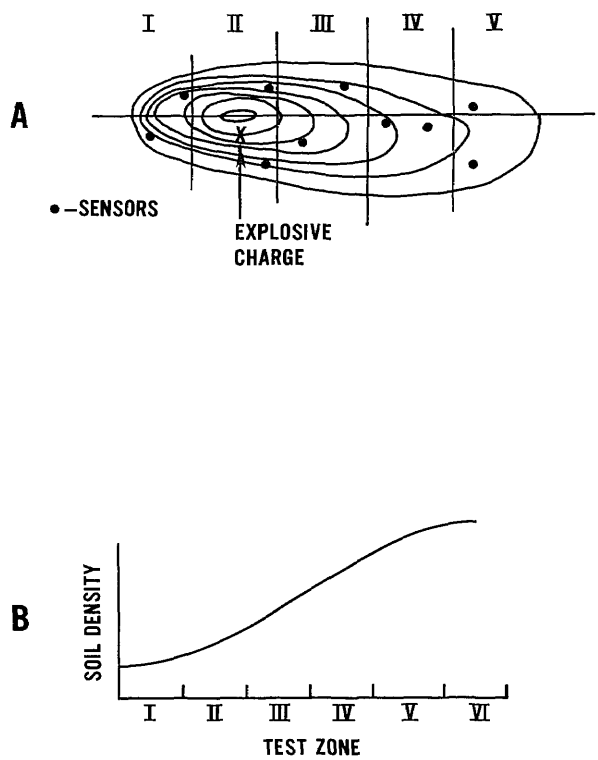

FIGURE 14. Schematic of seismic testing [9]
(A) Shock wave pattern (B) Seismic test data plot

values can then be related to load bearing capacities and foundation preparation requirements. Seismic testing can also be used to check structures for possible resonant frequencies that could cause failure under operating dynamic loads.

14.3. Limitations

Seismic testing is applicable only to monitoring soil conditions and structural vibrations. Multi-channel recording systems, power cables, and a large number of sensing devices are required for seismic testing. The hazards of explosives are also involved in the testing, but all components of a seismic test system are portable.

15. Surface Hardness Testing

Surface hardness methods are generally used to obtain an indication of the strength level or quality of a material rather than for flaw detection. Hardness in these tests refers to the resistance a material offers to indentation by an object. Indentation is produced under static or impact loading conditions; and the most common applications are in testing metals and concrete.

15.1. Static Indentation Tests

These methods are primarily used in testing metals. They commonly involve indenting the surface with an indentor of fixed geometry under specified loads [1]. The indenter has a small point and thereby produces high stresses in the metal at the point of contact. The stresses are sufficient to cause the metal to yield beneath the indenter and a permanent indentation results. The magnitude of the indentation will depend on the strength of the metal, the applied load, and geometry of the indenter. Therefore, by measuring the size of the indentation under a given set of conditions, an estimate of strength can be obtained.

15.1.1. Standard Methods

There are three widely used standard methods for hardness testing metals. The Brinell method [1] involves applying a constant load (500, 1500 or 3000 kg) on a 0.4 in (10 mm) diameter hardened steel ball-type indenter and measuring the diameter of the indentation on the test piece with a microscope. A hardness number is determined by substituting the values of the applied load, ball diameter, and indentation diameter into a standard formula. An example of a Brinell test result would be 400 HB, in which 400 is the number calculated from the standard formula, "H" stands for hardness and "B" for Brinell. For weaker metals a smaller load would be used to produce the indentation.

The Vickers method [1] is similar to the Brinell method except that a square-based pyramidal diamond indenter is used and the applied loads are much smaller. The diagonal of the square indentation is measured, and its value and the applied load are substituted into a standard equation to calculate the Vickers hardness number (HV).

The most common method is the Rockwell hardness test [1]. In this method the depth of additional permanent indentation that occurs as the load is increased from a small load to the test load is measured. The test instrument measures the depth automatically and the hardness number is read directly from a scale on the instrument. The Rockwell test can be performed much faster than the previously described methods. There are five different indenters and three different test loads that can be used; therefore, there are 15 different Rockwell hardness scales. For example, the result 60 HRC indicates a hardness number of 60 on the Rockwell C scale. The variety of scales permits testing a wide range of metals from very soft (weak) to very hard (strong).

15.1.2. Usefullness of Static Tests

Tables are available that permit conversion of the hardness number from one test method to the equivalent number of another test method (for example, ASTM E140)[25]. Tables are also available giving approximate tensile strengths of metals corresponding to the different hardness numbers. Care must be exercised in using the strength tables, because each is applicable to only certain types of metals.

Portable hardness testers are available for in-place testing of metal structures.

15.2. Rebound Hammer Method

The rebound method is based on the rebound theories of Shore [26]. He developed the Shore Scleroscope method in which the height of rebound of a steel hammer dropped on a metal test specimen is measured. The only commercially available instrument based on the rebound principle for testing concrete is the Schmidt Rebound Hammer [27].

The Schmidt Rebound Hammer has gained wide acceptance by researchers and concrete inspectors and is one of the most universally used nondestructive test methods for determining the in situ quality of concrete and for deciding when forms may be removed. Standards [28] have been drafted in Poland and Romania for the Rebound Hammer. The British Standards Institu-

tion has issued Building Standard 4408 which covers nondestructive test methods for concrete, and includes the rebound hammer method in part 4 of the Standard [28]. Recently, ASTM issued Standard C805, Test for Rebound Number of Hardened Concrete, which gives procedures for the use of the rebound hammer.

15.2.1. Description of Method

The Schmidt Rebound Hammer consists of a steel weight and a tension spring in a tubular frame (figure 15). When the plunger of the hammer is pushed against the surface of the concrete, the steel weight is retracted against the force of the spring. When the weight is completely retracted, the spring is automatically released, the weight is driven against the plunger and it rebounds.

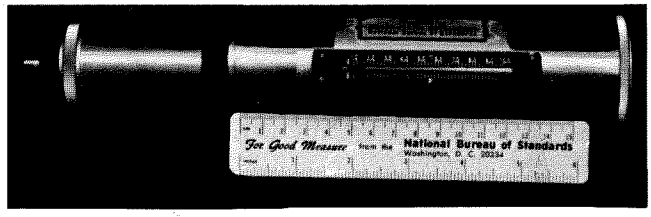

FIGURE 15. Schmidt rebound hammer.

The rebound distance is indicated by a pointer on a scale that is usually graduated from zero to 100, and the rebound readings are termed R-values. The determination of the R-values is outlined in the manual supplied by the manufacturer. R-values give an indication of the hardness of the concrete with values increasing with the hardness of the concrete.

Each hammer is furnished with a calibration chart, showing the relationship between compressive strength of the concrete and rebound readings based on data from tests conducted by the Swiss Federal Materials Testing and Experimental Institute. Users should not place too much confidence on the calibration chart, however, as they should develop their own for each concrete mix and for each rebound hammer.

15.2.2. Applications

Numerous investigators [29-31] have shown that there is some correlation between compressive strength of concrete and the hammer rebound number. Extensive disagreement exists, however, (e.g., Refs [32] and [33]) concerning the accuracy of the strength estimates from rebound measurements. Mitchel and Hoagland [34] found that the coefficient of variation for estimated compressive strength, for a wide variety of specimens from the same concrete, averaged 18.8 percent. Arni [21] found that the rebound hammer gave a less reliable estimate of compressive strength than the Windsor Probe.

Several investigators (33, 35] have attempted to establish correlations beteen the flexural strength of concrete and the hammer rebound number. Relationships similar to those obtained for compressive strengths were obtained, except that the statistical variations were even greater.

Mitchel and Hoagland [34] attempted to correlate rebound numbers with the modulus of elasticity of the concrete specimens. They concluded that no valid correlations could be made. Peterson and Stoll [29] and Klieger [36] have developed some empirical relations between the dynamic modulus of elasticity and hammer rebound.

The rebound hammer, like the Windsor Probe, is very useful in assessing the general quality of concrete and for locating areas in which poor quality concrete is located. A large number of measurements can be rapidly taken so that large exposed areas of concrete can be mapped within a few hours.

15.2.3. Advantages and Limitations

The rebound hammer provides a simple and quick method for the nondestructive testing of concrete in situ. The equipment is inexpensive, costing less than $1000, and can be operated by field personnel with a limited amount of instruction.

The rebound hammer, however, has recognized limitations. The rebound measurements on in situ concrete are affected by [4, 33, 37]:

(1) Smoothness of the concrete surface
(2) Moisture content of concrete
(3) Type of coarse aggregate
(4) Size, shape and rigidity of specimen, e.g., a thin wall or beam
(5) Carbonation of the concrete surface.

The rebound method is largely an imprecise test and it does not provide a reliable prediction of the strength of concrete. The rebound hammer, however, is very useful in the rapid assessment of the relative quality of concrete and for estimating the relative strength of concrete.

16. Thermal Inspection Methods

The presence of discontinuities in an object, such as cracks, voids or inclusions, will change the heat transfer characteristics of the object. Thus, if is a transient heat flow condition exists, there will be nonuniform surface temperatures, and the pattern of the surface temperatures can be used as an indirect indicator of sub-

surface anomalies [1]. Thermal inspection can also be used to detect anomalous operating characteristics of a system, such as over loaded electrical wiring or heat loss through walls and roofs of buildings. The following discussion will address primarily the application of thermal inspection to detect anomolies in the internal structure of test objects such as structural metallic components and roofing systems.

16.1. Principles of Thermal Inspection

To establish the conditions for thermal inspection, a heat flow situation must exist or be created. If necessary, this can be done by applying a temporary heat source to the front or back surface of the test object. The flow of heat from the warm to the cold surface will be affected by the thermal diffusivity of the material which is itself a function of its thermal conductivity, density, and specific heat. If discontinuities are present which have thermal diffusivities that differ from the bulk material, local "hot" or "cold" spots will exist on the surfaces directly over the location of the voids. Therefore, by measuring the pattern of surface temperatures under heat flow conditions, subsurface flaws can be detected.

Detection of surface temperatures can be accomplished by two methods: (1) contact inspection methods, and (2) non-contact inspection methods. With contact methods, the surface is covered with a temperature sensitive material and differences in surface temperature are recorded as a pattern of the coating material. Examples of coatings that have been developed for this application are [1]: heat sensitive paints and papers; phosphor coatings whose fluorescence under ultraviolet light is affected by temperature; melting point coatings which melt when a specific temperature is reached; and liquid crystals which undergo color changes as their temperatures are varied. Contact methods are generally not very sensitive, have relatively long response times, and require an application procedure prior to thermal inspection. Non-contact methods permit remote sensing of the thermal patterns, and are the most popular thermal inspection methods.

16.2. Infrared Thermography

16.2.1. Principle of Method

An object having a temperature above absolute zero will emit energy in the form of thermal photons. The wavelengths of the radiation fall within certain bands depending on the temperature. For example, at room temperature, the wavelengths are typically from 4 to 40 μm with a peak wavelength of about 10 μm [1]. At very high temperatures, the wavelengths of the emitted radiation are reduced to less than 1 micrometer and fall within the visible spectrum. The longer wavelength radiation associated with room temperature is not visible to the eye and is called infrared radiation. By using instruments that can detect infrared radiation, it is possible to "see" differences in surface temperatures. This is the basis of the thermal inspection method known as infrared thermography.

The rate of radiant energy emission per unit area of surface (W) is given by the Stefan Boltzmann Law:

$$W = e\delta T^4$$

where T is the absolute temperature,
e is the emissivity, and
δ is the Stefan Boltzmann constant
(5.67×10^{-12} watt/cm^2/°K^4).

Thus, changes in temperature of a surface produce more than proportional changes in emitted energy, and this enables the detection of temperature differences as low as 0.2 °C with the available detection equipment. Emissivity refers to the efficiency of energy radiation by the surface. The maximum radiation efficiency occurs in a "black body" and this is given an emissivity value of 1. All real surfaces have an emissivity while rough textured non-metals have high emissivity. Since detection methods are based on the intensity of emitted radiation, a change in emissivity at various points on the surface may be incorrectly interpreted as a change in temperature. Surfaces with non-uniform or low emissivity can be painted with high emissivity coatings.

16.2.2. Remote Inspection

Infrared thermography permits remote inspection of the test object. This is made possible because air is practically transparent to the infrared wavelengths associated with near room-temperature conditions [17]. However, high water content will reduce the transmission of infrared radiation through air so that problems may arise under humid conditions. The most common method for detecting infrared radiation is with semiconductor crystals whose electrical properties are altered by incident infrared radiation. For best sensitivity, the crystals should be kept cold with liquid nitrogen and this places some limitations on the portability of the detection systems. Dewar flasks are required to hold the liquid nitrogen, and the nitrogen needs to be replaced as it evaporates.

16.2.3. Infrared Scanners and Display

Infrared scanners consist of a sensing or camera-like unit and a display or recording unit. The elements of a camera unit are shown schematically in figure 16 and these components scan the viewed area and focus the individual "points" on a sensor or radiation detector. As shown in figure 16, the radiant flux which is related to the temperature of the selected viewing area passes through an infrared transparent lens and a mechanical-optical scanner. The mechanical-optical scanner, which consists of rotating or vibrating mirrors or prisms, provides a vertical and horizontal scan of the virtual image from the lens.

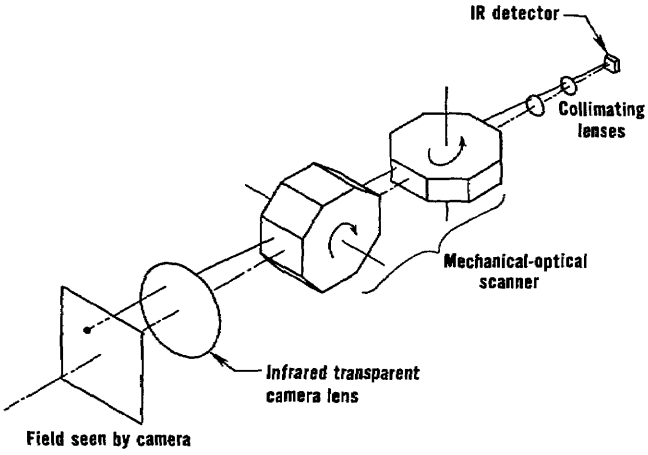

FIGURE 16. Schematic of infrared camera.

The picture is presented as shades of gray corresponding to variations in surface temperatures of the viewed object. A calibration strip is also shown so that the shades can be converted to absolute temperatures if desired. It is also possible to have a color display in which different temperatures are shown with different colors.

16.3. Applications

Thermal inspection methods have been applied for detecting disbonds in laminated materials, entrapped moisture, material density gradients, and anomalies in castings [1]. In the construction area, infrared thermography has been applied to compare thermal resistances of roofs, to detect water penetration into built-up roofs, to detect heat loss through walls and roofs of buildings, and to detect overloaded electrical circuits [17]. Recently, infrared thermography has been used to detect deteriorated regions in bridge decks [38].

16.4. Advantages and Limitations

Thermal inspection equipment is generally portable and a permanent record (photograph) can be made of the inspection results. By using thermal infrared thermography, inspections can be performed without direct access to the surface and large areas can be rapidly inspected.

In determining the size and location of detectable flaws, it should be recognized that under heat flow conditions the surface temperature patterns will be a function of the type and size of the discontinuity, the heat intensity applied or flowing to the surface of the object, and the observation time [1]. The sensitivity of infrared thermography in detecting internal flaws is a complex function of these variables. The results of such inspections, therefore, should be carefully interpreted.

17. Ultrasonic Pulse Methods

In the ultrasonic pulse methods sound waves which are beyond the audible range are induced in a test object generally by means of a peizoelectric transducer, and either reflected waves or those passing through the object are detected by a similar type of transducer [1, 4, 39-42]. When reflected waves are detected, the technique is referred to as "pulse-echo" and the transmitting transducer may also act as the receiver. Waves passing through the object (velocity method) are detected with a second transducer, i.e., a receiving transducer.

The application of ultrasonic inspection is based on two principles: (1) the velocity of the acoustic waves in a material is a function of its elastic constants and density; and (2) when an acoustic wave encounters an interface between dissimilar materials, a portion of the wave is reflected. The amount of reflection depends on the mismatch in acoustic impedance (product of wave velocity and density) of the materials with the amount of reflection increasing with the mismatch.

17.1. Ultrasonic Pulse Velocity Method

The ultrasonic pulse velocity method is one of the most universally used NDE methods for assessing the quality of concrete. It has been used in both the laboratory and in the field for the past 40 years. Some field applications have included checking the quality of concrete in bridge piers, pavements and dams.

17.1.1. Principle of Method

The ultrasonic pulse velocity method is based on measuring the travel time of an ultrasonic pulse passing

through a material. The pulse generated by an electroacoustic transducer is picked up by a receiver transducer and amplified.

The time of travel of the pulse is measured electronically [42]. A commercial instrument for measuring the ultrasonic pulse velocity of concrete is shown in figure 17.

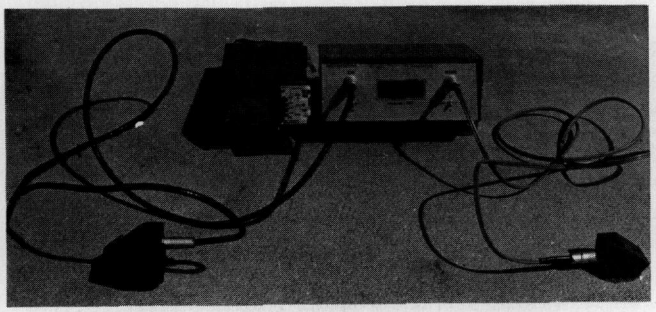

FIGURE 17. Ultrasonic pulse velocity equipment.

When a mechanical pulse is applied to a material by an electroacoustical transducer, waves are induced in the material. Usually longitudinal waves are used in testing concrete. These waves are transmitted by particles vibrating parallel to the direction of propagation. The velocity of the waves is controlled by the elastic properties and density of the material, and is virtually independent of the geometry of the object being tested.

If a longitudinal wave encounters a discontinuity such as a crack or void, it may "bend," i.e., be diffracted around the discontinuity. This increases the internal distance the wave must pass between the transmitting and pickup transducers, and consequently its travel time increases. Therefore, for a given separation of the transducers, and for a given concrete, the travel time of a longitudinal wave will be affected by changes in density and elastic properties along the travel path.

Several ultrasonic pulse velocity units are commercially available for testing concrete and cost about $4000. They can be used to test concrete having a thickness up to about 75 ft (30 m) depending on the specific model.

17.1.2. Application for Assessment of Condition of Concrete by Ultrasonic Pulse Velocity

The ultrasonic pulse velocity method is considered to be the best NDE method for determining the uniformity of in situ concrete, and ASTM Standard C 597 gives the standard test procedure to use. For example, velocity measurements have been successfully used to detect deteriorated regions in concrete bridges and the uniformity of concrete in walls [4]. In general, if substantial variations in pulse velocities are found in a structure, without any apparent reason (such as intentional changes in materials, concrete mix, or construction procedures), this indicates that unsound concrete is present.

A general rating which has been proposed [43] to assess the relative quality of concrete is presented in table . Three criteria should be used with caution as differences in the qualities of concrete cannot be as sharply delineated as indicated in table 12. In addition, velocity is affected by the density and amount of aggregate in the concrete. A crude assessment of the quality of similar types of concrete can be made, however, using these criteria. For example, if one concrete has a pulse velocity of 15,000 ft/s (4570 m/s) while another concrete with a similar composition has a velocity below 10,000 ft/s (3050 m/s), then there is clearly a significant difference in their qualities.

TABLE 2. *Pulse Velocities in Concrete* [43]

Pulse Velocity		
ft/s	m/s	General Condition
Above 15,000	(4570)	Excellent
12,000-15,000	(3660-4570)	Good
10,000-12,000	(3050-4570)	Questionable
7,000-10,000	(2130-3050)	Poor
Below 7,000	(2130)	Very Poor

17.1.3. Estimation of Strength Properties of Concrete

Numerous investigations have attempted to correlate compressive and flexural strengths of concrete with pulse velocity. Some correlations have been obtained in laboratory studies, provided that mix proportions, the cement, types of aggregate, and curing conditions were not varied. If these factors were varied, however, no usable correlations were obtained. For example, Parker [44] made a comparison of pulse velocities and compressive strengths for concretes made from only one type of aggregate but containing different cements from different sources and a variety of admixtures. His analysis of the total data indicated that at the 95 percent confidence level the estimate strength of 4440 psi (30.7 MN/m^2) concrete ranged from about 2100 to 6000 psi (14.5 to 41.8 MN/m^2). Obviously, the ultrasonic pulse method cannot be used to obtain reliable estimates of the compressive strength of concrete in structure when its composition is unknown.

Probably the best concluding remarks regarding strength prediction from wave propagation methods are those stated by Jones [45]:

"In spite of the promising results of the early investigations, it must be concluded that no general relation has been found between the dynamic modulus of elasticity and its flexural or compressive strength."

This statement still holds if one substitutes "pulse velocity" for "dynamic modulus of elasticity."

17.1.4. Extraneous Effects on Velocity Measurements

The measurement of the pulse velocity of concrete is affected by several factors which are not intrinsic properties of concrete, and, therefore, are not a function of the quality or strength of concrete [4]:

(1) Smoothness of concrete at transducer contact area. Good acoustical contact between the transducers and concrete is required. In addition, a coupling agent such as an oil or a jelly must be used.

(2) Concrete temperatures outside of the range between 41° and 86 °F (5° and 30 °C) affect the measured pulse velocity. Below this temperature range, the velocity is increased, and above the velocity is decreased.

(3) Moisture condition of concrete. Pulse velocity generally increases as the moisture content of concrete increases, while compressive strength decreases as moisture content increases.

(4) Presence of reinforcing steel. The pulse velocity in steel is 1.2 to 1.9 times the velocity in concrete. Measurements made near steel reinforcing bars, therefore, may not be representative of the concrete. If possible, measurements should be made perpendicular to the longitudinal axis of the bars. If measurements must be made parallel to the longitudinal axis of the steel bars, crude correction factors are available.

17.2. Ultrasonic Pulse Echo Method

17.2.1. Principle of Method

In the ultrasonic pulse echo method waves which are reflected off of discontinuities (e.g. cracks and voids) and from interfaces (e.g. interfaces between concrete and steel or between concrete and air) are recorded. Both the transmitting and receiving transducers are contained in the same probe, thus, only those waves which are reflected back at nearly 180° to the incident waves are detected. The penetrating ability of the ultrasonic pulse and the minimum size of detectable flaws are influenced by the frequency of the generated waves. High frequency results in less penetration but better sensitivity than low frequency.

17.2.2. Applications

Echo techniques have been extensively used to identify and locate discontinuities and defects in metals and welds [1, 39-41]. The echo technique is one of the most versatile and accepted NDE methods for metals. However, its application to concrete has been slow, largely because the extensive pore system, presence of cracking, and the heterogeneous nature of concrete result in multiple reflections when high frequency pulses are used which both significantly attenuate the reflected waves and complicate the interpretation of the observations. It may, however, be possible to combine the echo method with acoustic impact (see section 2) so that low frequency waves are generated which would be insensitive to microscopic flaws but could be used to detect large discontinuities. Commercial equipment is not at present available for this type of testing.

17.2.3. Advantages and Limitations

Ultrasonic pulse-echo inspection offers several advantages over other NDE methods capable of detecting internal flaws in a test object such as gamma radiography [1]. For example, acoustic waves have excellent penetrating ability, and with proper instrument selection thick sections on the order of 10 m or more can be inspected. Very small flaws may be detected and their location and geometry may be estimated with reasonable accuracy. In addition, test results are immediately available, the equipment is lightweight and portable, and acoustic waves pose no known health hazard.

Because of the indirect nature of flaw detection by ultrasonic pulse-echo inspection, a high level of expertise is required to plan an inspection program. A thorough understanding of the nature of the interactions between the acoustic waves and different discontinuities is required in order to properly interpret test results. The physical testing, on the other hand, may be performed by technical level personnel after proper training. Before ultrasonic inspection equipment can be used, calibration and referencing with standards must be performed, otherwise test results are difficult to interpret. The nature of the calibrations will depend on the particular inspection program.

18. Visual Inspection

Often surface defects can be detected visually using methods to enhance ordinary visual acuity. Optical magnification or other techniques which can be used to increase the apparent size of surface cracks are covered in this section.

18.1. Optical Magnification

Available magnifying instruments range from simple inexpensive glasses to expensive microscopes. Some fundamental principles about the operating characteristics of magnification instruments need to be understood before selecting a system for a particular application. First, the focal length decreases as the magnification power increases. This means that when high magnification is desired, the primary lens must be placed close to the test object. The field of view (that portion of the object that can be seen at any instant) also decreases as magnification power increases. A small field of view means that it will be tedious to examine a large surface area. Another important parameter is the depth of field, which refers to the elevation difference of rough textured surfaces that can be viewed in focus simultaneously; the depth of field decreases as the magnification power of the instrument increases. Therefore, to inspect a rough-textured surface, a magnification power should be selected that gives a sufficiently large depth of field so that the "hills" and "valleys" will be simultaneously in focus. Finally, the illumination intensity required to clearly see surface flaws will increase as the magnification power increases. High magnification may require using a supplementary light source to augment the available lighting.

A useful tool for field inspection is a pocket magnifier with a built-in measuring scale which enables measurement of flaw dimensions. A stereomicroscope is very useful when a three-dimensional view of the surface is required. With this instrument one can determine whether a crack is shallow or extends for considerable distance into the object. By calibrating the focus adjustment, a stereomicroscope can also be used as a depth gage to measure the approximate height of surface irregularities.

18.2. Fiberscope

Another useful instrument is the fiberscope, which is composed of a bundle of flexible optical fibes and lens systems. The fiberscope can be used to look inside a cavity by inserting it through a small access hole. Some of the fibers in the bundle are used to carry light into the cavity and illuminate the field of view. The viewing head can be rotated so that a wide viewing angle is possible from a single access hole. A fiberscope, because of the discrete nature of light transmission by the fibers may not have as good a resolution ability as a boroscope, which is a straight rigid tube using a lens system for viewing. The best resolution is obtained by an instrument with small diameter fibers in which the fiber density per unit area is high. To use a fiberscope requires drilling access holes if natural channels are not present, and the holes must intercept cavities. The acoustic impact technique (section 4.2) can be used to locate hollow spots for subsequent fiberscope inspection.

18.3. Liquid Penetrant Inspection

In this method a highly visible dye is used to coat the surface to be inspected [1, 46]. Any cracks that are open to the surface will soak up the dye because of surface tension and capillary effects. After application of the dye the surface is cleaned. The dye which penetrated into cracks remains and can be visually observed, thereby disclosing the presence of cracks. The method is one of the most inexpensive inspection methods available. It only enables detection, however, of open flaws that intersect the surface of the object.

18.3.1. Description of Method

Dye penetration inspection involves the following steps: (1) cleaning the surface; (2) applying the dye; (3) removing excess dye from surface; (4) applying a developer; and (5) interpreting the results.

The objective of the cleaning procedure is to remove foreign matter from within cracks so that dye can penetrate into them. The specific procedures to be used will depend on the condition of the surface. Care must be taken to ensure that the cleaning process does not smear the cracks or fill the cracks with residues. For example, sandblasting a soft metal may "hammer" the surface to such an extent that cracks become closed and undetectable.

The dye may be applied to the surface by spraying, painting or dipping. Two types of dye are available: one is for viewing under ordinary light and is usually a brilliant red color; the other is fluorescent and viewed under ultraviolet light. Fluorescent dyes offer the best sensitivity for detecting small cracks. The dye is allowed to remain on the surface from 10 to 30 min (dwell time) before cleaning the surface.

Cleaning can be done by flushing the surface with water or by wiping with a rag dampened with solvent. For water cleaning, the dye requires an emulsifying agent so that it can be completely removed with water.

The agent is either already included within the dye or it is added to the coated surface prior to washing. This phase is very important; all excess dye needs to be removed otherwise there will be false indications of cracks. If the surface is very porous, inspection by this method may be difficult; if dye is not removed from the pores, there will be a loss of contrast as the surface will take on a color that is a light shade of the dye. If dye is removed from all pores, it will probably also be removed from some of the cracks.

After cleaning, the surface is allowed to dry and a developer is added. Developer is a fine powder added for two reasons: (1) it provides a uniform colored background which increases contrast; and (2) it has a blotting effect, thereby drawing up the dye from within the cracks. The blotting action increases the apparent width of the cracks so that they become more visible. Developer can be applied as a dry powder or as a paint. The thickness of the developer layer is important, if it is too thin there may not be good contrast; and if it is too thick, it may mask the cracks.

Finally, the prepared surface is inspected. If the application procedure was correctly performed, the presence of cracks will be clearly shown. However, the inspector needs to be familiar with the patterns associated with "irrelevant indications," i.e., patterns not due to cracks but due to other sources such as improper cleaning.

18.3.2. Advantages and Limitations

Although dye penetrant inspection relies on simple principles, a certain amount of skill is necessary to properly carry out the process. The operator needs to know which materials to use for a particular application and to understand how the materials respond to different temperature conditions. Portable kits are available in which the various chemicals are contained in aerosol cans, thus making field inspection possible. At present, the technology has been developed primarily for inspection of metals, and the applicability of the procedures to masonry or concrete structures with surfaces of high porosity has not been demonstrated.

COMBINATIONS OF NONDESTRUCTIVE EVALUATION METHODS

While no single NDE method may be entirely satisfactory for predicting the strength or quality of a material, combinations of methods which respond to different factors may give more definite information. The combined NDE approach has been largely developed for evaluating concrete and, therefore, only applications to concrete will be described.

To predict the compressive strength of in situ concrete more accurately, the results of two or even three different NDE methods have been combined. The most popular combination has been the ultrasonic pulse velocity method in conjunction with the rebound hammer [47]. Other common combinations are the ultrasonic pulse velocity method and the measurement of the damping constant of concrete [48], and the ultrasonic pulse velocity and pulse attenuation methods [49]. The latter two combinations are essentially laboratory research techniques and therefore will not be discussed further.

The results of two methods can be combined in a linear equation of the form:

$$f'_c = A(\mathrm{NDE}_1) + B(\mathrm{NDE}_2) + C$$

where f'_c is the estimated compressive strength from the combined method, NDE_1 and NDE_2 are the results of the individual methods, and A, B, and C are empirically determined constants.

Combination of Ultrasonic Pulse Velocity and Rebound Hammer Methods

This combination of nondestructive tests has been used in Europe, primarily, with the most exhaustive studies being carried out by Facaoaru [50-53]. In this combined approach, measurements of ultrasonic pulse velocity and rebound number are made in situ on concrete. The pulse velocity and rebound number are substituted into a previously derived regression equation to predict compressive strength. It is believed that the multiple regression equation should give a more accurate estimate of compressive strength than either of the individual measurements alone.

Facaoaru [50] has developed calibration charts for standard concrete mixes from which the compressive strengths can be estimated when the pulse velocities and rebound numbers are known. Correction factors have also been developed to be used in the case of nonstandard concrete mixes. This combined method has been used often in Romania to estimate the compressive strength of in situ concrete [50, 52]. Based on his experiences, Facaorau contends that by using the combined method, the following accuracy in predictions of compressive strengths can be obtained:

(1) When composition is known and test specimens or cores are available for calibration purposes, accuracy is within 10 to 15 percent.

(2) When only the composition of the concrete is known, accuracy is within 15 to 20 percent.

(3) When neither the composition is known nor test specimens or cores are available, accuracy is within 20 to 30 percent.

This suggests that, for case (3), the combined method gives no better prediction of the compressive strength than can be obtained by measuring only the ultrasonic pulse velocity or only the rebound number; in case (2), the improvement is marginal. Therefore, only when the concrete is well characterized is this combined method better than the individual nondestructive methods.

SUMMARY

Nondestructive evaluation methods (NDE) offer significant advantages over traditional methods for determining the properties of building materials. One of these is the ability to make in-situ measurements of the materials, which virtually eliminates the specimen preparation costs used with ordinary strength testing methods. In-situ measurements are especially valuable in concrete technology because the characteristics of hardened concrete are affected by such factors as thermal history, presence of moisture and degree of compaction. Testing concrete in the structure ensures that these factors have been included. Another advantage of NDE methods is that they enable re-testing of the material or component at later ages so that material degradation with time can be determined. Finally, a majority of the NDE methods are economical and simple tests, permitting a larger number of tests for the same effort, compared with traditional test methods.

A key feature in the successful application of NDE methods is an understanding of their operating principles and their inherent limitations. These aspects have been emphasized in the paper are summarized in table 3. The numbers shown for each method refer to the section numbers in the text. The principle of operation will often dictate the types of materials and the nature of the characteristics that can be probed with each method.

In selecting which particular NDE method one should use, consideration should be given to the following factors: (1) the type of material, since many methods are applicable to only a particular type, such as concrete or steel; (2) the properties being sought; (3) the level of expertise required not only to perform but also to interpret the tests; and (4) the desired level of accuracy.

The required calibration procedure should also be considered as this may increase the total effort to perform an acceptable nondestructive inspection program.

The reliability of each method for a particular application depends on the relationship between the quantity measured directly by the method and the desired property. Methods are less reliable if their measurements are strongly affected by factors which have negligible effect on the desired properties. Reliability can often be improved by careful calibration of the method; this is especially critical to some of the NDE methods for concrete strength prediction.

The future offers many opportunities for the growth of NDE methods in building technology. The demand for such techniques is increasing, as is the level of research to refine existing methods and develop new ones. It is anticipated that the exploitation of microcomputers will lead to a new generation of methods capable of measuring characteristics that are presently beyond our reach.

Preparation of this report was sponsored by the U.S. Army Construction Engineering Laboratory, Champaign, IL 61820. The authors appreciate the valuable suggestions and information provided by Dr. Paul Howdyshell of the Engineering Laboratory and by Mr. Harry Berger, Office of Nondestructive Evaluation, National Bureau of Standards.

TABLE 3. *Survey of Commonly used NDE Methods for Inspection Building Materials*

Method	Principle	Main Applications	Equipment Cost	User Expertise	Advantages	Limitations
1. Acoustic Emission	During crack growth or plastic deformation, the rapid release of strain energy produces acoustic (sound) waves that can be detected by sensors attached to the surface of a test object.	Continuous monitoring of structure during service life to detect impending failure; monitoring performance of structure during proof testing.	$10,000 for single pickup, up to $100,000 for multichannel pickup.	Extensive knowledge required to plan test and to interpret results.	Monitors structural response to applied load; capable of detecting onset of failure; capable of locating source of possible failure.	Requires means of loading structure; complex electronic equipment is required.
2. Acoustic Impact (Hammer Test)	Surface of object is struck with hammer (usually metallic). The frequency, through transmission time, and damping characteristics of the "ringing" can give an indication of the presence of defects.	Detect delamination or disbonds in composite systems; detect voids and cracks in materials, e.g. hammer technique detect defective masonry units; "chain drag" method to detect delaminations in concrete pavements. Can be used to measure the modulus of elasticity of wood.	Negligible for manual technique, $3000 for measuring devices.	Low level of expertise required to use, but experience needed for interpreting results.	Portable; easy to perform; electronic device not needed for qualitative results.	Geometry and mass of test object influences results; poor discrimination; reference standards required for electronic testing.
3. Cast-in-Place Pullout	Measure the force required to pull out the steel rod with enlarged head cast in concrete. Pullout forces produce tensile and shear stresses in concrete.	Estimation of compressive and tensile strengths of concrete.	$1000 to $6000	Low, can be used by field concrete testers and inspectors.	Only NDE method which directly measures inplace strength of concrete; appears to give good prediction of concrete strength.	Pullout devices must be inserted during construction. Cone of concrete may be pulled out, necessitating minor repairs.
4. Electrical Potential Measurements	Electrical potential of steel reinforcement measured. Potential indicates probability of corrosion.	Determining condition of steel rebars in concrete	$1000 to $2000	Moderate. User must be able to recognize problems.	Portable equipment; field measurements readily made; appears to give reliable information.	Does not provide information on rate of corrosion. Requires access to reinforcing bars.
5.1 Eddy Current	An electrically excited coil induces eddy current flow and an associated electromagnetic field in metal. Flaws alter induced electromagnetic field which in turn	Inspection of metal parts for cracks, inclusions, seams and laps; measurement of thickness of nonmetalic coating on metals; detection of improper alloy composition.	Minimum $3000	Moderate.	Extremely sensitive to change in properties and characteristics of metal; portable.	Requires calibra- with standards; limited depth of penetration; only applicable to metals; sensitive to geometry of part.

TABLE 3. (*Cont.*)

	alters the impedance of the excitation coil. Change in coil impedance indicates presence of flaw or anomaly.					
Method	Principle	*Main* Applications	*Equipment* Cost	*User* Expertise	Advantages	Limitations
5.2 Magnetic Field Testing	An electrically energized primary coil is brought near test object, a voltage is induced in a secondary coil and its magnitude is compared to a reference standard. Magnetic properties of test object affect induced voltages.	Distinguishing between steels based on differences in composition, hardness, heat treatment, or residual stresses; locating hidden magnetic parts; measuring thickness of nonmagnetic coatings or films.	$3000	Low to moderate depending on application.	Portable; rapid test; easily detects magnetic objects even if embedded in nonmagnetic material.	Applicable only to ferromagnetic alloys; reference standards and calibration may be required for some applications.
5.3 Covermeter	Presence of steel affects the magnetic field of a probe. Closer probe is to steel, the greater the effect. Principle of operation is similar to eddy current method.	Determination of presence, location and depth of rebars in concrete and masonry units.	$800 to $1500	Moderate. Easy to operate. Training needed to interpret results.	Portable equipment, good results if concrete is lightly reinforced.	Difficult to interpret results if concrete is heavily reinforced or if wire mesh is present.
5.4 Magnetic Particle Inspection	Presence of discontinuities in ferromagnetic material will cause leakage field to be formed at or above the discontinuity when the material is magnetized. The presence of the discontinuity is detected by use of ferromagnetic magnetic particles applied over the surface which form an outline of the discontinuity.	Usually used to detect fatigue cracks inservice metal components and inspection during production control. Applicable to inspecting welds.	Minimum $2000	Expertise required to plan nonroutine tests. Moderate expertise to perform test.	Capable of detecting subsurface cracks if they are larger than surface cracks; size and shape of component poses no limitation; portable equipment available.	Non-ferromagnetic metal cannot be inspected; coatings affect sensitivity; demagnetization may be required after testing.
6. Leak Testing	Telltale substances added to piping system under pressure reveal presence of	Detection of leaks in pipes carrying fluids.	Wide range depending on detection method. $100 to $5000.	Low to high depending on application.	Can locate leaks too small to be found by any other NDE method.	Difficult to determine position of leaks in pipes hidden in wall or floor cavities.

TABLE 3 (*Cont.*)

Method	Principle	Main Applications	Equipment Cost	User Expertise	Advantages	Limitations
	leaks. Sound amplification to detect leak.					
8.1 Moisture Meter-Electrical Resistance Probe	Electrical resistance between two probes inserted into test component is measured. The resistance decreases with increased moisture contents.	Measurement of moisture contents of timber, roofing materials and soils.	$300 to $1000	Low	Equipment is inexpensive, simple to operate and many measurements can be rapidly made.	Not reliable at high moisture contents; needs to be calibrated; precise results are not usually obtained.
8.2 Moisture Meter-Capacitance	Water affects dielectric constant and the dielectric loss factor of materials. Measurement of either property can be used to estimate moisture contents.	Measurement of moisture contents of timber and roofing materials.	$2,000 to $5,000	Low level of expertise required to use but experience needed to plan test.	Portable; simple to operate; effective over a wide range of moisture contents.	Measurement is only of surface layer; calibration required; results affected by roofing aggregates; other factors affect accuracy.
8.3 Moisture Meter-Neutron	Fast neutrons are slowed by interactions with hydrogen atoms. Backscattered slowed neutrons are measured, the number of which are proportional to the amount of hydrogen atoms present in a material.	Moisture content measurements of soil and roofing materials.	$4000 to $6000	Must be operated by trained and licensed personnel.	Portable; moisture measurements can rapidly be made on in-service materials.	Only measures moisture content of surface layer (50 mm); dangerous radiation; hydrogen atoms of building materials are measured in addition to those of water.
8.3 Nuclear Density Meter	Gamma rays are used to measure mass density. The energy loss of the emitted gamma rays is proportional to the mass density of the material through which the rays pass.	Measurement of density of soils.	$4000 to $6000	Must be operated by trained and licensed personnel.	Portable; density measurements can be made without disturbing the soil.	Calibration necessary; dangerous radiation; only measures density of surface layers.
9. Tooke Gage	A V-groove is cut into the coating and an illuminated magnifier equipped with a reticle in the eyeplace is used to	Measurement of the number and thickness of paint layers.	$1300	Low	Simple to operate, portable; measurement can be made with any type of substrate.	Small scratch is made in coating and the substrate is exposed.

TABLE 3 (*Cont.*)

Method	Principle	Main Applications	Equipment Cost	User Expertise	Advantages	Limitations
	measure the number and thickness of the films.					
10. Pin Hole (Holiday) Meter	An earth load is connected to a conductive substrate and a probe (a moistened sponge) is passed directly over a coating. An alarm is sounded when the circuit is completed resulting from the probe contacting a pin hole (holiday).	Determining the presence of pin holes in non-conductive coatings over metals.	$200 to $1000	Low	Simple to operate; portable.	Results are qualitative, e.g., there is no measure of the pin hole size.
11. Proof Loading	Structure or system is subjected to loads and respond is measured.	Determining safe capacity and integrity of structures. Leak testing of pressure vessels and plumbing.	Wide, depending on application; often high.	Depends on nature of tests; can be high.	Entire structure can be tested in its "as-built" condition.	Can be very costly; instrumentation required to measure response; careful planning required; can damage structure.
12. Windsor Probe	Probe fired into concrete and depth of penetration is measured. Surface and subsurface hardness measured.	Estimations of compressive strength, uniformity and quality of concrete.	$1000 plus cost of probes.	Low, can be operated by field personnel.	Equipment is simple and durable; good for determining quality of concrete.	Slightly damages small area; does not give precise prediction of strength.
13.1 X-ray Radiography	Similar to gamma radiography, except X-rays are used.	To identify hidden construction features in wooden structures.	Field Equipment in excess of $5000	Should be operated by trained personnel because of radiation.	Portable equipment available, intensity of radiation can be varied.	Dangerous radiation; portable units have low intensities and field applications limited to wooden and thin components; opposite surface of component must be accessible.
13.2 Gamma Radiography	Gamma radiation attenuates when passing through a building component. Extent of attenuation controlled by density and thickness of the materials of the building component. Photo-	Locating internal cracks, voids and variations in density and composition of materials. Locating internal parts in a building component, e.g. reinforcing steel in concrete.	$5000 to $10,000	Must be operated by trained and licensed personnel.	Portable and relatively inexpensive compared to X-ray radiography; internal defects can be detected; applicable to a variety of materials.	Radiation intensity cannot be adjusted; long exposure times may be required; dangerous radiation; two opposite surfaces of component must be accessible.

TABLE 3. (*Cont.*)

Method	Principle	Main Applications	Equipment Cost	User Expertise	Advantages	Limitations
	graphic film record usually made, which is analyzed.					
14. Seismic Testing	Integrity of material evaluated by analysis of shock wave transmission and effects. Shock wave induced by explosive charges and transmission detected by transducers.	Determination of soil densities and variation in densities. Also vibrational characteristics of buildings can be determined.	Wide, depending on amount of information desired.	Experience required to plan test and to interpret results.	Large area of soil and entire structure in its "as-built" condition can be tested.	If incorrectly placed, explosive charge could damage structure; care must be exercised in handling explosives.
15.1 Indentation Hardness Test	Pointed probe is mechanically forced into surface of a material, usually a metal, under a specified load. The depth of identification is measured and strength of materials may be estimated.	Determination of effectiveness of heat treatment on hardness of metals. Estimating tensile strength of metals.	$600 to $4000	Low.	Portable equipment available; fast and easy test to perform.	Conversion tables give only approximate tensile strengths; feasibility of testing limited by size and geometry of component.
15.2 Rebound Hammer	Spring driven mass strikes surface of concrete and rebound distance is given in R-values. Surface hardness is measured.	Estimation of compressive strength, uniformity and equality of concrete.	$250 to $600	Low, can be readily operated by field personnel.	Inexpensive; large amount of data can be quickly obtained; good for determining uniformity of concrete.	Results affected by condition of concrete surface; does not give precise prediction of strength.
16. Thermal Inspection	Heat sensing devices are used to detect irregular temperature distributions due to presence of flaws or inhomogenities in a material or component that have different impedances to heat flow. Contours of equal temperature (thermography) or temperatures (thermometry) are measured over the test surface with	Detection of heat loss through walls and roofs; detection of moisture in roofs; detection of delamination in composite materials.	$30,000 for infrared scanning camera. Less expensive hand held equipment becoming commercially available.	Moderate to extensive depending on nature of test.	Portable; permanent record can be made; testing can be done without direct access to surface and large area can be rapidly inspected using infrared cameras.	Costly equipment; referenced standards needed; means of producing thermal gradient in test component or material is required.

TABLE 3. (*Cont.*)

Method	Principle	Main Applications	Equipment Cost	User Expertise	Advantages	Limitations
	contact or non-contact detection devices. A common detection device is an infrared scanning camera.					
17.1 Ultrasonic Pulse Velocity	Based on measuring the transit time of an induced pulsed compressional wave propagating through a material.	Estimation of the quality and uniformity of concrete.	$4000 to $6000	Low level required to make measurements.	Excellent for determining the quality and uniformity of concrete; test can be quickly performed.	Does not provide estimate of strength; skill required in analysis of results; moisture variation can affect results.
17.2 Ultrasonic Pulse Echo	Pulse compressional waves are induced in materials and those reflected back are detected. Both the transmitting and receiving transducers usually are contained in the same probe.	Inspecting metals for internal discontinuities. Some work has been performed on the use of the pulse echo method to inspect concrete.	Minimum $5000	High level of expertise required to interpret results.	Portable; internal discontinuities can be located and their sizes estimated.	Good coupling between transducer and test substrate critical; interpretation of results can be difficult; calibration standards required.
18.2 Fiberscope (Endoscope)	Bundle of flexible, optical fibers with lens and illuminating systems is inserted into small bore hole thus enabling view of interior of cavities.	Check condition of materials in cavity, such as thermal insulation in wall cavities, pipes and electrical wiring in cavity walls; check for unfilled cores in reinforced masonry construction; check for voids along grouted stressed tendons.	$3000 to $6000	Low.	Direct visual inspection of otherwise unaccessible parts is possible.	Probe holes usually must be drilled; probe holes must connect to a cavity.
18.3 Liquid Penetrant Inspection	Surface is covered with a liquid dye which is drawn into surface cracks and voids. Developer is applied to reveal presence and location of flaws.	Detection of surface cracks and flaws. Usually used to inspect metals.	$50 to $250 per 100 linear feet of inspection.	Low.	Inexpensive; easy to use; can be applied to complex parts; results are easy to interpret.	Detects only surface flaws, false indications possible on rough or porous materials; surface requires cleaning prior to testing.

REFERENCES

[1] Metals Handbook, Vol. 11, Nondestructive Inspection and Quality Control, 8th Edition (American Society of Metals, Metals Park, Ohio, 1976).

[2] Botsco, R.J., Specialized NDT Methods, Lesson 12, Fundamentals of Nondestructive Testing (Metals Engineering Institute, 1977).

[3] Tentative Test Method for Pullout Strength of Hardened Concrete, American Society for Testing and Materials (ASTM) Designation C900-78T.

[4] Malhotra, V.M., Testing Hardened Concrete: Nondestructive Methods, American Concrete Institute Monograph No. 9 (Detroit, 1976).

[5] Richards, O., Pullout Strength of Concrete, in Reproducibility and Accuracy of Mechanical Testing, ASTM STP626, pp. 32-40, (1977).

[6] Mailhot, G., Bisaillon, A., Carrette, G.G., and Malhotra, V.M., In-Place Concrete Strength: New Pullout Methods, ACI Journal. Vol. 76, pp. 1267-1282 (1979).

[7] Clear, K.C., and Hay, R.E., Time-to-Corrosion of Reinforcing Steel in Concrete Slabs, Vol. 1, Effects of Mix Design and Construction Parameters, Federal Highway Administration Report. No. FHWA-RD073-32 (Washington, D.C., 1973).

[8] McGonnagle, W.J., *Nondestructive Testing*, Gordan and Breach, New York, (1969).

[9] Sevall, G.W., Nondestructive Testing of Construction Materials and Operations, Construction Engineering Research Laboratory Technical Report M-67 (Champaign, Illinois, 1973).

[10] Dunn, F.W., Magnetic Particle Inspection Fundamentals, Lession 3, ref. 2.

[11] Betz, C.E., Magnetic Particle Inspection Applications, Lesson 4, ref. 2.

[12] Cantor, T.R. and Knecter, C.P., Verification of Radar NDE of 700 ft of the GWB, PAIVYNI Engineering R & D Report No. El-3 (New York Port Authority, 1981).

[13] Cantor, T.R. and Knecter, C.P., Radar and Acoustic Emission Applied to Study of Bridge Decks Suspension Cables and Masonry Tunnel, Transportation Research Paper 676 (1978).

[14] Alongi, A.V., Radar Examination of Condition of Two Interstate Highway Bridge decks, Penetradar Corp. (Niagara Falls, 1973).

[15] Bushing, H., Mathey, R., Rossiter, W., and Cullen, W., Effects of Moisture in Built-up Roofing—A State-of-the-Art Literature Survey, National Bureau of Standards Technical Note 965 (1978).

[16] Boot, A. and Watson, A., Applications of Centimetric Radiowaves in Nondestructive Testing, in Application of Advanced and Nuclear Physics to Testing Materials, ASTM STP-373, pp. 3-24 (1965).

17] Jenkins, D.R., Knab, L.J., and Mathey, R.G., Moisture Detection in Roofing by Nondestructive Means, A State-of-the-Art Survey, National Bureau of Standards Technical Note 146 (1981).

18] Knab, L., Mathey, R., and Jenkins, D., Laboratory Evaluation of Nondestructive Methods to Measure Moisture in Built-Up Roofing Systems, National Bureau of Standards Building Science Series 131 (1981).

19] Tobiasson, W. and Korhonen, C., Summary of Corps of Engineering Research on Roof Moisture Detection and the Thermal Resistance of Wet Insulation, Cold Regions Research and Engineering Laboratory Special Report 78-29 (1978).

[20] Test for Penetration Resistance of Hardened Concrete, ASTM Designation C803.

[21] Arni, H.T., Impact and Penetration Resistance Tests of Portland Cement Concrete, Federal Highway Administration Report No. FHWA-RD-73-5 (1972).

[22] Aman, J.K., Carney, G.M., McBride, D., and Turner, R.E., Radiographic Fundamentals, Lesson 8, ref. 2.

[23] McBride, D., Carney, G., Turner, R., and Lomerson, E.O., Fundamentals of Radiography, Lesson 9, ref. 2.

[24] Forrester, J.A., Gamma Radiography of Concrete, Proceedings of Symposium on Nondestructive Testing of Concrete and Timber, Session No. 2, pp. 9-13, Institute of Civil Engineers (London, 1969).

[25] Standard Hardness Conversion Tables for Metals, ASTM Designation E140.

[26] Shore, A.T., Properties of Hardness in Metals and Materials, Proceedings ASTM, Vol. 9, pg. 733, (1911).

[27] Schmidt, E., A Nondestructive Concrete Test, Concrete, Vol. 59, (No. 8), pg. 34 (1951).

[28] Clifton, J.R., Nondestructive Test to Determine Concrete Strength—A Status Report, NBSIR 75-729, National Bureau of Standards (1975).

[29] Peterson, P.H. and Stoll, V.W., Relation of Rebound Hammer Test Results to Sonic Modulus and Compressive-Strength Data, Proceedings, of Highway Research Board, Vol. 34, pg. 387, (1955).

[30] Boundy, C. and Hondrus, G., Rapid Field Assessment of Strength of Concrete by Accelerated Curing and Schmidt Rebound Hammer, Journal of American Concrete Institute, Vol. 61, (No. 1), pg. 1 (1964).

[31] Victor, D.J., Evaluation of Hardened Field Concrete with Rebound Hammer, Indian Concrete Journal, Vol. 37, (No. 11), pg. 407 (1963).

[32] Green, G.W., Test Hammer Provides New Method of Evaluating Hardened Concrete, Journal of American Concrete Institute, Vol. 26, (No. 3), pg. 249, (1954).

[33] Discussion of Reference 32, Journal of American Concrete Institute, Vol., 27 (No. 4), pg. 256, (1955).

[34] Mitchel. L.J., and Hoagland, G.G., Investigation of the Impact-Type Concrete Test Hammer, Highway Research Board Bulletin 305, pg. 14, (1961).

[35] Williams, C.H., Investigation of the Schmidt Concrete Test Hammer, Miscellaneous Report No. 6-267, U.S. Army Engineer Waterways Experiment Station (Vicksburg, Mississippi, 1958).

[36] Discussion of Reference 29 by Klieger, Proceedings of Highway Research Board, Vol. 34, pg. 392, (1955).

[37] Erickson, G.A., Investigation of the Impact-type Concrete Test Hammer, Model II, Concrete Laboratory Report C-928, Division of Engineering Laboratories, Dept. of the Interior (Denver, 1959).

[38] Manning, D.G. and Holt, F.B., Detecting Delamination of Concrete Bridge Decks, Concrete International, Vol. 2, No. 11, pg. 34-41 (1980).

[39] Smith, A.L., Ultrasonic Testing Fundamentals, Lesson 5, ref. 2.

[40] Lovelace, J.F., Ultrasonic Testing Equipment, Lesson 6, ref. 2.

[41] Moberg, A.J., Ultrasonic Testing Applications, Lesson 7, ref. 2.

[42] Whitehurst, E.A., Evaluation of Concrete Properties from Sonic Tests, American Concrete Institute Monograph No. 2 (Detroit, 1966).

[43] Leslie, J.R. and Cheesman, W.J., An Ultrasonic Method

of Studying Deterioration and Cracking in Concrete Structures, Journal of American Concrete Institute, Vol. **46**, (No. 1), pp. 17-36 (1949).

[44] Parker, W.E., Pulse Velocity Testing of Concrete, Proceedings ASTM, Vol. 53, pg. 1033 (1953).

[45] Jones, R., *Nondestructive Testing of Concrete*, Cambridge University Press, Oxford, (1962).

[46] Lomerson, E.O., Liquid Penetrants, Lesson 2, ref. 2.

[47] Jones, R. and Facaoaru, Analysis of Answers to a Questionnaire on the Ultrasonic Pulse Technique, RILEM Materials and Structures, Vol. 1 (No. 5), pg. 457 (1968).

[48] Wiebenga, J.G., A Comparison Between Various Combined Nondestructive Testing Methods to Derive the Comprehensive Strength of Concrete, Report No. B-168-61/IHI.8, Institut TNO Voor Bouwmaterialen en Bouwconstructies, (Delft, Netherlands, 1968).

[49] Galan, A., Estimate of Concrete Strength by Ultrasonic Pulse Velocity and Damping Constant, Journal of American Concrete Institute, Vol. **64**, No. 10, pg. 678 (1967).

[50] Facaoaru, I., Nondestructive Testing of Concrete in Romania, Paper 4C, Symposium on Nondestructive Testing of Concrete and Timber, Institution of Civil Engineers, (London, 1969).

[51] Facaoaru, I., Dumitrescu, I., and Constaninescu, L., Concrete Strength Determination by Nondestructive Combined Methods, RILEM Report, Aachen, 41 (1966).

[52] Facaoaru, I., Dumitrescu, I., and Stamate, G., New Developments and Experience in Applying Combined Nondestructive Methods for Testing Concrete, RILEM Report, Varna, 26 (1968).

[53] Facaoaru, I., Chairman's Report of the RILEM Committee on Nondestructive Testing of Concrete, RILEM, Materials and Structures, Vol. 2, No. 10, pg. 253 (1969).